INVESTIGATION INTO THE PERFORMANCE AND ACOUSTICAL CHARACTERISTICS OF PROTON EXCHANGE MEMBRANE FUEL CELLS

MOHMAD SALEM ALRWEG

A thesis submitted in partial fulfilment of the requirements of the
Manchester Metropolitan University for the degree of
Doctor of Philosophy

Department of Electrical and Electronic

The School of Engineering

Manchester Metropolitan University

2017

INVESTIGATION INTO THE PERFORMANCE AND ACOUSTICAL CHARACTERISTICS OF PROTON EXCHANGE MEMBRANE FUEL CELLS

M S ALRWEG

PhD 2017

Abstract

Over the last three decades, much research has been conducted into developing fuel cells (FCs) owing to their high efficiency and environmental friendly operation. Among different types of FCs, proton exchange membrane fuel cells (PEMFCs) are popular for stationary and mobile applications. They have a high-energy density, low operating temperatures, quick start-up times and zero emissions. However, their low reliability and unacceptable high costs limit their wider adoption in the above-mentioned applications. Lack of understanding and complexity of FC operations, mechanical failure, and the lack of root cause analysis and prevention techniques are obstacles that stand in the way of improving such low durability and reliability.

The aim of this PhD work is first to derive a realistic model that represents the complex operations of a single PEMFC and experimentally verify the effectiveness of the developed model. Second, to gain a clear understanding of PEMFCs' failure modes and effects analysis. Third, to assess the detectability of commonly used monitoring techniques and explore the acoustical characteristics of PEMFCs under normal and faulty conditions.

Power parameters are directly affecting the operating conditions of PEMFC and hence are expected to carry useful information about their conditions. Unfortunately, those measurements are intrusive and they do not detect faults at the early stages of onset. However, PEMFCs are dynamic chemical systems that involve phase transitions and thus are acoustically active. Chemical changes during interactions are usually accompanied by a transfer of energy and part of energy may be converted to an acoustic emission (AE).

Although, AE techniques are widely adopted for monitoring chemical and electrochemical systems, no rigorous work has undertaken to characterise the acoustical behaviour of PEMFCs. Therefore, the nature and source of AE in PEMFCs are identified and effect of load variations on them are experimentally investigated as part of this study.

It is anticipated the work presented in this thesis will open the door for more studies to build non-intrusive robust diagnostic systems, which will contribute to enhance the reliability of PEMFCs.

Declaration

No portion of the work referred to in this thesis has been submitted in support of an application for another degree or qualification at this, or any other university, or institute of learning.

Signature: Mohmad Alrweg

Acknowledgments

At this particular opportunity, I must thank Allah, who gives me the spirit and power to write this thesis and fulfil my ambitions, as it has been a challenging task to undertake such a project.

I have been fortunate to have the opportunity to undergo this intensive project work at Manchester Metropolitan University for three years as a PhD student.

My appreciation also goes to Dr Alhussein Albarbar, my director of studies, for his great contributions to the success of this thesis. His guidance has been extremely valuable to support and encourage me to achieve something that I had never thought to realise before. He has provided me with his valuable advice and knowledge during my study at MMU.

My deep gratitude goes to my mother, my father, and my lovely brothers and sisters for their love, encouragement, and unconditional support throughout my life.

I am grateful to my wife Nora for her continued loving support and companionship throughout everything I have done in my studies and beyond.

Finally, my loving greetings to my wonderful kids (Salem, Ahmed and Yumna) for their kind feelings and support to me.

Table of Contents

List of Figures

List of Tables

Abbreviations

A	Ampere
AE	Acoustic emission
AFC	Alkaline fuel cell
AST	accelerated stress-testing
Bp	Bipolar plate
CHP	Combined heat and power
CTE	Coefficient of thermal expansion
CL	Catalyst layer
CNTs	Carbon nanotubes
CO_2	Carbon dioxide
D_f	Diffusion flux of reactant species
E_o	Open-circuit voltage
EIS	Electrochemical impedance spectroscopy
F	Faraday constant
FFT	Fast Fourier transformer
J	Joule
FC	Fuel cell
GDL	Gas diffusion layer
GL	Gas channel
H_2	Hydrogen
H_2O	Water
HFCs	Hydrogen fuel cells
HO•	Peroxide
HOO•	Hydro-peroxide
HP	Hydropower
HRES	Hybrid renewable energy system
Hrs	Hours
HHV	Higher heating value
i	Current density (A/cm^2)
i_a	Current density at anode side (A/cm^2)
I_c	Current density at cathode side (A/cm^2)
LHV	Lower heating value

I	Actual cell current.
i_o	Exchange current density
M	Molecular weight of reactant species
MCFC	Molten fluid Carbonate fuel cell
MEA	Membrane electrode assembly
N	Number of electrons
Nb	Niobium
Ni	Nickel
O.C	Open circuit
O_2	Oxygen
ORR	Oxygen redaction reaction
PAFC	Phosphoric acid fuel cell
PEM	Proton exchange membrane
PEMFC	Proton exchange membrane fuel cell
PFSA	Perfluorinated sulfonic acid
P_{H2}	Pressure of hydrogen
P_{input}	Power input
P_{O2}	Pressure of oxygen
P_{out}	Power output
PRR	Proton reduction reaction
Pt	Platinum
PTFE	Polytetrafluoroethylene
PV	Photovoltaic
R	Universal gas constant, 8.314 (J/mole. K)
R_e	Conductive FC components
RH	Relative humidity
RHE	Reversible hydrogen electrode
R_i	Ionic resistance of the electrolyte
Ru	Ruthenium
S	Source term
SHE	Standard hydrogen electrode
SOFC	Solid oxide fuel cell
T	Temperature
T_a	Tantalum
T_i	Titanium

u	Velocity vector
UPS	Uninterrupted power supply
V	Voltage
WT	Wind turbine
Z_r	Zirconium
E	Reverse voltage
P	Pressure
K	Permeability of the porous medium
Greek Symbols	
$\boldsymbol{\eta_{Ohm}}$	Ohmic polarisation
$\boldsymbol{\eta_{act}}$	Activation polarisation
$\boldsymbol{\eta}$	Cell efficiency
$\boldsymbol{\eta_{thermal}}$	Thermal efficiency
$\boldsymbol{\delta_{thick}}$	The thickness of the membrane
$\boldsymbol{\sigma}$	The conductivity
$\boldsymbol{\eta_{conc}}$	Concentration polarisation
$\boldsymbol{\Omega}$	Ohm
$\boldsymbol{\eta_{thermal}}$	Thermal efficiency
$\Delta \boldsymbol{G_f}$	Change of standard free energy
$\Delta \boldsymbol{G_{f\,(product)}}$	Standard enthalpies
$\Delta \boldsymbol{G_{f\,(reactant)}}$	Entropies of reaction
$\Delta \boldsymbol{g_f}$	Enthalpy
$\boldsymbol{\alpha}$	Charge transfer coefficient
$\boldsymbol{\psi}$	Fuel utilisation efficiency

CHAPTER 1

INTRODUCTION AND BACKGROUND

This chapter provides an overview of fuel cells' technology in terms of their types, advantages and disadvantages and discusses the novelty of the project. The aim and objectives are also outlined at the end of the chapter.

1.1 Overview

Costs of fossil fuel and the growing concerns about greenhouse gas emissions has prompted scientists and researchers to look for other sources of energy that are sustainable with low costs, highly efficient energy conversion and minimal environmental impact. Therefore, interest in green renewable power generation systems, such as photovoltaic (PV), wind turbine (WT), hydropower (HP) and hydrogen fuel cells (HFCs), has increased (Rodrigues *et al.*, 2015). Although, PV, WT and HP renewable systems represent an effective way to substantially reduce fuel consumption and emissions, these systems have their own drawbacks and limitations. For example, solar and wind energy systems experience large variations in their power output since they mainly rely on weather conditions, while hydropower depends on geographic position and water availability (International Energy Agency, 2015). Usually PVs and WTs are combined with the use of an energy storage system, such as batteries and fuel cells, as a type of energy-balancing medium. This system is known as the hybrid renewable energy system (HRES) and it is employed to overcome the drawbacks of PVs and WTs (Panwar *et al*., 2011; Rodrigues *et al.*, 2015). Unlike other renewable energy power generations, FCs do not rely on weather conditions or geographic position.

Hydrogen fuel cells (HFCs) are part of the energy economy, which is a renewable resource when produced from the electrolysis of water using electricity from solar, wind, and bioenergy sources (see Figure 1.1). Hydrogen is an attractive alternative since water is a by-product when it reacts with air in a fuel cell. Therefore, hydrogen and FC technologies can address two essential challenges, which are reducing CO_2 emissions and reducing overall dependence on fossil fuels.

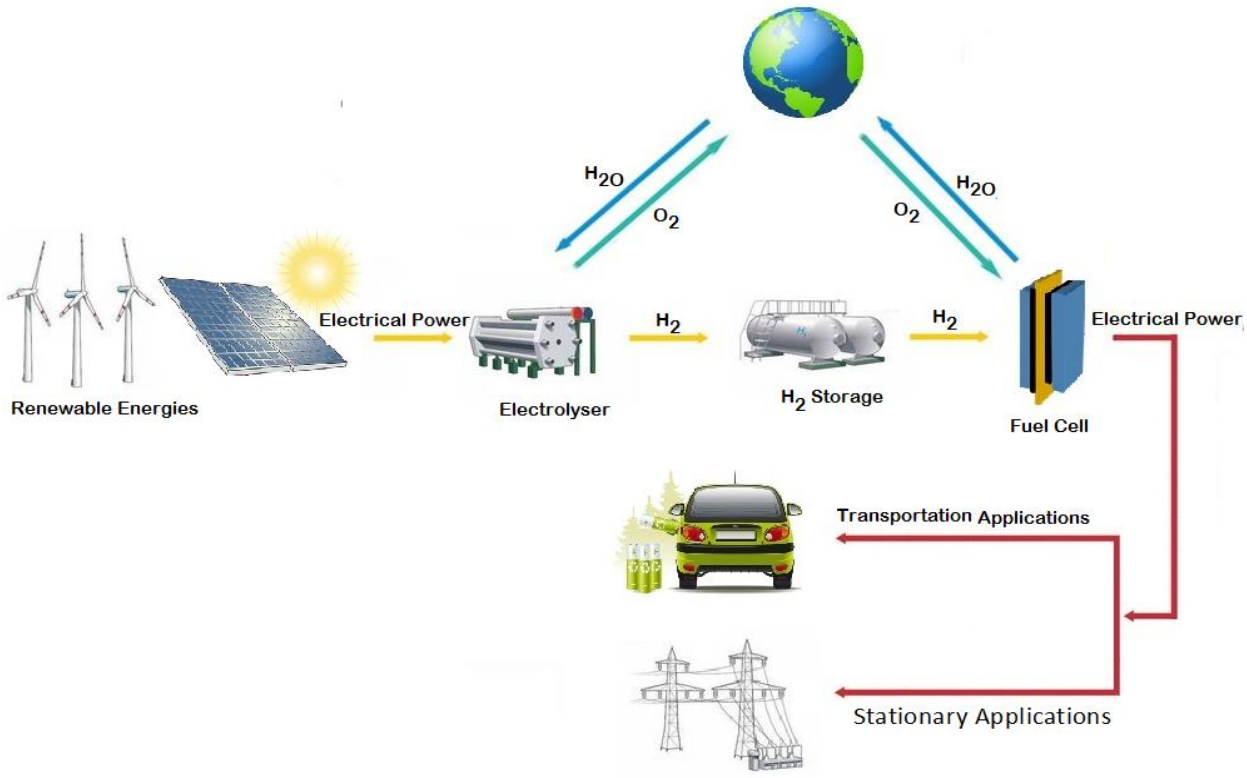

Figure 1.1: Renewable energy, fuel cell and hydrogen economy.

1.2 Fuel Cell Technologies

A fuel cell is an electrochemical device that converts chemical energy into electrical energy. Due to the electrochemical reactions occurring at both electrodes of the FC, the fuel at the negative electrode (anode) is oxidised to release electrons and protons. The electrons are transferred to the positive electrode (cathode) via an external circuit, reducing the oxidant species (air or oxygen). The flow of electrons during these electrochemical processes gives rise to direct current ($I_{d.c}$) in the electrical circuit, while potential differences exist over the two electrodes based upon the nature of the redox reactions. The electrical energy obtained by FCs can be utilised in many sectors such as in residential, stationary, phone cells, and communication and transport applications. The greatest advantage of FC energy compared to the traditional one is its high efficiency. Unlike internal combustion and steam engines, heat exchange and mechanical work are no longer the major energy conversion methods. The electrons from the chemical reactions themselves are collected and converted directly to supply power. FC is a clean source of energy if proper selection of fuel, such as pure hydrogen has been used, showing great potential of mitigating the environmental pollution problems of the modern industrial

world. State-of-the-art FCs are appearing on the market in two forms: stand-alone or networked, to certain residential and industrial applications or as an uninterrupted power supply (UPS), as a major power system for adventure and telecommunications in distant locations, and as demonstration units in universities and automobile companies.

Over the last 50 years, much research has been conducted to develop FC products due to their high efficiency and environmental friendly operations. However, the results have only slightly improved performance. The durability and reliability have shown no major benefits. FCs have not been widely adopted in the open market due to their low durability and reliability and unacceptably high cost. Those weaknesses remain strong research issues and appear to be the most important considerations in achieving successful commercialisation of FCs (targets: 40,000 hrs for stationary and about 5,000 hrs for automotive applications) (Bose *et al*., 2011; Kirsten, 2014).

1.2.1 Fuel Cell Types and Applications

1.2.1.1 Fuel Cell Types

Fuel cells can be classified according to the type of fuel used, which can be pure hydrogen or gases saturated with hydrogen. Also, depending on the specified reaction temperature where some FCs work at low temperatures (less than 100^0C) such as the proton exchange membrane (also known as the polymer electrolyte membrane fuel cell, PEMFC), while other work with high temperature (600-1000)^{0}C such as solid oxide fuel cells (SOFC).

In this research, the classification adopted is one based on the type of material used for the electrochemical material (i.e. electrolyte) and their types according to this classification are:

1. Alkaline Fuel Cells (AFCs).
2. Solid Oxide Fuel Cells (SOFCs).
3. Direct Methanol Fuel Cell (DMFCs).
4. Phosphoric Acid fuel cells (PAFCs).
5. Molten Fluid Carbonate Fuel cells (MCFCs).
6. Proton Exchange Membrane Fuel Cells (PEMFCs).

1.2.2 Fuel Cell Applications

Based on each FC type's characteristics, FCs may have specific applications in three main categories: transportation, stationary, and portable applications. For instance, FCs have been used as the auxiliary power supply in the Apollo and Gemini space programmes respectively. FCs may become the future replacement of current internal combustion engines in automobiles. High temperature FCs such as MCFCs and SOFCs have been applied in static power stations to generate electrical power and heat for the community. In addition, researchers are investigating the possibility of DMFCs as the power supplier for portable electronic apparatus including cell phones and laptops. In addition, PEMFCs have been used in transit utility vehicles, breath alcohol testers and outdoor activity power sources (Murray *et al*., 1999; Dutta *et al*., 2001; Bianchi *et al*., 2015).

1.2.3 Full Cell Advantages

Fuel cells can be considered as batteries, except that FCs do not need to be recharged and fuel is stored outside the cells. In FCs, fuel constantly flows through the cell and it is easily replenished outside the cell, so it never stops providing electrical current. If there is a flow of fuel through the cell, the electricity flows out of it. A FC is an energy-producing device while a battery is an energy-storage device. For batteries, the fuel is stored inside the battery and cannot easily be replenished. Another unique feature that FCs possess is the ability to scale between power (specified via the FC's size) and capacity (specified by the reservoir size). Batteries cannot scale well at large sizes. This is not applied for FCs that scale well from 1W range to megawatt ranges. Moreover, FCs provide energy with high densities compared to batteries. In addition, FCs can be quickly recharged via refuelling while batteries are not rechargeable or need a long time to be recharged (Dutta *et al*., 2011).

Unlike the conventional energy conversion through the combustion process, FCs convert the chemical energy of the fuel directly to electrical energy, which is not subject to Carnot thermodynamic inefficiency. FCs possess 45 – 60% efficiency compared with the 33% efficiency of a fossil fuel plant, as shown in Figure 1.2. FCs allow conversion of a wide range of gasifier hydrocarbon fuels such as ammonia, natural gas, gassified coal, etc.

Unlike conventional combustion-based power generation technologies, FCs can significantly decrease any detrimental environmental impact (Murray *et al*., 1999; Bianchi *et al*., 2015). The pollution reductions can be seen from figure 1.3, where PEMFC emits virtually no gas emissions, and the emitted CO_2 is significantly reduced by more than 50% (Panwar *et al*., 2011).

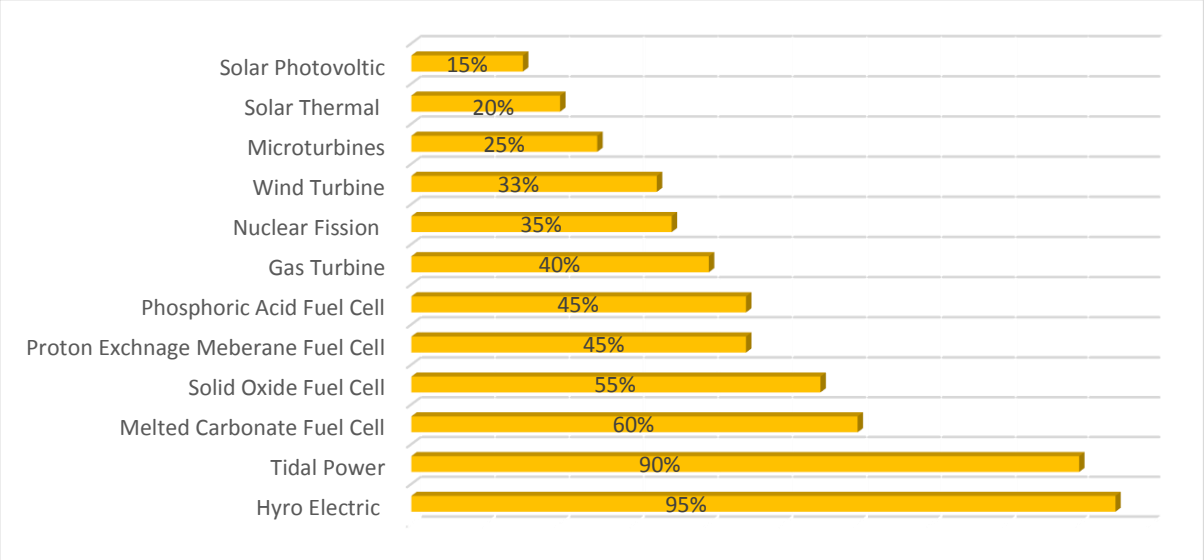

Figure 1.2: Comparison of the efficiency of different sources of electrical power (from Panwar *et al.*, 2011).

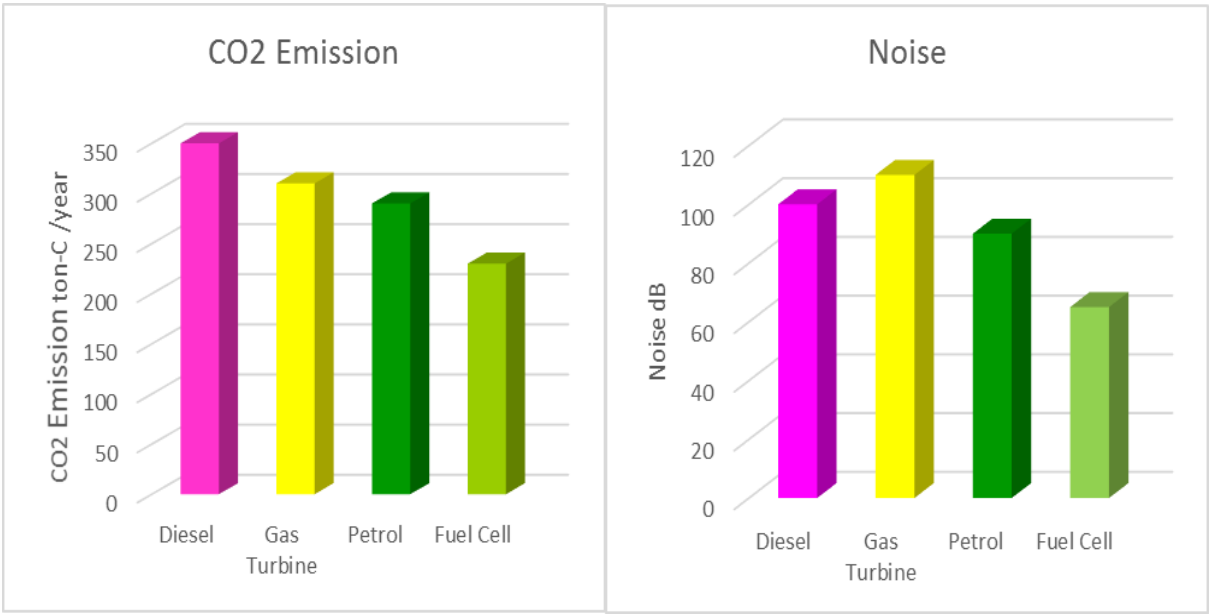

Figure 1.3: Fuel cell emission environmental benefits (from Panwar *et.al*., 2011).

1.2.4 Fuel Cell Disadvantages

Despite the advantages that FCs have, they also possess several disadvantages. The first one is the implementation cost, which limits FC application. Although there are great efforts to bring FCs into the energy markets, the high cost remains an obstacle. The power density, which is the power produced by the FC per volume or per unit mass, is dependent on many parameters such as pressure, temperature and the size of the active area of the catalyst and its material. Despite recent improvements in power density, more improvements are needed for FCs to be applied in portable and automotive applications. Generally, engines and batteries are more effective than FCs in terms of volumetric power density. However, in terms of gravimetric power density, FCs, batteries, and engines have a comparable performance.

A further two issues are availability and storage. FCs work perfectly with hydrogen gas, which is not widely available, and the source of pure hydrogen remains an unresolved issue for PEMFC application. Although hydrogen can be obtained from many sources, for example: water electrolysis, methanol/natural gas/gasoline reformation and bacterial production, the cost of hydrogen generation, storage and the building of hydrogen refuelling infrastructure is high.

Reformation of hydrocarbon compounds cannot eliminate the dependence of power generation on naturally conserved fossil resources and has carbon dioxide (CO_2) as one of the products, causing environmental issues by itself. Moreover, they have low volumetric power density and these FCs are hard to store.

Alternative fuels such as gasoline and formic acid are difficult to use directly and they usually need reformation. These problems reduce the FC performance. Gasoline is a good alternative fuel from the energy density point of view; however, it is not suitable for FC use.

Some additional limitations of FCs include the operational temperature compatibility issues, lack of environmental safety and durability (Jouin *et al*., 2014).

Table 1.1 briefly lists some of the properties of these cells.

Table 1.1: Types of fuel cells and their characteristics and usages.

Proton Exchange Membrane Fuel Cell (PEMFC)	**Membrane**	**Solid Polymer**
	Operating Temperature	20-180 ^{O}C
	Anode Reaction	$H_2 \rightarrow 2H^+ + 2e^-$
	Cathode Reaction	$^1/_2\, O_2 + 2H^+ + 2e^- \rightarrow H_2O + heat$
	Mobile Ion	H^+
	Stack size	< 1-100 kW
	Efficiency	60% transportation 35% stationary
	Applications	Portable power Transportation Stationary power
	Advantages	Solid membrane Low temperature Quick start-up
	Disadvantages	Expensive catalyst Sensitive to fuel impurities
Alkaline Fuel Cell (AFC)	Membrane	Solution (KOH)
	Operating Temperature	60-120^{O}C
	Anode Reaction	$H_2 + 2(OH)^- \rightarrow H_2O + 2e^-$
	Cathode Reaction	$^1/_2\, O_2 + H_2O + 2e^- \rightarrow\ 2(OH)^-$
	Mobile Ion	OH^-
	Stack size	10-100 kW
	Efficiency	60%
	Applications	Military uses Spacecraft

	Advantages	High performance due to the fast electrochemical reactions Low cost of components
	Disadvantages	Sensitivity to carbon oxide poisoning Electrolyte management
Phosphoric Acid Fuel Cell (FAFC)	Membrane	Phosphoric acid
	Operating Temperature	160-200^{O}C
	Anode Reaction	$H_2 \rightarrow 2H^+ + 2e^-$
	Cathode Reaction	$^1/_2\, O_2 + 2H^+ + 2e^- \rightarrow H_2O$
	Mobile Ion	H^+
	Stack size	400 KW
	Efficiency	85% Combined Heat & Power (CHP) 37-42% (generation of power)
	Applications	Distributed generations
	Advantages	Higher temperature Tolerant of fuel impurities
	Disadvantages	Pt catalyst Long start-up time Large and heavy Expensive Low output power
Molten Carbonate Fuel Cell (MCFC)	Membrane	Molten carbonate
	Operating Temperature	500-650^{O}C
	Anode Reaction	$H_2 \rightarrow 2H^+ + 2e^-$
	Cathode Reaction	$^1/_2\, O_2 + 2H^+ + 2e^- \rightarrow H_2O$
	Mobile Ion	H^+
	Stack size	0.3-3 MW

	Efficiency	45-50%
	Applications	Distributed generations
	Advantages	Higher temperature Tolerant of impurities fuel.
	Disadvantages	Corrosion and breakdown of cell components Long start-up time Low current density
Solid Oxide Fuel Cell (SOFC)	Membrane	Ceramic compound
	Operating Temperature	600-1000^{O}C
	Anode Reaction	$H_2 + O^- \rightarrow H_2O + 2e^-$ $CO + O^- \rightarrow CO_2 + 2e^-$ $CH_4 + 4O^- \rightarrow 2H_2O + CO_2 + 8e^-$
	Cathode Reaction	$^1/_2\, O_2 + CO_2 + 2e^- \rightarrow CO_3^{-2}$
	Mobile Ion	O^-
	Stack Size	1KW-3MW
	Efficiency	85% Combined Heat & Power (CHP) 60% (generation of power)
	Applications	Auxiliary power Electrical utility Distribution generation
	Advantages	High efficiency Fuel flexibility Variety of catalysts Solid membrane
	Disadvantages	High temperature Corrosion and breakdown of cell components Long start up time

1.3 Motivation

A fuel cell is a complex technology that cuts across multiple disciplines, including materials science, electrical, electrochemistry and catalysis.

It is always a major challenge to fully understand all the phenomena and processes that occur within the FC such as thermodynamics, fluid mechanics, FC dynamics, and electrochemical processes (Dutta *et al*., 2001).

Most researchers have focused on operational performance and little attention has been given to investigate the phenomena that occur in the cell and then link it to the FC's performance evaluation and enhancement. Understanding the fundamentals and principles of those phenomena will be the key to understanding the mechanism of faults and their causes that will help to enhance reliability and performance, ultimately reducing the cost owing to improving the drawbacks and increasing the lifespan of FCs.

Electrochemical acoustic emissions (AEs) are usually defined as the spontaneous fluctuations of potential and/or current generated by electrochemical processes. In the last decade, acoustic emission (AE) has become a widespread technique that has been shown to be well-adapted to the study of electrochemical systems such as corrosion (Murray *et al*., 1999), gas evolution (Bianchi *et al*., 2015) and batteries (Jouin *et al*., 2014). AE occurs within FCs because of explosion and movement of water bubbles at the cathode side. This phenomenon can be utilised to study FC behaviour and investigate its state of health.

This research is an attempt to study and investigate AEs' capabilities to enhance the performance and efficiency of FCs by providing rigorous investigations into the generation mechanisms and characteristics of FCs, particularly for proton exchange membrane fuel cells' (PEMFs') emitted acoustic signature.

1.4 Research Aim and Objectives

1.4.1 Research Aim

This research aims to investigate the design and performance of PEMFCs. In addition, their fundamental acoustical characteristics and generation mechanisms will be also studied.

1.4.2 Research Objectives

To effectively achieve the above-mentioned aim, the research objectives are outlined as below:

1. Explore the design and working principles of Proton Exchange Membrane Fuel Cells (PEMFCs) and their associated parameters.
2. Gain clear a understanding of Proton Exchange Membrane Fuel Cells' (PEMFCs') failure modes, and comprehend control and condition monitoring techniques e.g. temperature, voltage, power and current analysis.
3. Develop a mathematical model for Proton Exchange Membrane Fuel Cells' (PEMFCs') operations and effect of faults on their efficiency and performance.
4. Design and construct a test rig with associated instrumentation for various operating conditions and fault simulation, namely load variations, hydration and dehydration, data collection and subsequent data analysis.
5. Carry out experimental investigation on the use of power parameter-based techniques such as current, voltage and power in diagnosing the simulated conditions. This also includes determining their operating efficiency using only the measured current and the manufacturer's data available from the datasheet to detect, diagnose and assess the relative fault severity of the seeded faults.
6. Upgrade the developed test rig to include measuring and recording acoustic emissions (AE) data, under varying operating conditions and different electric loads.
7. Develop and apply signal-processing methods to assess the effectiveness of AE signals to detect load variations. Those processing techniques include multiband filtration, root mean square values, variance, and kurtosis.

1.5 Thesis Organization

The remainder of the thesis is divided into six chapters:

Chapter 2: Presents the physical construction of proton exchange membrane fuel cells (PEMFs) as well as studying the characteristics of the cells and polarisation curves. In addition, the dynamic behaviour (thermodynamic) and efficiency of the PEMFCs are covered in this chapter.

Chapter 3: Covers all the literature regarding performance evaluation and efficiency calculation related to PEMFCs. In addition, it concentrates on reviewing the causes of the degradation in FCs and the diagnosis and monitoring techniques currently in use.

Chapter 4: Illustrates the failure modes that occur within FCs and their effect on the performance, reliability, and efficiency of FCs. Additionally, this chapter will cover the fault mitigation strategies that are used to reduce the negative impact for most common faults. Finally, some diagnosis and monitoring techniques are presented.

Chapter 5: Presents the proposed and developed fundamental theory-based numerical and Simulink models to evaluate the effects of parameter variations such as temperature, pressure and water content on the performance and reliability of the PEMFC.

Chapter 6: Presents the experimental set-up to study and investigate the effect of the load variation on acoustic emission and cell flooding. Outcomes and dissuasion of result are the core element of this chapter.

Chapter 7: In this last chapter, a summary of the work carried out in this thesis and the conclusions drawn from the results are presented. In the last section, some of the areas for future work are explored.

CHAPTER 2

DESIGN AND WORK PRINCIPLES OF PROTON EXCHANGE MEMBRANE FUEL CELLS

This chapter covers the structure and fundamental principles of proton exchange membrane fuel cell (PEMFC) systems and their operations. A good understanding of these concepts is essential to sufficiently understand the phenomena that occur within the fuel cell systems, which is the focus of the following chapter.

2.1 Overview

A fuel cell (FC) is a device that is capable of converting chemical energy into electrical energy, and generating a direct electrical current ($I_{d.c}$) with weak direct voltage ($V_{d.c}$), gathered in a pack (i.e. a FC stack). Humidified hydrogen or other hydrocarbon fuel, such as methanol, is used as fuel enters the anode side while an oxygen gas stream is used as oxidant at the cathode side. These cells are connected in series to give the demand voltage and the current.

Proton exchange membrane fuel cells (PEMFCs) have many advantages such as:

1- High current and power density.
2- Low operating temperature.
3- Quick start-up.
4- No gas emission if pure hydrogen is used.
5- Flexibility of applications, where PEMFC can be used in stationary, transportation and mobile applications.

2.2 Working Principles of Hydrogen Fuel Cells

The basic physical structure of a FC is depicted in figure 3.1. The mode of operation depends on the presence of a membrane separator and the catalyst, which is usually made of platinum powder and the carbon paper or cloth is coated with a very thin layer of the platinum powder (Kircheva *et al*., 2001; Shao *et al*., 2007; Laberty-Robert *et al*., 2011). The platinum coats the sides of the plate and it is placed next to the proton exchange membrane. Once hydrogen (fuel) supplied to the cell, the platinum (catalyst) works on separating H_2, (which is the simplest atom consisting of just one proton and electron), is spilt into a positive proton ion and a negatively charged electron. This operation occurs at the anode side and is known as the oxidation of the fuel. If the oxygen and hydrogen are mixed directly, the products will be water and heat due to this reaction being exothermic. This reaction needs to be controlled where the electrical current is used to provide the load by damned electrical energy is created due to hydrogen oxidation resulting in two protons and two electrons.

The membrane separator allows protons to pass but not electrons. Therefore, electrons should pass only through the current collectors, and this produces direct electrical current ($I_{d.c}$). On the opposite side of the membrane (i.e. at the cathode side), the electron binds with the proton in the presence of a catalyst again and with the presence of oxygen, the water, H_2O, is produced and the heat spreads.

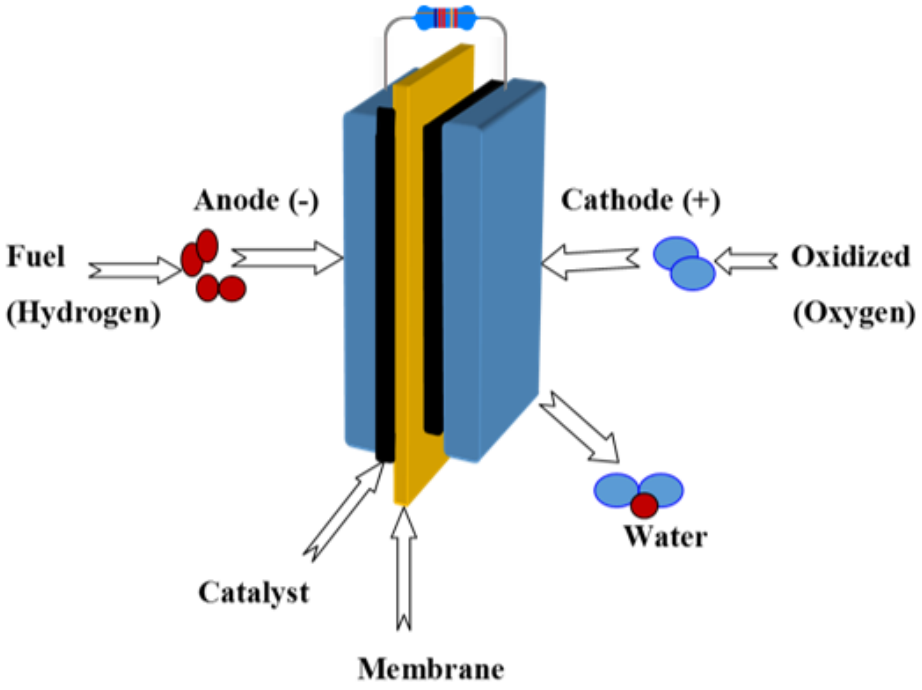

Figure 2.1: The functionality of the proton exchange membrane fuel cell.

2.2.1 Proton Exchange Membrane Fuel Cells

Niedrach and Grubb invented the PEMFC in 1960 at the General Electric Company. The PEMFC is the most commonly used type of FC; it is used in various fields due to its small size and its low temperature of operation. A PEMFC uses a polymer as membrane (Nafion), which plays the role of mediator in the electrochemical cell, in a solid state and thus it reduces the reaction temperature and increases the efficiency (speed of interaction in the start-up and response when loading).

The polymer separation membrane is positioned between two electrodes of perforated platinum and it causes no risk of pollution due to its solid nature. Interaction takes place under 80^0C and when the membrane is exposed to water, it becomes a conductive material for ions (Cheng et al., 2006; Sutharssan et al.,

2016). The electrodes are made of platinum. The efficiency of such cells is up to 45-50% (Panwar et al., 2011) and their power density is high compared with other types of cells being up to 350-600 mW/cm^2 and the reactions are defined in equation (2.1).

$$at\ Anode:\ 2H_2 \rightarrow 2H^+ + 4e^- \quad (2.1a)$$

$$\text{at Cathode}:\ O_2 + 4H^+ + 4e^- \rightarrow 2H_2O \quad (2.1b)$$

$$Overall\ reaction: 2H_2 + O_2 \rightarrow 2H_2O + \text{electricity} + \text{heat} \quad (2.1c)$$

Another type of polymeric cell runs directly on methane gas, and it differs from the first type in terms of the electrode's materials. These cells have a device for the preparation of fuel, where it works on the saturation of methane with hydrogen. The problem in this type of cell is the crossing of methane from the membrane and there is currently a lot of research to address this issue (Chatenet *et al*., 2010).

2.3 Thermodynamic Analysis

Thermodynamics is the science that deals with the transformation of energy from one state to another. As the chemical energy is transferred to electrical energy in a FC, predictions that can be obtained using the equations of thermodynamics are essential to understand and model the performance of the FC.

2.3.1 The Mechanism of Proton Exchange Membrane Fuel Cells

The thermodynamics in a FC is the study of the mechanism of electrochemical, thermal, and electrical reactions within it, to indicate the performance and efficiency of the FC.

Studying the topics mentioned is based on the study of change in Gibbs free energy, which is defined as the actual capacity of the production operation outside of the FC, without addressing the consumption of this energy to change the pressure and volume. It is the energy of the electrons in the external circuit, measured in $KJ\ /mol$, and written as follows:

$$\Delta G_f = \Delta G_{f\,(product)} - \Delta G_{f\,(reactant)} \quad (2.2)$$

Where:

ΔG_f : Change of standard free energy,

$\Delta G_{f\,(product)}$: Standard enthalpies,

$\Delta G_{f\,(reactant)}$: Entropies of reaction.

The free energy (Gibbs energy) resulted from the chemical reaction is that for one molecule the energy is equal to the total energy enthalpy $\Delta g_{f\,(product)}$ minus the entropy losses $\Delta g_{f\,(reactant)}$ as depicted in equation (2.2) :

$$\Delta g_f = \Delta g_{f\,(product)} - \Delta g_{f\,(reactant)} \tag{2.3}$$

Hydrogen and oxygen gases interact in FCs and this reaction produces water, so the equation becomes:

$$\Delta g_f = \Delta g_f(H_2O) - \Delta g_f(H_2) - \Delta g_f(O_2) \tag{2.4}$$

The free energy that enters the cell is not totally converted into electrical energy. The chemical energy (Δg_f) is present as the total chemical energy that can be obtained from the electrochemical interaction.

This energy is not equal to the amount of change in Gibbs free energy transformed into electrical energy. This is due, in a FC, to the two electrons 2e on each molecule of hydrogen (pure hydrogen fuel), i.e., if there is a molecule of hydrogen and it is assumed that the atoms of this molecule all interact at the negative pole (anode), the result will be $2\ e * N\ electrons$, where N is Avogadro's number.

The load which is connected with the external circuit gets 2e* N of electrons where e is the charge of one electron. The Faraday constant (F), which is equal to (96487 J/V-mole), is the result of the production of e in N of electrons.

$$2e * N = 2F \tag{2.5}$$

The variation of voltage between the cathode and the anode (potential energy) is E, thus we will have:

$$Voltage\,x\ electric\ current = eclectic\ - 2FE \text{ [Joules]} \tag{2.6}$$

This assumes that the reaction in the cell is reversible; therefore, as has been explained previously, the electrical supply is different in the Gibbs free energy

resulting from the interactions that took place in the cell (Nu *et al*., 2007; Spurgeon *et al*., 2011):

$$\Delta g^{-} = -2FE \rightarrow E = \frac{-\Delta g}{2F} \tag{2.7}$$

$$E_o = \frac{219100}{2*96487} = 1.135\ volt \tag{2.8}$$

In addition, this equation shows the open-circuit voltage of the FC, and gives the free energy in the data manual to a FC. Table 2.1 shows the values of the free energy, outcome and voltage of the open circuit in the event of the output water or water vapour to the cells and its fuel being hydrogen and oxygen.

Table 2.1: Free energy, yield stress and the open circuit if the output is water or water vapour.

$\boldsymbol{H_2 + \frac{1}{2}O_2 \rightarrow H_2O}$ **1 atmosphere reactant pressure (standard condition)**						
Temp (ºC)	Product H_2O phase	ΔH_f $(\frac{KJ}{mol})$	$\Delta\ G_f$ $(\frac{KJ}{mol})$	η (%)	$E_{O.C}$ (V)	E_{rev} (V)
25	LHV(vapour) HHV(liquid)	-241.8 -286	-228.6 -237.3	94.5 83	1.253 1.482	1.185 1.229
80	LHV HHV	-242.3 -283.8	-226.2 -233.7	93.3 82.3	1.256 1.471	1.172 1.212
130	LHV HHV	-242.8 -282.1	-223.9 -230.4	92.2 81.7	1.258 1.462	1.160 1.195
200	LHV	-243.8	-219.1	89.8	1.259	1.131
600	LHV	-247.2	-198.1	80.1	1.277	1.023
1000	LHV	-249.4	-175.8	70.5	1.288	0.908

Figure 2.2 shows the entropy energy of hydrogen, oxygen and water as functions of temperature at a reactant pressure of one atmosphere.

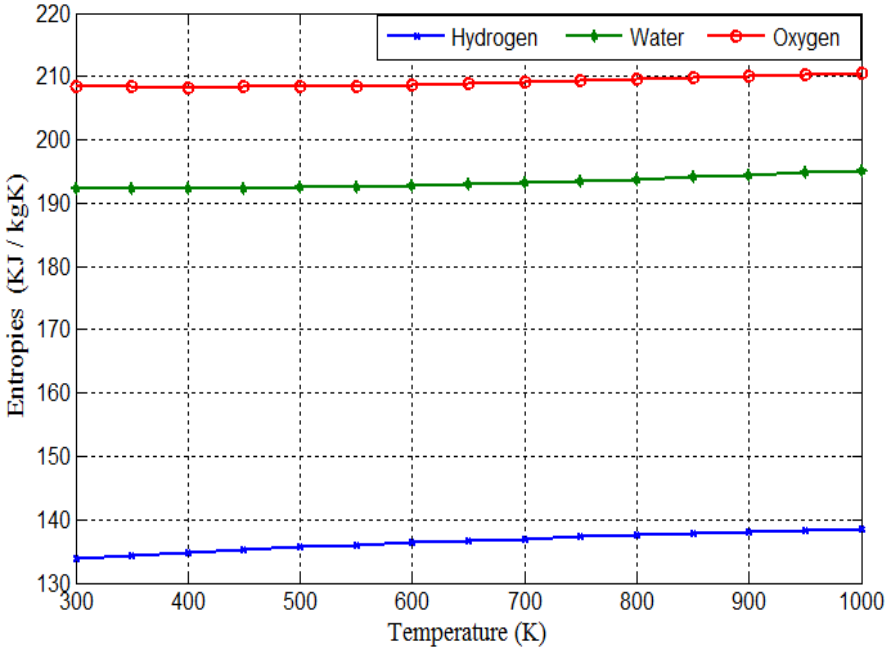

Figure 2.2: The entropy of hydrogen, oxygen and water.

The open circuit voltage is associated with the real operating conditions at operating temperature, where the Gibbs energy changes when the fuel enters the cell, and this results in operating temperature increase and water is production, based on the electrochemical reactions that take place in FCs (Ural et al., 2007).

The Nernst equation shows the relationship between the open-circuit voltage (E_o) under typical conditions ($T = 25^O C$, $P_{H2} = P_{O2} = 1atm$) and the operating voltage for FC (E) at different temperatures and pressures.

$$\Delta G = \Delta G\, o + RTInQ \tag{2.9}$$

FCs that work at low operating temperatures, such as PEMFCs and PAFCs need to contain expensive metals to function as a catalyst to accelerate the reaction in the electrodes. Hydrogen, in general, is the only fuel used in these types of cells, whereas in cells with high temperatures such as Molten Fluid Carbonate Fuel Clles (MCFCs) and Solid Oxide Fuel Cells (SOFCs), the catalysts and fuel used are varied and diverse. The equations below describe the energy of a chemical reaction (Q) and the voltage of the FC produced as result of the oxidation reaction at the anode side.

$$aA + bB \rightarrow cC + dD \Longrightarrow where\ , Q = \frac{[C]^c[D]^d}{[A]^{ca}[B]^b} \tag{2.10}$$

$$\frac{1}{2}O_2 + H_2 \longrightarrow H_2O \Longrightarrow Q = \frac{[H_2][O_2]^{\frac{1}{2}}}{[H_2O]} \quad (2.11)$$

$$E = E_o + \frac{RT}{2F}\left[\frac{\alpha\beta^{\frac{1}{2}}}{\delta}\right] + \frac{RT}{2F}ln(p) \quad (2.12)$$

The above equations can be expressed as follow:

$$E = 1.23 - 0.9 * 10^{-3}(T - 298) + \frac{RT}{4F}ln(P^2H_2 * P_{O2}) \quad (2.13)$$

If the pressure of the gases (fuel and oxidiser) and the water pressure generated by the electrochemical reaction are taken into account, and then by dividing both sides of the equation (2.13) by (-1/2F), the Nernst equation depending on the equations mentioned becomes as follow:

$$E = E_o + \frac{RT}{2F} + ln\frac{P_{H2}*(P_{O2})^{\frac{1}{2}}}{P_{H2O}} \quad (2.14)$$

Equation (2.14) expresses the total pressure in terms of the partial pressure of gases, multiplied by a gas constant of each gas separately:

$$P_{O2} = \beta p \ \& \ P_{H_2} = \alpha P \ \& P_{H2O} = \ \delta P \quad (2.15)$$

By substituting the value of P_{O2} in equation (2.14), it will produce the final form of equations (2.16) and (2.17) that express the influence of heat and pressure on the work of the cell as follows:

$$E = E_o + \frac{RT}{2F}\left[\frac{\alpha\beta^{\frac{1}{2}}}{\delta}\right] + \frac{RT}{2F}ln(p) \quad (2.16)$$

$$E = 1.23 - 0.9 * 10^{-3}(T - 298) + \frac{RT}{4F}ln\left(P^2H_2 * P_{O_2}\right) \quad (2.17)$$

Where:

R : Gas constant $(8.314\ (J\ /\ mol.K)$,

T : Temperature in Kelvin, P the gas pressure in the anode and the cathode (bar),

F : Faraday's constant (96487 joules/volt-mole),

β: The hydrogen gas constant and δ the water vapour constant.

2.4 Polarisation Phenomenon

When a PEMFC is loaded, the voltage goes down by 60% or 70% of the open-circuit voltage. Both the output voltage and current density determine the characteristics of the *V-I* curve. The output voltage of the PEMFC is closely related to that thermodynamically predicted in FCs and three major losses, which are Activation losses, Ohmic losses, and Concentration losses. Activation losses occur due to the electrochemical reaction. Ohmic losses occur due to the ionic electronic conditions while Concentration losses are produced due to mass transport (Al-Baghdadi *et al*., 2005; Offer *et al*., 2009).

The main reason for this loss is the fuel crossover and internal currents through the electrolyte through which only ions should transport. However, a small amount of fuel and fewer electrons will be conducted through the electrolyte. The electrolyte has a reducing effect on the open circuit voltage, as depicted from the polarisation curve. When the current moves away from the zero point, and the voltage initially and rapidly drops, this drop is due to the activation losses which are caused by the slowness of the reaction taking place on the surface of the electrodes. A small part of the voltage generated is lost since it drives the chemical reaction responsible for transferring the electrons to and from the electrode.

At medium current densities, the voltage losses become linear and decrease less slowly. The linearity characteristics represent the Ohmic losses which are also known as “resistive losses” and they stem from the straightforward resistance to the flow of electrons in the various FC components, as well as the resistance to the flow of ions in the electrolyte. This voltage drop is linear and it is proportional to the current density.

At higher current density, the voltage falls rapidly due to mass transport limitations in the cell. These are usually known as “Mass transport or concentration losses”, and they result from the change in the concentration of the reactants at the surfaces of the electrodes.

The possible reasons for this change are:

1. The obstruction that prevents the gases from reaching the reaction sites on the membrane.

2. The accumulation of product water blocking the flow channels in the bi-polar plates or the GDL. To avoid the drastic decrease in power density in this region, the optimal operating system for a FC is up to the maximum power density.

It is noteworthy that the terms used for losses are variable from one discipline to another, they are called: losses, voltage drop or conversely overvoltage, which gives the impression that the voltage increases instead of decreasing. However, it is the term usually used in electrochemical literature. In the following sections, each one of these losses will be described separately, and presented in mathematical and graphical forms.

The effects of varying certain operating conditions such as temperature and pressure on the performance of the FC, as well as certain geometric-dependant parameters such as the values of exchange current density and charge transfer coefficient, which are dependent on the electrode material and catalyst loading of the FC electrodes.

It is obvious from figure 2.3 that the open circuit voltage (E_O) is less than the theoretical value of the reversible voltage (Offer *et al*., 2009; Alrewq & Albarbar, 2016). This is proof that there is a loss of voltage even when there is no load connected to the FC.

The analysis takes into consideration the following assumptions:

1. The FC operates under steady state conditions.
2. The gases (fuel and oxidiser) are assumed to be ideal compressible gases.
3. Due to the low velocity of the gases, their flow is laminar.
4. The product water assumed to be in liquid form.
5. The electronic resistance of the FC components and the external circuit are constant over the range of operating temperatures.
6. The pressures at both electrodes are assumed to be the same.
7. The internal currents in the FC are equal to fuel crossover.

Table 2.2: Values of constant parameters utilised to plot the polarisation curve in figure 2.3.

Parameter	Value	Units
E_o	1.23	*Volt*
b	0.032	*KJ.Mole/kg. °C*
R	$3*10^{-3}$	*Ohm*
α	0.3	--------
$P_{O2} = P_{H2}$	2	*atm*
T	353	*Kelvin*

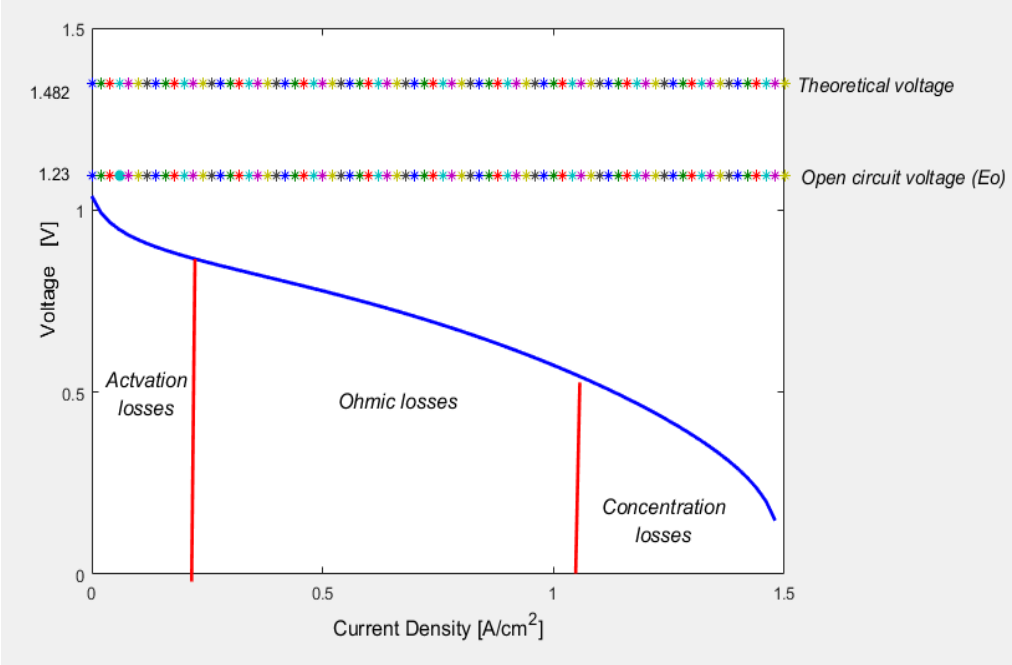

Figure 2.3: The schematic diagram of the FC through the production cycle and three losses.

2.4.1 Activation Polarisation

When the cell is loaded, the non-linear voltage drops suddenly by (ηact > 50-100 mV) and then remains constant because of the energy needed to trigger the interaction between the fuel and oxidiser (Alrewq & Albarbar, 2016). The activation polarisation (η_{act}) is non-linear and it has large values at low current density. Both electrochemical and chemical reactions are very similar since they involve an activation barrier that needs to be overcome by the reacting species.

Consequently, part of the electrode potential is lost since it drives the electron transfer rate to the one required by the current demand.

The reaction kinetics are expressed by the Butler-Volmer equation where the mass transfer effects are neglected (Wang *et al*., 2013; Al Zahrani *et al*., 2015):

$$i = i_0 \left[e^{\frac{\alpha n \eta_{actc}}{RT}} - e^{\frac{(1-\alpha) nF \eta_{acta}}{RT}} \right] \quad (2.18)$$

Where:

R: the universal gas constant $(8.314\ \mathrm{kJ/kmol.K})$,

T: the temperature of cell operation in Kelvin,

n: the number of electrons involved per mole of electrolysed component,

α: the charge transfer coefficient, which is the portion of the electrical energy assisting the forward reaction, $1 - \alpha$: hinders the reverse process.

The value of charge transfer coefficient (α) is relies on the reaction involved and the material that the electrode is made from, and it must be in the range of 0< α <1.

F: is Faraday's constant $(96485\ C/mole)$,

η_{actc} and η_{acta}: are the activation polarisation s on the cathode and anode respectively,

i: current density (A/cm^2) and,

i_o: the exchange current density, which is the rate of flow of electrons to and from the electrolyte.

In equation (2.18), the first exponential term expresses the forward reaction voltage that occurs at cathode side as result of the reduction reaction, while the second term expresses the backward reaction voltage as result of the oxidation reaction on the anode side. The equation can be written in the logarithmic form as:

$$ln\left(\frac{i}{i_o}\right) = \frac{-\alpha n F \eta_{actc}}{RT} + \frac{(1-\alpha) nF \eta_{acta}}{RT} \quad (2.19)$$

If the activation polarisation value on the cathode side is considerably higher than that on the anode side, the first part of the equation which expresses the oxidation reaction prevails and the second part can be ignored, and vice a versa in the case of prevailing anodic over- potential.

Tafel's laws represents these two expressions separately for anode and cathode. To express the net cathodic overvoltage, the backward activation overvoltage (anodic reaction) is negligible, and the equation becomes:

$$\eta_{act} = -\frac{RT}{\alpha nF} ln\left(\frac{i_c}{i_a}\right) \tag{2.20}$$

The 'exchange current density' can be defined as 'the current flowing equally in each direction at the reversible potential'. The chemical reaction's 'equilibrium' is initiated when the forward and backward rates are the same.

For electrochemical reactions, the rates of reaction define the current which, at equilibrium, would be the exchange current density. For a net, anodic overvoltage, the anodic reaction becomes the forward reaction and the cathodic reaction can be neglected, equation (2.20) becomes:

$$\eta_{act} = \frac{RT}{(1-\alpha)nF} ln\left(\frac{i_c}{i_o}\right) \tag{2.21}$$

Subscripts a and c utilised in equations (2.19) and (2.20) are used to express the anodic and cathodic current densities respectively. Both equations are in the form known as Tafel's Law, which can be written in terms of current density as follows:

$$\eta_{act} = x + ylni_c \tag{2.22}$$

This equation can also be written in terms of both current density and exchange current in the following form:

$$\eta_{act} = blog\left(\frac{l_c}{i_o}\right) \tag{2.23}$$

Where: b in this equation is equal to:

$$b = -\frac{RT}{\alpha nF} \tag{2.24}$$

Tafel's equation can be used in situations where the activities of the species involved in the reaction are not very much affected by the current flow. This equation can be utilised to deduce the exchange current density which takes place when $\eta_{act} = 0$.

Equation (2.22) can be re-arranged to give 'lni_c' in terms of 'η_{act}' , and considering the other terms as constant gives:

$$\eta_{act} = -\frac{RT}{\alpha nF} lni_a + \frac{RT}{\alpha nF} lni_c \tag{2.25}$$

Writing the equation using the coefficient 'b':

$$\eta_{act} = bln(i_a) - bln(i_c) \tag{2.26}$$

The first exponential term in equation (2.25) that expresses the anodic part of the total activation potential can be ignored as reported in most studies made of PEMFCs. Therefore, the equation can be simplified to Tafel's law.

If proper values were substituted in equation (2.25) and putting $n = 4$ for the cathode side and $\alpha = 0.5$ and the operating temperature$T = 353\,K$, the corresponding value of 'b' $= 0.016$ (Al Zahrani *et al*., 2015).

Figure 2.4 depicts the equation plotting for various exchange current densities

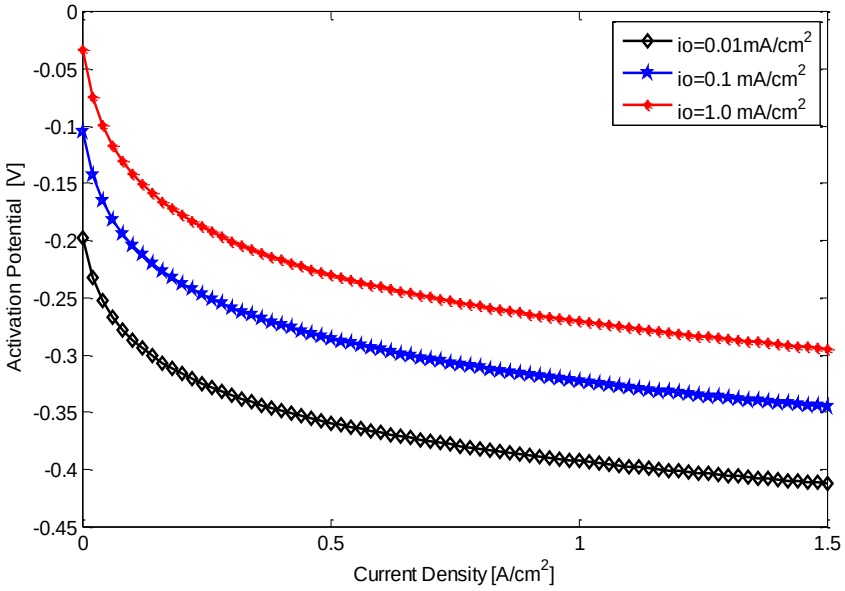

Figure 2.4: The impact of exchange current density on the activation potential.

It is obvious from the figure 2.4 that increasing the exchange current density results in reducing the activation losses. A typical value for the exchange current density(i_o) would be about $0.1\,mA/cm^2$ at the cathode and about $200\,mA/cm^2$ at the anode (for a FC running on air at ambient pressure and low temperature). This

makes losses due to activation over-voltage much greater on the cathode side and therefore it requires more catalyst loading to improve the kinetics of the reaction.

It can also be seen from the figure 2.4 that the current density has an adverse effect on the voltage, as it drops exponentially as the current density increases.

From the literature (Al Zahrani *et al*., 2015), it was found that the exchange current density; i_0 also depends on the partial oxygen (air) pressure. Jaouen *et al*. (2013) conducted experiments on a PEMFC at a temperature of 50^0C. The study found that there is a linear relationship between the logarithm of the oxygen partial pressure and logarithm of the exchange current density i_0, according to:

$$i_0 = x.e^{(yP_{o2})} \tag{2.27}$$

Where : $x = 1.27 \times 10^{-8}$ and $y = 2.06$. However, this relationship is only applicable to the conditions of the experiment performed in the study and hence it is not applicable to other FCs. The exchange potential, particularly at the cathode side, is a mixed potential due to electrochemical reactions. In addition, there are other geometric variables and operating conditions that contribute to the value of the exchange current density. The study (Jaouen *et al*., 2013) also showed from the experiments, that the oxygen partial pressure is a factor in determining the value of 'i_0'. To understand the impact of the charge transfer coefficient on the activation overvoltage, Tafel's equation is plotted for different values of the charge transfer coefficient (α) for a given value of exchange current density $i_0 = 0.01$ and an operating temperature of $T = 353K$.

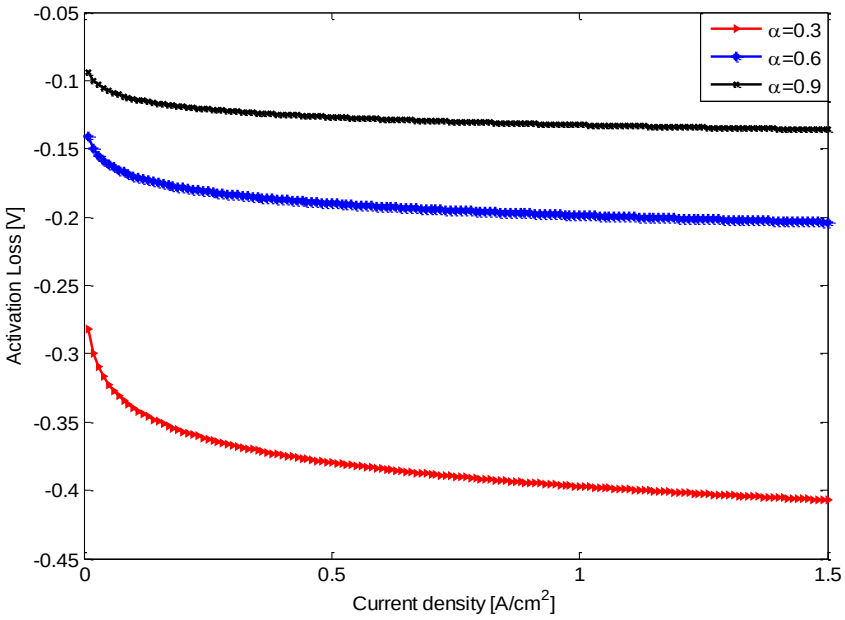

Figure 2.5: The effect of varying the values of α in the activation overvoltage, for exchange current density (i_o =0.01) and operating temperature T=353K.

As the charge transfer coefficient decreases, the activation overvoltage increases exponentially. This shows the importance of the charge transfer coefficient which depends on the type of electrode material. Therefore, the type of electrode material is an important factor in improving the power output of the FC. When the same equation is plotted with various operating temperatures and current densities, it is obvious that the activation losses increase at higher temperatures. However, this effect is balanced by the increased activities of the reactants due to higher temperatures, in accordance with the kinetic theory of gases. For a PEMFC, with effective catalyst action, the hydrogen electrode operates close to thermodynamic equilibrium conditions. The hydrogen oxidation reaction proceeds readily so that the anodic activation potential; 'η_{acta}' is negligible.

In contrast, at the thermodynamic equilibrium potential; the rate at which the oxygen is reduced, in aqueous media, is around 5-10 times slower than that of hydrogen, even with the best catalysts currently available. Thus, the cathodic reaction activation can be attributed to the voltage drop. However, this is not applicable for other types of FCs, such as the Direct Methanol FC (DMFC) which is like the PEMFC in using the same type of membrane electrolyte with a different catalyst and the same construction, but the activation over-voltages on the anode are significant and should be taken into consideration in the equation.

Many methods have been proposed to reduce the activation polarisation (Al-Baghdadi, 2005; Jaouen *et al*., 2013) such as:

1. Increasing cell temperature;
2. Doping the electrode with effective catalysts;
3. Increasing the surface area of the electrode by making it rougher;
4. Increasing the reactant concentration of air, and
5. Increasing the pressure (through increasing catalyst site occupancy which increases the open circuit voltage).

2.4.2 Ohmic Polarisation

All materials have internal (or intrinsic) resistance to the flow of charges. This cell resistance causes Ohmic polarisation, which leads to the loss of FC voltage. The components of the FC, including the membrane, the catalyst layers (CLs), and the gas diffusion layers (GDLs), bi-polar plates (Bp), and terminal connections and interface contacts, contribute to its electrical resistance. The resulting voltage reduction is known as the 'Ohmic loss' and it includes the electronic (R_e) and ionic (R_i) contributions to FC resistance. This can be written as equation (2.28):

$$\eta_{ohm} = IR_{internal} \quad = I(R_e + R_i) \tag{2.28}$$

Since the transportation of the protons is more difficult than electronic transportation, the R_i dominates the reaction. In equation (2.28) R_i represents the ionic resistance of the membrane while the R_e represents the total electrical resistance of all conductive FC components, which includes bi-polar plates, cell interconnects, and contacts.

The Ohmic polarisation (ηohm) is positively proportional to the current density and internal resistance such as the electrode resistance, the bulk electrolyte (membrane) resistance and interface contact resistance between electrodes and electrolyte. Since the cell's resistance is almost constant, the Ohmic polarisation changes linearly and this is due to the emergence of resistance while crossing of ions in the electrolyte and Ohmic resistance electrodes.

The reduction of these resistances by using the appropriate electrolyte and metals in the electrodes can be adopted to overcome this problem. In addition, the Ohmic

losses may be reduced by using high conductive membranes as well as reducing the space between electrodes.

The ability of a material to support the charge flow through itself is known as conductivity.

The electrical resistance of FC components is often referred to as conductance (s) in the state of the area, which is the inverse of resistance:

$$\sigma = \frac{I}{R_{internal}} \tag{2.29}$$

Resistance characterises the size, shape, and properties of the material, as expressed by equation (2.30):

$$R = \frac{\rho_{ele} l}{A} \tag{2.30}$$

Where:

$$\rho_{ele} = \frac{1}{\sigma}$$

Where: ρ_{ele} is the electrical conductivity (ohm^{-1} cm^2), l is the length (cm) of the conductor, and A is the area (cm^2) of the conductor.

Equation (2.30) can be rewritten as follows:

$$R = \frac{l}{\sigma A} \tag{2.31}$$

The current density, which expresses the number of the electrons in a square metre can be expressed by the following equation:

$$i = \frac{I}{A} \tag{2.32}$$

Current density (I) can also be determined by the number and the average velocity of carriers as in equation (2.33):

$$i = Q n_{carriers} * u = \sigma \xi \tag{2.33}$$

Where: A is the active area of FC, $n_{carriers}$ is the number of charge carriers, Q is the charge of the electrons (1.6×10^{-19}), u is the average drift velocity (cm s^{-1}) with which the charge carriers move, and ξ is the electric field.

The final equation for conductivity is:

$$\sigma = Qn_{carriers}\frac{v}{\xi} \tag{2.34}$$

The part $\frac{v}{\xi}$ in equation (2.34) is known as the mobility. Two main factors can characterise an equation for material conductivity in a specific way; these are:

1- The number of carriers available;
2- The mobility of those carriers in the material, which can be expressed as:

$$\sigma_i = (|s_i| * F) * d_i * u_i \tag{2.35}$$

Where: d_i is the number of moles of charge carriers per unit volume, u_i is the mobility of the charge carriers within the material, s_i is the charge number (electrons) for the carrier, and F: is Faraday's constant.

The reduction of FC resistance will lead to FC performance improvement, since the FC resistance changes with area. When studying Ohmic polarisation, it is essential to compare resistances on a per-area basis using the current density. Ohmic polarisation can be determined from current density using equation (2.36):

$$\eta_{ohm} = i(AS\ R_{ohmic}) = i(A * R_{ohmic}) \tag{2.36}$$

Where: $\mathrm{AS\ R_{ohmic}}$ is the area-specific resistance of the PEMFC.

Figure 2.6 illustrates the relationship between the Ohmic losses and cell area. The ohmic losses will increase be increase the cell area as noticed in figure 2.6.

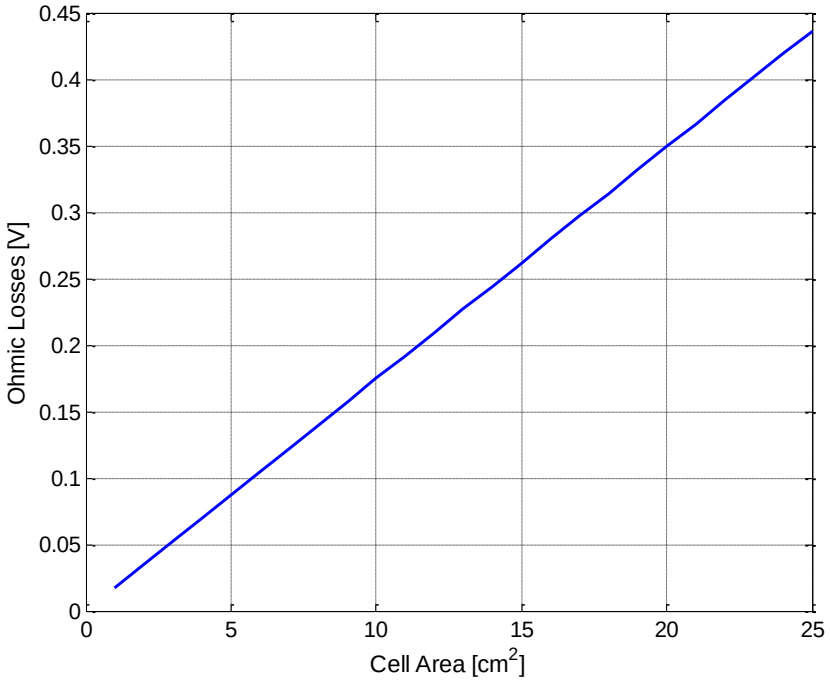

Figure 2.6: Ohmic losses as a function of fuel cell area.

The conduction mechanisms are different for ionic conduction versus electronic conduction. In a metallic conductor, valence electrons associated with the atoms of the metal become free to move around in the metal.

In a typical ionic conductor, the ions migrate from anode side to cathode side, hopping to ionic charge sites in the material. The number of charge carriers in an ionic conductor is much lower than in an electronic conductor. Electronic and ionic transportation are shown in figures 2.7 and 2.8 respectively.

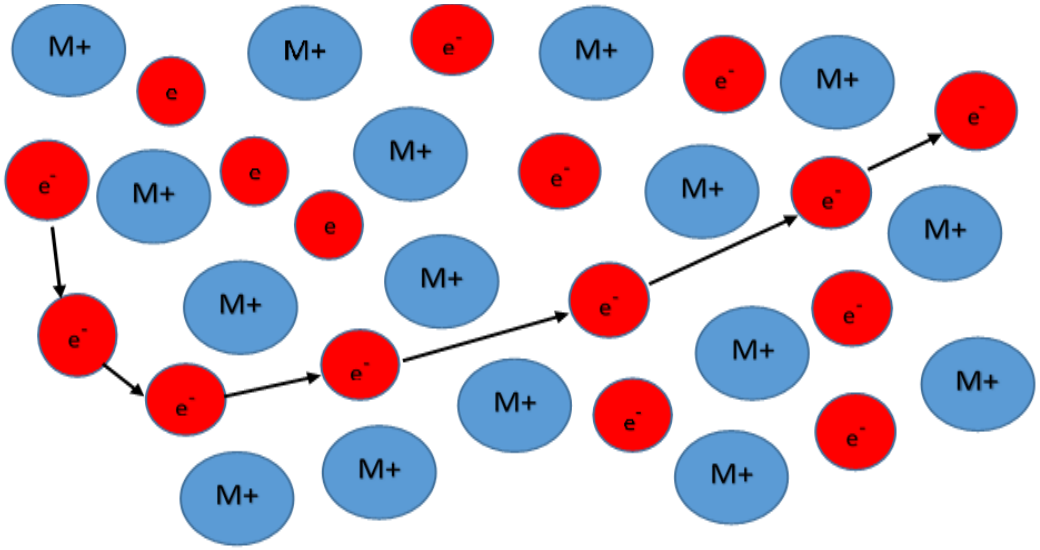

Figure 2.7: The transportation of electrons in a metal.

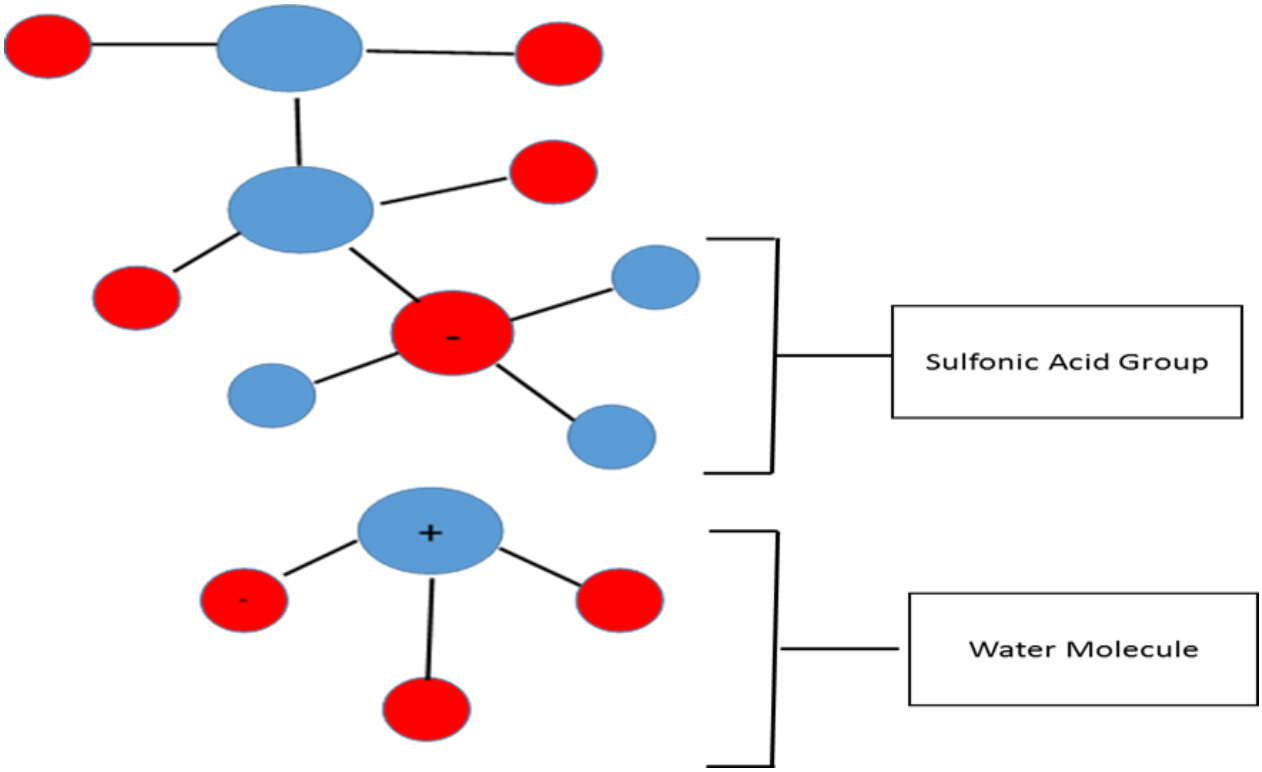

Figure 2.8: Ionic transportation in an electrolyte.

The losses from Ohmic contact can be reduced by either increasing the active area or decreasing the channels area. This will help to optimise the voltage and current and ultimately improve the performance and efficiency of the FC. The most effective way to reduce Ohmic loss is to use either a membrane that has high ionic conductivity, or a thinner membrane layer.

Thinner membranes are advantageous for PEMFCs because they guarantee the saturation of the anode through back diffusion of water molecules from the cathode side. For very high current densities (which means fast fluid flows of water), mass transportation causes a rapid drop-off in cell potential.

Hydrogen and oxygen are unable to diffuse through the electrodes and ionise quickly enough; therefore, products cannot move out at the necessary speed.

Ionic resistance in the electrolyte mainly causes Ohmic over-potential for the FC, and this can be expressed as:

$$\eta_{ohm} = iR_{internal} \quad = iA\left(\frac{\delta_{thick}}{\sigma A}\right) = \frac{\delta_{thick}}{\sigma} \tag{2.37}$$

Where: A is the active area of FC, $\boldsymbol{\delta_{thick}}$: thick is the thickness of the electrolyte layer, and $\boldsymbol{\sigma}$ is the conductivity of the electrolyte .

It is obvious from equation (2.37) and figures 2.9 and 2.10 that the Ohmic potential can be reduced by employing a thinner electrolyte layer, or a higher ionic conductivity electrolyte.

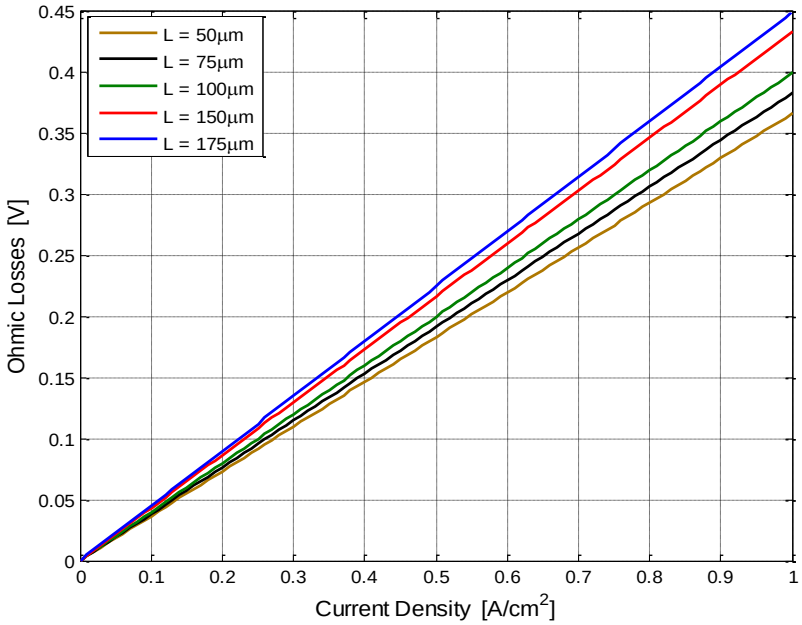

Figure 2.9: Ohmic losses as a function of membrane thickness [cm].

Figure 2.10 shows the local conductivity as a function of membrane thickness.

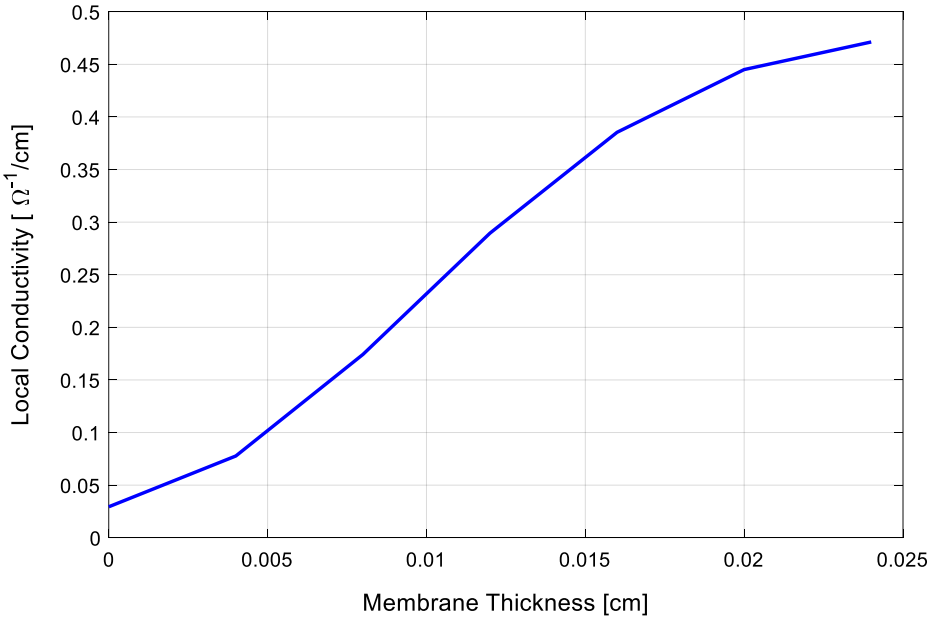

Figure 2.10: Membrane thickness and local conductivity.

The total Ohmic losses for the FC can be expressed as follows:

$$\eta_{ohm} = iA\sum R = IA\left[\frac{I_a}{\sigma_A A} + \frac{I_e}{\sigma_e A} + \frac{I_c}{\sigma_c A}\right] \quad (2.38)$$

Where: I is the thickness or length of the material.

The first term in equation (2.38) applies to the anode, the second to the membrane, and the third to the cathode. In the polar plates, the 'land area' can vary depending on the gas channel area. When the land area is reduced, the contact resistance increases accordingly, since the land area is the term in the denominator of the contact resistance.

2.4.3 Concentration Polarisation

The concentration polarisation , which also is known as "mass transport losses'', occurs when there is a change in the concentration of one of the gasses at the surface of the electrodes and this occurs when a chemical species contributes to the reaction (in a small amount) because of obstruction in the pathway of those species. This loss type is also known as concentration polarisation. This phenomenon is also known as "Nernstian" as it is related to the concentration effects modelled by the Nernst equation.

The reduction of concentration of reactants depends on the rate at which they are being consumed. This concentration reduction depends on the current drawn from the FC as well as on the physical characteristics of the system (Alrewq & Albarbar, 2016).

Obviously, these factors are dependent on the variation in pressures, concentrations of the gases and on the gas transportation rate (the rate at which gases move from the flow channel to the surface of the membrane through the catalyst layer and the GDL). The initial concentrations of the reactant gases, represented by their partial pressures, have an effect on the open circuit voltage. The pressure of the gases decreases in the FC while being consumed, until the point where the amount of reactant gases reaching the electrolyte is equal to the rate of their consumption. At this point, the partial pressure of the reactant gas equals zero. Therefore, it is not possible to increase the current output of the FC beyond this point, as it has reached its maximum current density. This density is termed the "limiting current density".

Since the pressure is assumed to have dropped to zero at the limiting current density linearly due to mass transport, the initial pressure at zero current was assumed zero as well. It can be seen from the similarity of triangles depicted in figure 2.11 that by substituting this value in the Nernst equation (2.17), which expresses the relationship between the voltage drop and partial pressures of the reactant gases, the following expression is obtained (Alrewq & Albarbar, 2016):

$$\eta_{conc} = -\frac{RT}{nF}\left\{1 - \frac{i}{i_o}\right\} \tag{2.39}$$

Where:

n :is the number of electrons migrated from anode side to the cathode side per molecule in the oxidation reaction, in the case of a hydrogen-oxygen FC n = 2 for hydrogen, and n = 4 for oxygen;

R: is the universal gas constant, which equals$(8.314\,\frac{\mathrm{KJ}}{\mathrm{k}}\,\mathrm{mole})$;

T: is the cell temperature of operation in Kelvin, and

F: is Faraday’ s constant, which equals 96485.33289 C/ mole.

This can be compared to equation (2.24) where:

$$\mathrm{b} = -\frac{\mathrm{RT}}{\alpha \mathrm{nF}} \tag{2.24}$$

Therefore, equation (2.38) can be written as:

$$\eta_{conc} = \alpha ln\left\{1 - \frac{i}{i_o}\right\} \tag{2.40}$$

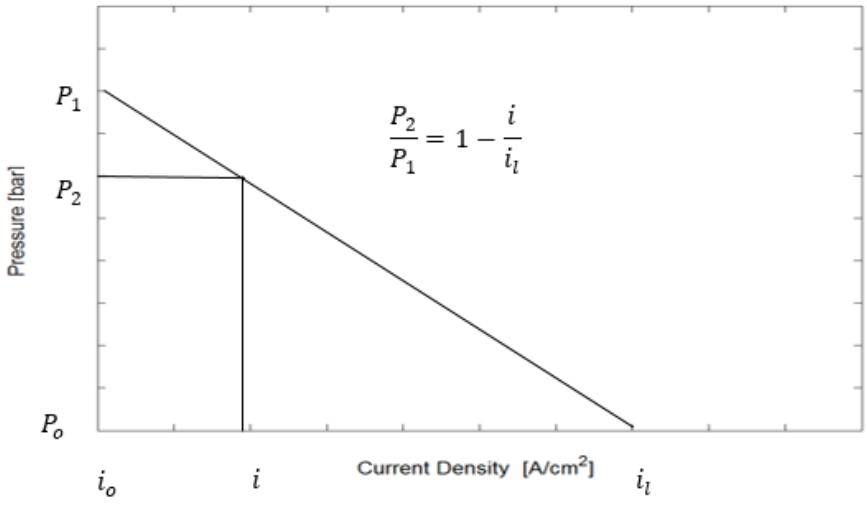

Figure 2.11: Assumed variation of current density with concentration pressure.

Equation(2.40) can be employed to characterise the concentration potential for H_2 and O_2 using appropriate values of 'n' at a temperature of 353K and charge transfer coefficient '$\alpha = 0.5$' (Kim *et al.*, 2011), the corresponding plots are depicted in figure 2.13, where the open circuit voltage is taken as 1 Volt.

In figure 2.13, the effect of the concentration polarisation is significant at the anode compared to the cathode. This is due to the significant speed of the reaction kinetics on the anode. Meanwhile, any effect that results in a delay to the reaction will be more noticeable on the anode. For "limiting current", it does not occur immediately and the curve decreases gradually at the anode side. Whereas, at the cathode side, the curve's drop-down is more gradual. Both curves drop down to the limiting current value simultaneously.

Therefore, the final drop at the cathode side is more rapid and it is not possible to draw more current from the FC beyond this point since this attempt will result in a sharp drop in cell voltage, which decreases the power output.

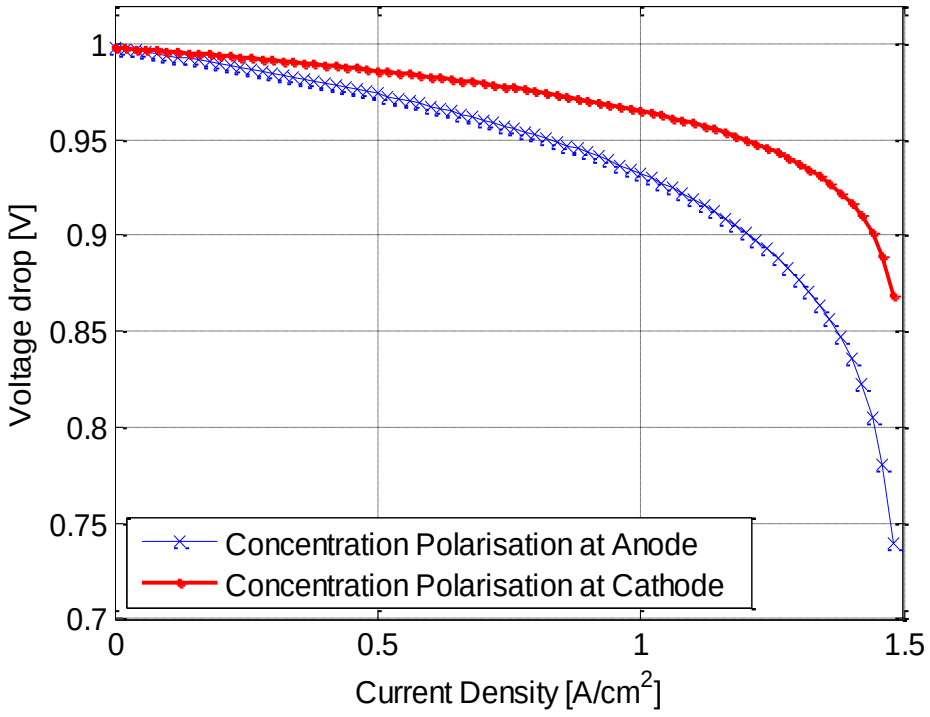

Figure 2.12: Concentration overvoltage at the anode and cathode at 353 K, open circuit voltage is taken as 1 volt.

Kim *et al.* (2011) presented different methods to model the concentration potential through the empirical equation based on experimental data and this equation is expressed as follows:

$$\eta_{conc} = Memexp(Gi) \tag{2.41}$$

The parameters 'm' and 'n' were not physically interpreted, however, the interpretation was made by Belvedere *et al*., 2013) that 'Mem' correlates to the membrane conductivity and 'G' to the porosity of the GDL.

Consequently, it can be concluded that both 'Mem' and 'G' relate to water management issues. The partially dehydrated membrane causes the decrease in conductivity and this can be represented by 'Mem', while the increase in liquid water in the cell will lead to a reduction in porosity and hence to an early onset of mass transport limitations, can be captured by the parameter 'G' (Berger, 1968; Wang, 2004).

It is noteworthy that the equation is derived based on curve fitting techniques and thus it can only be applied to the FC and operating parameters of the particular experiments carried out by the authors (Wandschneider *et al*., 2014).

Typical values for 'Mem'and 'G' parameters are $Mem = 2.11e^{-5}$ and $G = 0.008$, as recommended (Ercolino *et al*., 2015).

Another parameter that can be taken into consideration to minimise the concentration losses is the FC's geometry. This parameter helps in increasing the value of the limiting current and improving the range of operation of the FC. This can be achieved through reducing the pressure drop in the flow channels and increasing the active area of the membrane. Also, by improved water management which removes the water produced by the redaction reaction at the cathode side, in order to maintain access for the reactants to reach the active sites on the membrane.

2.4.4 Overall Voltage

The three kinds of overvoltage are Activation, Ohmic and Concentration incorporate throughout the operation modes of FCs. The effect of that overvoltage will cause the non-linearity of the performance curve of the FC which is also known as the polarisation curve, plotted with respect to the current required from the FC.

To visualise the combined effect of these losses, a general equation that expresses the summation of their basic equation captures the total impact of the losses. The basic equation (Adjemian *et al*., 2002; Raunija *et al*., 2016) is:

$$E = E_o - \eta_{act} - \eta_{ohm} - \eta_{con} \tag{2.42}$$

2.4.5 Notes and Observations on the Polarisation Curve

The following notes can be concluded from the graph:

1. Figure 2.3 presents the typical shape of the FC's performance curve. However, under practical conditions, some deviation from this shape is expected, due to the idealistic assumptions made during derivation of the equation and does not consider all the factors affecting the practical applications.
2. This study applies only to the changes in both pressure and temperature and their effect on the performance of the FC. However, these changes will also affect the conductivity of the various components, and the viscosity of the fluids. In addition, some parameters that were assumed to be constant, such as the specific heat at constant pressure, will also vary.

2.5 Efficiency of the Hydrogen Fuel Cell

Efficiency is a term that may refer to the process efficiency or the system efficiency. Process efficiency indicates how efficient a process in the system is performing. This definition does not express the total system efficiency, such as the combustion process in a heat engine which could reach 95% while the system efficiency is in the range of 28%. The efficiency of the thermodynamic process occurring in the FC is the theoretical maximum efficiency allowed by the second law of thermodynamics and can be written as:

$$\eta_{thermal} = \frac{\Delta G_T}{\Delta H^o} \tag{2.43}$$

Where $\Delta \mathrm{GT}$ is the Gibbs free energy at the cell operating at temperature T is $\Delta \mathrm{H}^{\mathrm{o}}$ is the reaction enthalpy at the standard temperature and pressure 101.3 Pa, 298 K.

For a PEMFC and other FCs that utilise hydrogen as fuel, it is vital to determine the proper value of enthalpy depending on the phase at which water is produced.

Higher heating value,(HHV) is used when the water product is liquid at 298K (25^0C) and lower heating value (LHV) is used when the water product is vapour at 423K (150^0C), due to the use of part of the enthalpy in converting water to vapour. It is noteworthy that in PEMFC, the water product is produced at 353K (80^0C), and the calorific value of the fuel should be between the lower and higher heating value, as indicated in the definitions of the heating values.

Table 2.3: Gibbs free energy, enthalpy, and calorific value for hydrogen.

Value	ΔG_T KJ/mole	ΔH^o KJ/mole	Calorific Value MJ/Kg
LHV	223	240.4	120.21
HHV	237.1	285.8	142.18
Interpolated value at 353K	230.5	264.6	132

From standard thermodynamic values, the values for the Gibbs free energy 'ΔG' for hydrogen and the enthalpy of the reaction 'ΔH' at 353K (80^0C) are approximated by linear interpolation, table 2.3. Applying equation (2.43) for thermal efficiency above, using the interpolated values at 353K from table 2.3, it follows that the maximum thermal efficiency is approximately equal to 0.87. Hence, from the equation of thermodynamic efficiency above, it can be concluded that:

$$\Delta G_T = 0.87 * \Delta H^o \tag{2.44}$$

Gibbs free energy expresses the maximum thermodynamic output possible in an electrochemical process. However, in real operation, the actual power output derived from the FC is:

$$P_{cell} = VI \tag{2.45}$$

Where fuel cell's current is equal to:

$$I = n * \bar{m} * F \tag{2.46}$$

Where:

$\bar{m}$: the molar flow rate of fuel,

n: the number of electrons transferred per molecule in the reaction.

To determine the FC's electrical efficiency, the actual output should be compared to the actual input, which is the total enthalpy of the reaction, hence:

$$\eta = \frac{Actual\ electrical\ output\ power}{\bar{m}\Delta H^o} = \frac{IV_{cell}}{\bar{m}\Delta H^o} \quad (2.47)$$

Hence, from equation (2.47) the value of ΔH^o can be re-written as below:

$$|\Delta H^o| = \frac{|\Delta G_T|}{0.87} = \frac{|-nFE_o|}{0.87} \quad (2.48)$$

Absolute numerical values are considered for efficiency calculation (since the negative sign indicates the direction of energy transfer). The substituting equations (2.47) and (2.48) in (2.49) yields the electrical efficiency of the PEMFC:

$$\eta_{ele} = 0.87\frac{V_{cell}}{E_0} \quad (2.49)$$

Where V_{cell} is the measured cell voltage; which is a function of current density, and E_0 is the reversible voltage of the cell.

The expression can be interpreted as the maximum theoretical efficiency multiplied by the electrical efficiency; i.e. (the $\eta = \eta_{thermal} * \eta_{ele}$).

Following the same lines, the electrical efficiency is the ratio of measured power output to the actual power input, which can be written as:

$$\eta_{ele} = \frac{iV_{cell}}{(i+i_{int})*E_o} \quad (2.50)$$

Where:

i: the current density,

i_{int}: the cross-over current which is assumed to be equal to the internal current (both currents are defining the input electrical power together with the theoretical reversible electrical potential of the PEMFC). The maximum fuel cell efficiency (thermal and electrical) can be found as below:

$$\eta_{FC} = \frac{0.87*iV_{cell}}{(i+i_{int})*E_o} \quad (2.51)$$

This relationship between the maximum fuel cell efficiency and current density is plotted in figure 2.13.

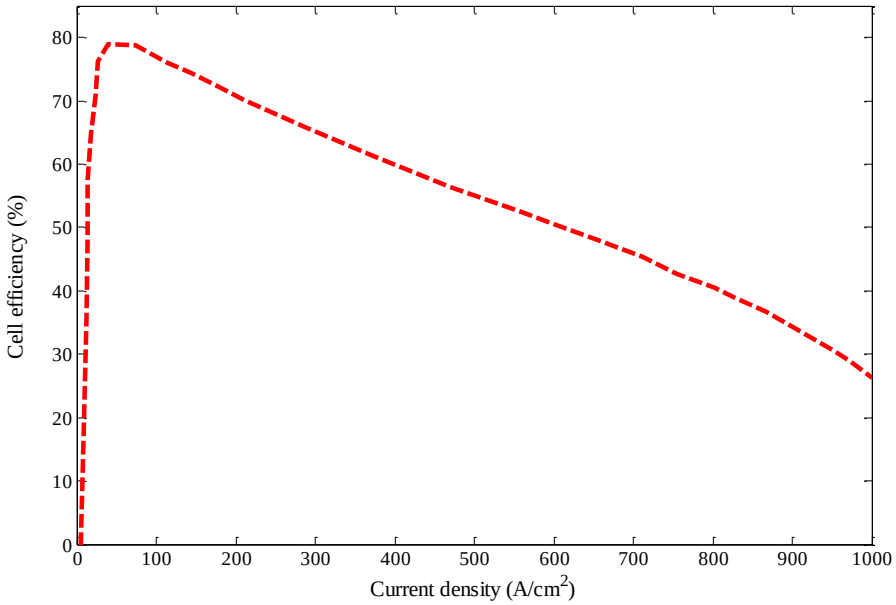

Figure 2.13: Efficiency as function of current density.

It is clear from figure 2.13 that the efficiency of the FC is higher at low fuel flow rates, which corresponds to low current densities. The efficiency curve has similar behaviour to that of the voltage curve. More effort is needed to improve FC voltage and to reduce voltage losses to enhance the performance of the FC.

According to the definition of efficiency in thermodynamics, another approach can be used to define the FC's efficiency, namely, by comparing the actual output with the input calorific value.

In this case, the system efficiency of the FC can be written as:

$$\eta_{FC}\% = \frac{V_{cell} * I}{mH_2 * Calorific\ value(LHV)} * 100 \tag{2.52}$$

Using the expression for current, for a hydrogen FC:

$$I = \frac{mH_2 * 2F}{MH_2} \tag{2.53}$$

Equation (2.53) can be rewritten after the compensation for the value of I as follows:

$$\eta_{FC}\% = \frac{V_{cell} * 2F}{MH_2 * Calorific\ value(LHV)} * 100 \tag{2.54}$$

By substituting the values for Faraday's constant, molar mass of hydrogen and the interpolated calorific value for hydrogen, the efficiency of the FC becomes:

$$\eta_{FC}\% = \frac{V_{cell}}{1.38} * 100 \tag{2.55}$$

Comparing the two expressions for efficiency as in equations (2.54) and (2.55), the theoretical open circuit voltage of a pure hydrogen FC can be found as follows:

$$\eta_{FC}\% = \frac{V_{cell}}{1.38} = 0.87 \frac{V_{cell}}{E_o} \tag{2.56}$$

Therefore, the reversible voltage of the FC if the water product is steam at 80^0 is:

$$E_o = 0.87 * 1.38 = 1.2006\, V \tag{2.57}$$

This value is almost equal to the value of the potential of equilibrium for hydrogen FCs which is 1.229 V, and this proves the above method for calculating the efficiency of the FC.

2.5.1 Fuel Utilization Efficiency

There is a significant issue in FCs which is the venting of the fuel out of the cell. However, this issue can be overcome by operating the FC dead ended or in the case where the excess fuel is recalculated or used in another process. In this way, the fuel is utilised properly.

The final efficiency of the FC has to be multiplied by the fuel utilisation value to calculate the exact efficiency of the FC. By assuming fuel utilisation efficiency was given the term 'ψ', the above expression of efficiency equation (2.51) becomes:

$$\eta = \psi * \frac{iV_{cell}}{(i+i_{int})*E_o} \tag{2.58}$$

2.6 Summary

The main features and functionality of PEMFCs have been presented starting with the contents and basic components of FCs and the fundamentals of PEMFCs. A thermodynamic investigation followed to establish the relationship between current and voltage and their relationship with other operations, such as pressure,

temperature, exchange current density, charge transfer coefficient and gas concentrations in the FC. The analysis based on the polytrophic index is used to study the effects of pressure and temperature on FC performance, which shows the effects of irreversibility on output voltage of the FC.

A comprehensive study and analysis of the FC takes into consideration the actual operating conditions, internal currents, fuel utilisation efficiency and thermal and electrical efficiencies that involve expressions for the efficiency of the FC, and the formula for FC efficiency is derived and employed to plot the complete curve of efficiency against current density.

All derived equations can be utilised in performing parametric studies on FC performance.

The graphical representations of the solutions of the derived equations would help in finding the optimum combination of the design variables for changing operating conditions. They can also be employed in making a more complex numerical model of the system which can be resolved using computational methods to simulate the FC performance and then finding opportunities for optimisation.

The knowledge and findings acquired in this study will be useful in understanding the parameters that have an influence on PEMFCs and formulating the mathematical model, which will be used to study the performance and efficiency issues of FCs.

CHAPTER 3

LITERATURE REVIEW

In this chapter, studies made by current academic and industrial researchers on the performance and efficiency of PEMFCs have been summarised. It includes the operating conditions of fuel cells operating at steady state or accelerated conditions.

3.1 Overview

A considerable body of research work has been carried out to develop highly efficient and reliable single PEMFCs and stacks to be utilised in various applications such as portable devices e.g. as a power source, stationary and automotive applications. Significant development has been achieved recently, especially in materials and the level of increased current density, which will eventually lead to increasing the power density and make FCs more efficient and reliable. It was expected that proton exchange membrane fuel cells (PEMFCs) would be commercialised static applications by 2001 and in transport applications in 2003 (James and Spisak, 2012; Fecarotti *et al*., 2016; Robin *et al*., 2016). However, some of the technical challenges remain as obstacles to achieving this target, especially concerning the infrastructure and storage of hydrogen fuel (HF) in addition to the FC systems. One of the major issues of the FC system is the high cost of the FC itself. Other technical barriers to adopting FC technology in practical power source applications are the performance, reliability, and durability under different operating conditions. The requirements for FC lifetime vary significantly, per the nature of the application, ranging from 5,000 hrs for cars to 20,000 hrs for buses and 40,000 hrs for static applications with continuous operation. Despite the target age for FCs, in the transport sector these are much lower than for static applications, the operating conditions such as the operations of start-up and shut-down, dynamic load including load cycling, and freeze/thaw make this target very challenging for current FC technologies.

Fabrication and assembly of FCs, as well as the operational conditions, control strategies, degradation of materials, impurities and contaminants are the major concerns that must be considered when evaluating both the performance and reliability of FCs.

Although it is impossible to avoid degradation of performance and reliability, it is possible to reduce degradation rates by a comprehensive and sufficient understanding of degradation and failure mechanisms. Some related terms and definitions will be clarified first in order to visibly understand the concepts of PEMFCs' performance deterioration and lifetime:

- Reliability: the capability of FCs to accomplish the required functions while working under normal operating conditions within the defined run- time. That covers the failure modes, which cause a major reliability issue and performance under the acceptable level.
- Durability: the capability of a FC to resist performance degradation over time. Degradation in durability leads to an unrecoverable failure. This accountability is closely linked to the operational cell's age.
- Stability: the capability of a FC to recover loss of energy while the cell is in operating. Stability decay is closely associated with the operating conditions of the FCs, such as poor water and heat management.

The reliability and performance of a FC's overall deterioration rate is usually measured when the cell is operating in a continuous condition without any interruption for a specific time. Performance of the FC can be expressed as the sum of the durability and stability decay rates.

Throughout this chapter, studies made by academic and industrial researchers on the performance, efficiency, and reliability for PEMFCs have been summarised. It includes the operating conditions of a FC operating at steady state or accelerated conditions. Steady state and accelerated conditions include air and/or fuel starvation load or thermal cycles.

3.2 Lifetime Tests for Proton Exchange Membrane Fuel Cells

Several studies have been conducted to understand the mechanics of the deterioration of PEMFC components such as membranes, catalyst layers (CLs), bipolar plates (Bps), gas channels (GLs) and gas diffusion layers (GDLs). However, only a few studies have focused on real PEMFC reliability and lifetime due to several reasons such as high cost of the tests as well as long test periods. For instance, approximately 4.5 years of uninterrupted testing are needed for a PEMFC system for stationary applications and it costs around US $2 million to test a FC bus system (Zhou *et al*., 2010).

Increasing the sample productivity and reducing the testing time required are the targets of many FC designers and companies, such as General Motors, Gore, DuPont, and Ballard Power Systems. To achieve this goal, various accelerated stress tests (ASTs) have been suggested and carried out to set the reliability, durability, and performance of present FC components.

Most the experiments on FC lifetime under steady state conditions were conducted for much less than 4,000 hrs (despite demonstrating a degradation rate of between 2 -10 μVh^{-1}).

To commercialise FCs, the degradation rate must be less than 10 μVh^{-1}. If the cell degradation rate exceeds this value (10μVh^{-1}), additional investigations on the components as well as the failure modes system are required (De &Janssen., 2008).

3.3 A review of Performance Degradation and Common Failure Modes

The faults that occur inside proton exchange membrane fuel cells (PEMFCs) are many, ranging from chemical faults, electrochemical, electrical, and mechanical faults. This chapter covers the faults that have significant impact on the performance and reliability of PEMFCs.

3.3.1 Membrane Degradation

The membrane (electrolyte) is one of the essential and expensive components in PEMFCs. In typical PEMFCs, the membrane is placed between two catalyst layers of electrodes. The membrane achieves several functions such as allowing the proton to pass from negative electrode (anode) to positive electrode (cathode), supporting the CLs for both electrodes, and more significantly, separation of oxidising gases at the anode and reducing gases at the cathode.

A set of characteristics must be contained in the membrane to ensure the achievement of all the functions such as stability of thermal, high ionic conductivity, and chemical and flow reactant gas permeability (Devanthan, 2013; Subianto, *et al.,* 2013; Scott, *et al.*, 2014). Nafion® (Dupont TM), Aciplex®, Flemion® (Asahi TM) and Gore-Select® (Gore TM) membranes are most commonly used in PEMFCs. Several studies have been conducted on the operation/mechanism of the

membranes' decay and failure in the FCs. There are three main issues related to PEMFCs, which are still under investigation, namely: performance, reliability, efficiency and durability of the polymer exchange membrane (PEM).

3.3.1.1 Mechanisms of Membrane Degradation

It has been established that the rates of air and hydrogen that travel through both sides of the proton exchange membrane (PEM) are comparatively slow. The slow rates result in a loss of FC efficiency of only (1–3) percentage (Tang *et al* 2006; Cheng *et al,* 2007) but ,in spite of this, the above-mentioned extremely exothermal combustion of H_2 and O_2 can probably cause pinholes in the membrane, causing disastrous problems and leading to damage of the membrane electrode assembly (MEA). Under severe conditions, the chemical reaction taking place at the catalyst layers of both electrodes can produce hydro-peroxide (HOO•) and peroxide (HO•) radicals, which are generally considered as the cause of chemical damage to the membrane and catalysts On further analysis, it was discovered that the rate of production of these radical (Gubler & Scherer, 2009; Young *et al*., 2010; Gittleman, 2011) and the resulting chemical destruction of the membrane become more accelerated at low humidity rates and at open circuit voltage (O.C.) (Wang *et al*., 2009).

Several procedures have been suggested, which provide contrasting theories on whether the radicals are produced at the cathode, at the anode, or on either side of the membrane. A few studies indicate that the ionic groups' loss starts on the negative side of the membrane and eventually advances towards the positive side (Young, 2010; Carmo *et al*., 2013). However, Zhou *et al*. (2014) and many other researchers (Tang *et al*., 2007; Chandan *et al*., 2013) have substantiated the occurrence of predominant cathode degradation. On the other hand, Subban *et al*. (2010) found no noticeable difference between the negative side and the positive side of the membrane. Foreign cationic ions, if present, can drastically reduce the FC performance by adsorption on the CLs and/or membrane.

The potential sources of multi-valent ion contaminants are many, such as impurities in the air stream and corrosion of FC stack components, humidifier reservoirs, etc. (Wu *et al*., 2008). A stronger affinity than H^+ was exhibited by many cations towards

the sulfonic acid group in perfluorinated sulfonic acid (PFSA) membranes (Kratysberg & Ein-Eli, 2014; Abdo & Easton, 2016).

A greater number of active sites were filled by the multi-valent ions during the operation of the FC. As a result, the major membrane features, such as water molecules, H^+ transference numbers, changed in proportion to the charge of cation ionic, and membrane ionic conductivity (Okada *et al*., 1998). This impact under normal conditions is not severe, unless the concentration of contamination exceeds 50% of the sulfonic acid sets in the PEM (Ganes *et al*., 2007).

The other probable mode of PEM degradation, because of contaminated ions, is caused by the changed water flux inside the membrane, and just 5% contamination is adequate for damage to take place.

The proton conductivity and attenuation of water flux are also caused by the movement of H^+ with foreign cations, which in turn result in much more rapid and extensive membrane drying, particularly near the negative electrode (Gubler *et al*., 2009; Gittleman *et al*., 2011].

Trace metal ions are produced because of the corrosion of metal bipolar plates (Bps) or end of plates. Trace metal ions include, $Cu^{2+}$and Fe^{2+}, which can result in contamination and strongly hasten the membrane thinning process and performance degradation of PEMFC by catalysing the reactions of the radicals' formation, as expressed in the equations below (Inaba *et al*., 2006):

$$H_2O_2 + Fe^{2+} \rightarrow HO^{\bullet} + HO^- + Fe^{3+} \quad (3.1)$$

$$Fe^{2+} + HO^{\bullet} \rightarrow Fe^{3+} + HO^- \quad (3.2)$$

$$H_2O_2 + HO^{\bullet} \rightarrow HO^{\bullet}{}_2 + H_2 \quad (3.3)$$

$$Fe^{2+} + HO_2{\bullet} \rightarrow Fe^{2+} + H^+ + O_2 \quad (3.4)$$

As discussed, this mechanism could result in the occurrence of pinholes or thinning in the membrane, and subsequently cause an irreversible failure of the PEMFC. Based on the kind of the membrane, the HOO• and HO• radicals produced during the reaction can displace the aromatic group in carbon, such as the branching points of the electrolyte (polymer), or ether links. On the other hand, some H-containing terminal bonds with carboxylate end-groups, are inexorably created during the production process of the polymer, and are considered to be the inducing agent for

the chemical degradation of PFSA membranes that have high susceptibility to radical attacks. The unzipping reaction is a commonly accepted procedure that initiates the releasing of hydrogen from the end-groups, free hydrogen fluoride (FHF) and carbon dioxide (CO_2), and creates new carboxylate groups at the chain ends (Rowshanzamir *et al*., 2015).

The radical attack might circulate along the main chain as the process repeats, and ultimately lead to the decomposition of the polymer into low-molecular weight compounds. Jeon *et al*. (2016) suggested another probable mechanism which is the separation of the main chains of the polymer, where the ether linkages are considered to be the most-targeted side-chain sites for attack by radicals, generating vulnerable –COOH groups. Consequently, the number of –COOH groups increases, while the average molecular weight of the polymers decreased together with time. Even in the absence of susceptible end-groups, the polymer chain of the PFSA membrane might selectively interact under exposure to H_2.

3.3.1.2 Mitigation Techniques for Membrane Degradation

To avoid or mitigate the mechanical failure of the proton exchange membrane (PEM), the membrane electrode assembly (MEA) and flow field structure of the cell should be carefully designed. In addition, preventing the hydration levels of the membrane to lower than the allowable limit is essential, specifically at the reactant inlet area. Gore FC Technologies developed a PEM reinforced with e-PTFE, which demonstrated a lifetime much longer than a non-reinforced PEM of relative thickness. Koh *et al*. (2007) reported similar results for a PEM with enhanced mechanical strength through the use of “Nafion®–Teflon®–phosphotungstic acid’’ composite membranes and reinforced Aciplex® membranes, respectively.

The contemporary membrane development and fabrication methodologies that intend to attain prolonged durability above 100ºC have been covered in numerous review papers (Viestich *et al*., 2009; Zhang and Shen, 2012; Dubau *et al*., 2014).

The membranes formed so far can be categorised into three groups: (1) acid–based PEMs, such as phosphoric acid-doped Nafion®–PBI complex membranes; (2) modified PFSA membranes, which incorporate hydrophilic oxides and solid

inorganic proton conductors; and (3) complex membranes, such as PVDF, PBI and SPSF, which are made from alternative sulphonated polymers.

Regarding the membrane chemical and electrochemical decomposition, the development of chemically stable membranes against proxy radicals, has gained significant awareness from researchers. One way to solve this is to develop new membranes that have high chemical stability. For example, because of its low resistance to radicals, the radiation-grafted FEP-g-polystyrene membrane is utilised as a sacrificial material (Dubau *et al*., 2014; Jeon *et al*., 2015).

During membrane fabrication, free-radical inhibitors, as well as stabilisers such as anti-oxidants or hindered amines, can be mixed with the membrane through the modification of its structure. The chemical stability of the membrane was remarkably augmented (Peighambardoust *et al*., 2010; Rowshanzamir *et al*., 2015) by excluding the unstable end-group. In addition, by re-designing the MEA, the chemical damage that can occur due to hydrogen peroxide can be diminished. For example, (Jouin et al. 2013), proposed a complex membrane where a thin modified Nafion membrane was bonded with a membrane of PSSA, and when it was fixed at the positive electrode of the FC, the degradation of the PSSA membrane that occurred due to oxidation might successfully be avoided.

The addition of peroxide-decomposition catalysts such as heteropoly acids within the membrane has led to the moderation or elimination of membrane degradation because of exposure to peroxide. However, the benefit of this mechanism would be partially countered by a reduction in membrane stability and conductivity resulting from the blending of the catalysts. Lastly, the long-term target is to enhance the durability of the membrane, which can be achieved by development, improvement and application of new metal coatings that enhance the ability of the membrane to resist corrosion, and to use catalysts that produce less hydrogen peroxide.

3.3.2 Degradation of Catalyst Layers and Electro-Catalysts

The electro-catalysts in PEMFCs that have been proposed and applied include ternary-Pt, binary-Pt and quaternary Pt-transition metal alloys, on conductive supports. The supports that are generally used include high-surface-area carbon materials, such as Black pearls BP2000, Ketjen black, or Vulcan-XC 72. In theory,

these catalysts can meet the cost requirements and performance expectations of high-volume FC applications. However, when catalyst durability is considered, the performance and reliability of the presently identified materials is still sub-standard under a severe operating environment, such as high humidity, dynamic loads or low pH values, in combination with an oxidising or reducing environment, and elevated temperature.

3.3.2.1 Mechanisms of Catalyst Layer Degradation

Significant efforts have been made to examine in detail the process of Platinum (Pt) catalyst degradation in a hard environment and under long-term operation. Initially, a pure Pt catalyst might be exposed to the impure by impurities obtained from the FC system or supply reactants, (Xin et al., 2011). Moreover, there is a possibility that the catalyst may become non-active to migration or sintering of Pt particles on the carbon support, corrosion of the carbon support, detachment, and dissolution of Pt into the membrane. Several techniques have been suggested to demonstrate the factors and operating conditions of FC which contribute to coarsening and the size of the catalyst particle:

(1) small Pt particles may dissolve in the ionomer phase and be deposited again on the surface of large particles, causing the particle to grow, a phenomenon known as Ostwald ripening (Nakagawa *et al*., 2010). On the contrary, the dissolved Pt species may diffuse into the ionomer phase and eventually precipitate in the membrane through reduction of Pt ions by the crossover hydrogen from the anode side, drastically reducing the membrane conductivity and stability;

(2) As a result of random cluster–cluster collisions, the agglomeration of Pt particles on the carbon support may take place at the nanometre scale causing a typical log-normal distribution of particle sizes with a maximum at smaller particle sizes and a tail towards the larger particle sizes;

(3) By the minimisation of the clusters' Gibbs free energy, the catalyst particles may grow according to the atomic scale. Here, the distribution of the particle size can be characterised/identified by a tail where the particle size is small and a maximum at the larger particle sizes Xin et al., 2011).

To date, no agreement has been achieved on identifying the mechanism that governs and is principally responsible for the catalyst particle growth. Coalescence on the carbon support and coarsening of the catalyst because of movement of particles can cause the catalytically active surface area (ASE) to reduce. Lastly, there is probably an increase in particle sizes that leads to the reduction in catalyst activity due to the development of metal oxides at the anode or cathode side.

Another significant matter related to CL and electro-catalysts' performance and reliability, which has been the subject of considerable attention lately for both academic and industry research, is the catalyst carbon support corrosion (Meier *et al*., 2012). Both modes are considered to induce carbon corrosion in PEMFCs and stacks: (1) starvation of fuel because of H_2 obstruction from a section of the anode under steady-state conditions, and (2) transitioning between start-up and shut-down cycles.

The first mode, which is starvation of fuel in individual fuel cells, may arise from imbalanced flow-sharing between one cell and other cells during high complete stack application or from gas flow obstruction ascribed to ice formation when FCs work in sub-zero temperatures. The second mode, denoted as the air-fuel front, can result from non-uniform allocation of fuel on the anode and the probable crossover of oxygen through the membrane during start-up and shut-down of the PEMFC. In either of the cases, the anode electrode is moderately covered with hydrogen. Under the conditions of hydrogen exhaustion, the anode voltage is driven to negative until water and carbon oxidation occurs.

Despite the thermodynamic variability, carbon corrosion in a typical PEMFC is insignificant at voltages less than 1.1V compared to reversible hydrogen electrodes because of slow kinetics. Recent experiments have validated that the occurrence of Pt/C or PtRu/C electro-catalysts can contribute to hasten carbon corrosion and decrease the voltage for carbon oxidation to lower than, or equal to, 0.55V vs RHE) (Inaba *et al*., 2006; Yuan *et al*., 201l).

Carbon, in general, is protected from corrosion by the process of water oxidation when there is adequate water in the FC, unless the water in the electrodes is exhausted or the cell is exposed to a high current density not supportable by water oxidation alone. There is a potential that cell reversal, because of fuel starvation,

can affect the durability of the GDL, the Bp, or the CL. As an outcome, the comparative percentage of conductive material in the electrodes may decrease, while the internal resistance of the cell, and the contact resistance with the current collector, may eventually increase. Under acute conditions, the availability of the number of sites for anchoring the catalyst reduces with carbon corrosion, resulting in catalyst metal sintering (Pedersen *et al*., 2015), and in severe cases, a disintegration of the electrodes structure. At sub-zero temperatures, there is another significant hazard to PEM FC durability, which is the impact of volume changes of water and phase transformation on the physical characteristics of the PEM, and on the electrode's interface and structure. It was observed by Schmittinger & Vahidi, 2008 that there is a decline in performance at a rate of about 2.3% per freeze–thaw cycle from −10 to 80^{o} C. The physical damage of the electrode's structure and MEA integrity caused by ice expansion during freezing is often considered to be a factor behind the degradation in cell performance observed in thermal cycles. Kusoglu *et al*. (2006) presented analytical formulae that validated the impact of temperature cycling between −40 and 80^{o} C on the ionic conductivity, membrane structure, mechanical strength, water management, and gas permeability. A comprehensive synopsis of the research on PEMFC freeze and rapid start-up has been provided by Xie *et al*. (2005).

Their experimental results showed the variation in hydrophobic properties of the CLs that take place eventually because of the dissolution of PTFE or Nafion, which adversely impacts the mass transport potential of the ions and water management.

3.3.2.2 Mitigation Techniques for Electro-Catalyst and Catalyst Layers' Degradation

Several strategies have been suggested by recent researchers which have been successfully implemented to augment the durability of the catalyst. To begin with, FC operating environments have a significant role to play in the process of catalyst degradation. The Pt catalysts are more stable at the anode side than those at the cathode side, as the dissolution of Pt from the carbon support is less favourable at low electrode potentials. The experimental results obtained by Zarrin *et al*. (2011) indicate that the loss or reduced active surface areas of Pt that are linked with an

increase in testing time, can be remarkably reduced by making FCs operate at low relative temperature and low RH. Borup *et al*. (2007) discovered that the carbon corrosion of the CLs increases with a decrease in RH. It was further found that the increase in cathode Pt particle size was significantly less during steady-state testing than during potential-cycling experiments. The Pt particle size increased with an increase in voltage, which was validated during the recent application of an AST method to analyse the stability of the electro-catalyst. Then, by improving the water retention on the anode, the corrosion of the carbon support, as a result of fuel starvation, can be lessened through the addition of water-blocking components such as graphite, modifications to the PTFE and/or ionomer, and the use of improved catalysts for water electrolysis, as explained by Lohoff, *et al*. (2016). Based on whether the system uses extra power when starting-up or parking, two principal strategies have been suggested to mitigate FC performance degradation with respect to PEMFC rapid start-up and freeze issues.

The “keep-warm” technique (Assarabowski *et al*., 2004; Alink *et al*., 2008; Jung and Um, 2011), which is the first solution, is based on consuming energy from an intermittent or continuous low power source (from a hydrogen fuel converter or an extra battery) to ensure that the temperature of the system is above a particular threshold when the system is in a non-operational state. The second solution is to increase the temperature of the FC system to ensure that the water temperature inside the FC is above freezing point when the FC starts up. As a higher energy temperature is required for this solution, it is highly recommended that the technique be combined with efficient elimination of residual water to alleviate any of the physical damage to the MEA due to ice expansion, and to enable energy saving. Gas disinfection or washing with an anti-freeze solution before stopping the FC, are some feasible techniques to get rid of the water. Third, compared to pure Pt catalysts and Pt-alloy catalysts, for example Pt–Cr–Ni and PtCo have exhibited good stability and activity.

The improvement observed may be attributed to an increased sintering resistance due to the large size of the alloy particles or the alloying elements. In spite of this, X-ray diffraction analysis has detected a skin that constitutes a monolayer of pure Pt formed on the surface of the alloys after long-term testing (Shao *et al*., 2006a; Shao *et al*., 2010). This implies that the non-noble metals present in the Pt-transition

metal alloy catalysts are more pre-disposed to being dissolved in the ionomer phase, and thus the benefit of Pt-alloy catalysts is partly neutralised. Cr, Co, Ni, V, and Fe are some metals that are verified as being capable of dissolution in a FC operating environment. On the other hand, Pt–Co/C has gained a lot of attention lately because of its enhanced stability, in comparison to that of the other Pt-transition alloy catalysts (Jia et *al*., 2016). It is worth mentioning that recently Adzic et al., (2007) considerably augmented the stability of Pt against dissolution under prospective cycling regimes by using gold (Au) clusters to alter the Pt nanoparticles. Under oxidising environments and prospective cycling between 0.6 and 1.1V after over 30,000 cycles, no noticeable changes were observed in the activity and surface area of Au-altered Pt nanoparticles. The significant enhancement in the stability of the Au/Pt/C catalyst was primarily due to the occurrence of insoluble Au clusters. The sintering and dissolution potential of the metal alloy catalysts can be improved by reinforcing the interaction between the carbon support and the metal particles. As an example, Maiyalagan *et al*., (2008) proposed and initiated a nitrogen-based carbon functionality to the carbon support surface through chemical alteration and, thus, a considerable improvement was noted in the ability of the treated support to anchor metal particles as well as in its catalyst activity. In PEMFC applications, multi-walled carbon nanotubes (CNTs) have also exhibited the potential of catalyst supports. Shao *et al*., (2015), in a recent publication, mentioned that under the same conditions of the accelerated durability test, the rate of degradation of Pt/CNTs was almost two times lower than that of Pt/C. This phenomenon was ascribed to the distinctive interaction between CNTs and Pt, and to the increased resistance of the CNTs to the oxidation reactions. Moreover, the reduction in support surface area or graphitisation of the carbon support can increase the support's resistance to oxidation and carbon corrosion. In spite of this, the number of active surface sites that anchor the metal particles correspondingly reduces, which is possibly detrimental to the accumulation of metal on the carbon support.

3.3.3 Gas Diffusion Layers

3.3.3.1 Degradation Mechanism of Gas Diffusion Layers

In general, the gas diffusion layers (GDLs) are a carbon-based dual-layer made up of porous material, which consists of carbon cloth substrate or microporous carbon fibre paper protected by a thinner microporous layer consisting of a hydrophobic agent and carbon black powder. In earlier research of GDLs, the focus was on the effect of GDL design and materials on PEMFC performance, instead of durability. Nevertheless, after 11,000 hrs of operation and cold-start conditions (Meng, 2008), augmented GDL surface hydrophilicity has evidently been observed and implies with certainty that further investigation of the GDL is necessary. So far, only a few studies have concentrated on the correlation between GDL properties and FC performance decay, or the degradation mechanisms of GDLs. To sum up, these studies have primarily used *ex-situ* GDL aging methodologies to escape the potential confounding effects from the adjacent elements such as the bipolar plate (Bp) and the CL.

The results of the experiments of Yang *et al*., (2015) indicate that the loss of GDL hydrophobicity improves with operating temperature and with the use of air sparging in place of nitrogen. Moreover, the conclusion was reached that alterations in the GDL characteristics were ascribed typically to the micro-porous layer. Tanuma *et al*. (2011) made the GDLs grow by immersing the samples in 15wt percentage hydrogen peroxide at 82ºC. With this experiment, it was discovered that the greater the time of exposure, the greater was the weight loss and the MPL contact angle and the increase was accredited to oxidation of the carbon in the micro-porous layer. Kangasniemi *et al*. (2004) explained the impact of electrochemical surface oxidation on the GDL characteristics and discovered that the contact angle of the micro-porous layer surface reduced significantly with time when the GDL samples were submerged in 1M H_2SO_4 under potentiostatic treatment of 1.2V vs. the standard hydrogen electrode (SHE). More recently, Oberholzer *et al*.,(2011) researched the GDL characteristics in depth, which included bending stiffness, electrical resistivity, surface contact angle, air permeability, water vapour diffusion, porosity, and after degradation tests at steady-state conditions (over 1,500 hrs having time at 80ºC and 13.6 atm) and freezing (54 freeze/thaw cycles between −35 to 20ºC) conditions.

The carbon composite and PTFE of the GDLs are pre-disposed to electrochemical (voltage) oxidation and chemical attack (that is, OH• radicals as electrochemical by-products), during the FC operation. With the loss of carbon and PTFE, alterations are observed in the physical characteristics of GDL changes, such as there is a reduction in the GDL conductivity and hydrophobicity, which further decrease the MEA performance and negatively impact the durability of the complete (or overall) FC. With respect to the quantitative relationship between the changes in GDL characteristics and performance loss, Lim *et al*.,(2014) recently discovered that the decay of PTFE in both the electrodes induced a two times higher performance loss (approximately) compared to that of the clustering of the Pt catalysts after 1,000 hrs of FC operation. Then again, the impact of PTFE degradation on the GDL and CLs was not individually analysed in their paper and the disintegration mechanism of PTFE was not discussed in detail.

3.3.3.2 Mitigation Techniques for Gas Diffusion Layer Degradation

To the best of the author's knowledge, the literature provides no information about mitigating GDL degradation. To enhance the electro-oxidative and stability of the GDL, Borup et al., (2007) proposed the use of graphitised fibres during GDL preparation. Borup further suggested that higher PTFE loading may prove to be advantageous to the water management potential of aged GDLs. Ha *et al*. (2011) found a 25% increase in the start/stop degradation rate at $1.2\ (A/cm^2)$ by incorporating graphitised carbon material Pureblack® in the MPL.

3.3.4 Bipolar Plate

3.3.4.1 Degradation Mechanisms of Bipolar Plate

The bipolar plate (Bp) that functions as a separator between the coolant hydrogen and air is a multi-functional component of the FC system, which consistently distributes the reactants and produces streams, providing a path to current that is produced during the electrochemical reactions. A significant amount of research has been made on the Bp component and several literature reviews (Iranzo *et al.*, 2010; Karimi *et.al*., 2012; Taherian, 2014) have also been published. Several characteristics are required for the materials to be suitable for the Bp component so

that all the necessary functions are accomplished. These characteristics include, but are not restricted to, low gas permeability, high ionic and protonic conductivity, sufficient strength, low thermal resistance, high resistance to corrosion, and reasonable manufacturing costs. At present, researchers are evaluating many materials such as polymer-based composites with conductive carbon/graphite fillers and graphite (Hu *et al*., 2014).

The combination of high thermal and electrical conductivity, high current density, and high corrosion and chemical resistance are advantageous properties of graphite and graphite composites. In spite of that, their permeability to hydrogen, manufacturability, durability under shock and vibration are detrimental in comparison to metals. To overcome these inadequacies, the volume and weight of electrodes should be increased. Common metals used with Bps are Nb, Pt, Zr, and Ta. These noble metals are extremely resistant to corrosion and can be produced into lightweight thin Bps, however, the raw material overheads for these Bps forbid their use in commercial applications. Commercially obtainable metals and their alloys such as Ni, Al, and Ti have shown strong potential for their use in Bps due to their good mechanical characteristics, high electrical conductivity, and low cost. Nevertheless, these metallic Bps pose a significant challenge because of their contact resistance between the Bp and the GDL, which is ascribed to the formation of electrically resistant oxide films on the surfaces that unavoidably increase the FC's internal electrical resistance. For researchers, stainless steel has been the focus of significant attention because of its extensive range of alloy selections and applicability to mass production. However, stainless steel is susceptible to corrosion in aggressive humid and acidic environments inside a PEMFC (Antunes *et al*., 2010), which further increases the contact resistance. In addition, metallic materials undergo corrosion to produce multi-valent cations, which may completely affect the membrane and catalyst durability (Hu *et al*., 2014). After 100 hrs of cell operation, the MEA chemical analysis showed that untreated stainless steel 316L (Gabreab *et al*., 2014) discharged large amounts of Ni and Fe atoms, and traces of Cr. As a result, the corrosion of this Bps material led to an electrical potential drop of up to 300 mV at a measured current of 700 mA/cm^2. Brady *et al*. (2013) conducted an *ex-situ* experiment to analyse the chemical corrosion in eight commercial stainless steels exposed to an acidic solution. A controlled voltage was applied, and to

simulate either cathodic or anodic conditions, the solution was bubbled with a gas (H_2 or air). Once 72 hrs of aging were completed, the solution was found to contain dissolved metal cations (including Fe^{+3}, Cr^{+3} Ni^{+2}).

3.3.4.2 Mitigation Techniques for Bipolar Plate Degradation

To improve the resistance of corrosion in simulated or real FC environments, the recent work in this key area was directed towards the use of graphite/polymer composites, carbide-based alloys or various nitride, or metallic materials coated with noble metals (Gabeab *et al*., 2014). A number of developed coating methods that are widely employed in other industrial areas, for example, electro less deposition, spraying, electroplating, immersion coating, painting and electrolytic anodisation (Brady *et al*., 2013), were examined for Bp materials. Considering the manufacturing cost-effectiveness for continuous high-volume production (Wang *et al*., 2013), has started concentrating on chemical vapour deposition (CVD) and physical vapour deposition (PVD) processes. However, the protective coating methods may face the potential risk of coating material deformation during the operation of PEMFC under high thermal conditions.

Kakati *et al*. (2013) have suggested a sensible description, that the difference in the coefficients of thermal expansion (CTE) of a coating material and the substrate causes their expansion and contraction at various rates. The deformation of the coating layer may cause micro-cracks and micro-pores, which expose the substrate metal directly to an extremely corrosive environment. This subsequently leads to the diffusion of dissolved metal ions into the PEM, thus being trapped in the ion exchange sites, which adversely affects the performance of the FC. One effective strategy to buffer the CTE differential is to add intermediate coating layers with high bonding strength and introduce a gradient of CTEs between coating and adjacent layers of the Bp.

The compressive forces employed to guarantee electric contact between the layers and reactant sealing when the cell is in an operating state may cause deformation or even fracture, which is a common concern related to Bps. In addition, operational factors such as non-uniform current, thermal cycling or thermal misdistributions over the active area can affect the bipolar plate's mechanical properties. Lee *et al*. (2006),

in the presence of an acidic electrolyte, introduced electrical current to the surface of a metallic material (nickel-rich alloys or stainless steel). This treatment enhanced the corrosion resistance property of the metallic Bp due to the surface composition and/or the modification of the surface morphology. Delamination was not an issue as the surface treatment method used here modifies only the surface rather than the coating procedure.

Although carbon–carbon composites lack the mechanical strength, as well as needing the lengthy and costly process of chemical vapour impregnation (CVI), however they offer many advantages. In recent times, carbon–polymer materials, particularly those with thermoset resins, are quickly gaining popularity as alternatives for Bps in terms of dimensional tolerance and good conductivity. However, obtaining the required electrical conductivity requires high carbon loadings, which may cause difficulties in the ability to process. The degradation of the resins in PEMFCs' working environments, owing to the polymer's inherent properties, is another issue related to the materials of carbon–polymers. The heavy atoms, such as magnesium, calcium or zinc, released from these resins may diffuse into and contaminate the membrane, which reduces the performance and durability of the FC.

Wu *et al*. (2010) discovered Bp requirements and design rules for PEMFCs) that follow the principles of environmental impact and stack manufacturing. Considering the state-of-the-art alternatives for Bp, no material has met all the intended target properties that are suitable for industrial applications. However, each material will eventually find its specific application field based on its own specific advantages and disadvantages. The driving constraints of the application determine the choice of material and are always a compromise between reliability, durability, efficiency, performance, lifetime, size, cost, local climate, and operational range flexibility, among others (Kakati *et.al*., 2013).

3.4 Monitoring Techniques in Proton Exchange Membrane Fuel Cells

In the field of engineering, the traditional durability data analysis used to quantify the life characteristics of products, systems, or components includes evaluation of

times-to-failure data obtained under normal operating conditions. In the case of FCs, obtaining such times-to-failure data is always challenging due to issues such as high costs and prolonged test periods. A FC stack is a complicated system that consists of several components. Establishing commercial viability of FCs requires in-depth understanding of component interactions, degradation mechanisms and the effects of operating conditions.

Many approaches have been implemented by several FC developers to evaluate FC performance, reliability, durability as well as failure modes of current FC components to reduce experimental time and increase overall sample throughput. Currently, the US FC Council (USFCC) and the US Department of Energy (DOE) are putting efforts into establishing PEMFC performance, durability and reliability testing protocols and set standards for operating procedures and test conditions to examine new structures and cell component materials.

Typical tests made through this suite include: electrochemical, electrical and mechanical tests and associated measurements performed according to two modes: operating FC and in *ex situ* measurements.

The most common *ex-situ* tests for the operating FC are described in this section together with reference to applications to contamination testing.

3.4.1 Polarisation Curve

The polarisation curve (also known as the V-I curve) is one of the most widely used performance testing approaches. This curve consists of several recordings of cell voltages as a response to current or current density levels. When the current increases from zero to the Nernst voltage, the electrodes begin to polarise, producing lower cell voltage. This curve includes essential operating characteristics for various applications of FC, since it indicates the available power. The curve's shape provides vital information about the magnitude of the polarisation losses, categorised as kinetic, Ohmic and mass transport (see figure 3.1). (Wu *et al*., 2010; Ni, 2013; Ramija *et al*., 2016).

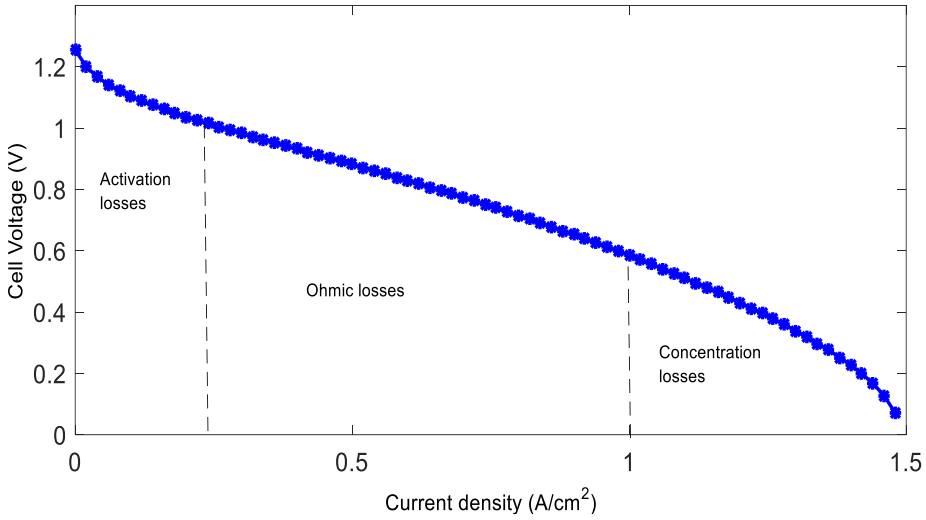

Figure 3.1: Polarisation curve of a single PEMFC.

3.4.2 Steady-State Testing

This is the second common test and it is used to investigate the durability of the FC. Such a type of test is quite simple and easy to perform, as it only requires setting the FC at a constant load or current or, in some cases, a constant voltage. Then the FC is operated for a specific period or until a failure criterion is reached while the change in voltage or current is recorded. The rat-cycle and type of FC performance degradation can be characterised by conducting diagnostic schemes, which can be made through polarisation curves, or some of the other tests described in the following sections.

This test is among those for contamination testing. The FC is run for a short period to produce a baseline performance and the contaminants are introduced into one of the inlet reactant streams to enable the monitoring of performance degradation. The contaminant may then be stopped and the test continues to determine the possibility of having spontaneous recovery of any performance losses or that there is a need to conduct further tests, e.g. to detect the presence of the adsorbed species on the catalyst (Ni, 2013).

3.4.3 Duty Cycle Testing

Depending on the application in question, FC simulation may be quite a complex process. An example, of the efforts involved, is a study that was conducted by

Sandia National Laboratories robotic vehicle. This study showed the effort made in characterising the duty cycle of the vehicle with a data acquisition system (Najafi *et al*., 2015). Despite being a valuable tool, duty cycle testing is rarely used in the literature since it requires an automated test station and a good understanding of the intended duty cycle.

3.4.4 Oxygen Testing

The oxygen polarisation curve provides a measure of the activation and Ohmic losses, with minimal contribution from mass transport or concentration losses, as the diffusion rate of the oxygen is much higher than that of the binary gas diffusion with air. This justifies the need to separate the kinetic, Ohmic, and mass transport losses.

3.4.5 Voltage Decay

The voltage diagnostic technique is based on the analysis of the transient voltage response after step change in load from zero to a constant current. The test is performed whilst running the cell under the conditions of interest until it becomes stable, and the cell is then set to 'open circuit'. The current value increases from zero to the specific value depending on the load, and the transient voltage response is measured.

The initial response occurs because the reactants are at a uniform concentration as there is no current being generated. Just after the load is applied, the voltage (V_o) rises before a diffusion gradient can be established in the electrodes, while the reactant concentration at the CL is the same as the bulk gas concentration. It is worth mentioning that with a uniform distribution of temperature and reactant concentration, V_o should occur with a uniform current distribution. Repeating this test (via stepping to different load points) can produce a mass transport free polarisation curve. As the reactants are being consumed, a diffusion gradient is established, and the subsequent response provides information about mass transport.

3.4.6 Alternating Current Impedance Testing

Alternating current (AC) impedance testing is different from the majority of other diagnostic techniques as it applies a very small perturbation to the system in the form of an alternating signal. The small signal results in reduced errors introduced by the measurement technique. The theory uses an equivalent electronic circuit consisting of resistors, a capacitor and inductors to represent the impedance to electron flow in an electrochemical cell, such as the slow electrode kinetics and diffusion resistance. Relatively simple equivalent circuit models are frequently good approximations of a real system and data can be fitted to yield reasonably accurate results. By introducing a perturbation in the direct current (DC) delivered by the FC and measuring both the voltage response and the perturbed current, an AC impedance can be calculated. Electrochemical impedance spectroscopy (EIS) involves the measurement of the response at several frequencies.

Vengatesan *et al*. (2012) provided an example of the use of AC impedance for assessing the degradation over a lifetime test. When measuring the AC impedance spectra at different current densities for new and lifetime–tested cells, the resistance to transport, or diffusion processes, significantly increased between the new cell and the life-tested cell. By applying the proposed technique under different humidification levels, the authors were able to confirm that there is a connection between the presence of water and the increased resistance to diffusion. The study also considered the change in ionic conductivity of the electrodes.

3.4.7 Cyclic Voltammetry Testing

This type of test is commonly used to investigate the FC electrodes and hydrogen crossover. In this technique, a linear ‘sweep’ potential is applied to one electrode, while the other is held constant. The potential is cycled in a 'triangular wave' pattern and the current produced is monitored.

The information expressed by the shape and magnitude of the current response are useful quantitative and qualitative information regarding the amount of catalyst that is electrochemically active, the double layer capacitance, hydrogen crossover, and the presence of oxide layers and contaminants. Wu *et al*. (2010) provide a description of this technique with examples of voltammograms.

3.4.8 Single Cell versus Stack Testing

PEMFC developers commonly use a mixture of single test and stack testing. Both testing types have several advantages as follows:

The main advantages of single testing are: 1) it is a cost-effective test; 2) it provides great control of operating conditions and 3) it is more useful for fundamental studies.

The main advantage of stack testing is the ability to simulate very closely the operation under realistic conditions including the range of conditions experienced by the cells in the stack.

The main differences for operation in a stack are due to uneven thermal, electrical and flow distribution effects between the cells. Moreover, the heat loss from a single cell is quite large, and this makes it quite difficult to simulate the same thermal conditions, as a cell would see in a stack. This can lead to some differences for contamination studies and it is well known that temperature effects are very important for adsorption and desorption phenomena.

3.4.9 Accelerated Durability Testing

To make the FC test more realistic, long-life requirement should be considered in the test. Applications such as stationary power generation at 40,000 hrs and bus application at 20,000 hrs will take several years to test and will need significant quantities of fuel. The development and design cycle require turnaround in a make-break-fix cycle involving determination of failure modes, followed by technology development, and, finally, implementation of mitigating materials and designs. Therefore, the main features are whether the FC testing approach is sufficient for the required lifetime, thus accelerated testing techniques are being developed by many FC developers and material suppliers and are an important component of FC testing strategy.

The use of an accelerated stress-testing method not only stimulates the specific component’s targeted failure mode but also minimises the confounding effects from other components. As the components undergo different degradation mechanisms under various conditions, AST protocol for catalyst supports differ when compared with electro-catalysts. Similarly, AST requires isolating and distinguishing the effects

of membrane chemical degradation for understanding membrane mechanical degradation.

3.5 Summary

By reviewing the above-mentioned research efforts, it has been noted that performance, reliability, and durability are three major issues which are obstacles to the commercialisation of FCs.

The performance, efficiency and reliability of a PEMFC are affected by many internal and external factors, such as the degradation of materials, operational conditions, and impurities or poisons. Undoubtedly, whilst more conventional experimental approaches dedicated to cell state assessment (electrochemical impedance spectroscopy, current interruption, pressure drop and X-ray methods) are undoubtedly powerful, they remain unsuitable in terms of handling the heterogeneous, transient and even stochastic elements of the phenomena witnessed in the membrane of the FC.

Phenomena occurring within PEMFCs are many. Sufficient understanding of these phenomena will lead to good understanding of the failures that occur in FC systems. This will help to establish diagnostic and monitoring systems that are highly reliable, and ultimately enhance the reliability of the cell and reduce its cost. Essentially, due to the cell geometry, chemical, electrical and physical values, uniformity is not flawlessly achieved. In some regards, an approach facilitating the membrane hydrogen state measurement that needs to be sensitive to localised phenomena, would contribute significantly to developments made in water management.

Although all methods used to diagnose FCs are generally well understood and give acceptable results, using them with stack FCs is a difficult task, and they require more complex procedures in order to obtain good quality data. Another issue is the cost, as all techniques utilising monitoring and diagnosis faults are expensive. Accordingly, the acoustic emission (AE) technique was chosen for three main reasons:

1. AE is non-invasive, meaning it causes minimal perturbation.

2. Unlike other methods, AE depends on electrochemical reactions, hence it can be used as a non-intrusive technique to investigate and indicate the FC state.

AE occurs because of the reaction between hydrogen and oxygen molecules at the cathode side. Another possible acoustic source is the movement and bursting of bubbles generated by reactions at the cathode side of the cell. The nature of AE means that it carries very useful information about the condition of PEMFCs and factors influencing their operation.

AE emitted by PEMFCs, could play a crucial role in increasing performance, reliability and even the lifetime of FCs. As AE is directly associated with many phenomena and factors of PEMFCs, such as electro-osmotic drag, water content, temperature , and pressure incidents resulting from electrochemical reactions within FCs, it becomes possible to reliably detect and diagnose faults.

CHAPTER 4

COMMON FAILURE MODES

The fuel cell is known as a complex device where many phenomena occur within it. This complexity includes the geometry of the cell and the source of faults. This chapter presents the failure modes that have significant impact on fuel cell performance efficiency and lifetime.

4.1 Overview

The faults that affect FCs are many, ranging from transient to permanent faults. Electrical and chemical faults are the significant faults leading to a reduction in performance and, in the advanced stage of faults, may destroy the cell. The failures that occur within a FC system can be divided into three kinds, which are:

1. Permanent Faults (irreversible faults).
2. Transient Faults (reversible faults).
3. External Faults.

The external faults include, faults in compressors, converters and control systems.

4.2 Permanent Faults (Irreversible Faults)

These kinds of fault are permanent and in time will lead to permanent damage to the FC. The cell's performance and efficiency will degrade when such a fault occurs. The possible solution in this case is to replace the damaged FC.

4.2.1 Membrane Degradation

Degradation of membranes is one of the most common faults that affect PEMFC performance, efficiency, and their lifetime. This kind of fault takes place over time such that the system's evolution is looking for new equilibrium points. In this case, the diffusion constants of the system are changed as well as the pressure gradients between the two electrodes. The temperature and humidification, besides chemical attack, cause changes in the membrane characteristics and the mechanical degradation. The chemical attack is caused by radicals initiating membrane degradation because of their unpaired electrons being highly reactive. Electrochemical impedance spectroscopy (EIS) is employed to detect the membrane degradation, however the EIS is suitable for one or a small number of cells (10 cells or fewer), owing to the technological limits of the classical impedance meters. One of the most common factors that cause membrane degradation, leading to reduced FC performance and reliability, is chemical stability of the membrane. Because of their good features and properties such as composition of per fluorinated membrane which is relatively stable in terms of chemical and thermal

sense. For ion exchange, DuPont's Nafion and Gore's Primea membrane series are utilised. The lifetime of such membranes may be extended to thousands of hours. However, when temperatures are lowered to sub-zero, these membranes becomes more sensitive and vulnerable with the chance of rapid degradation. This happens especially in the case of transportation when the start-up and shut-down phases are in freezing duration Kircheva *et al*. 2011)

4.2.2 Absence of Catalyst

This kind of fault occurs when the cell is flooded or when the fuel is contaminated with CO that will lead to reducing the active area of the catalyst, which ultimately reduces the cell's performance. The output power that could be used to diagnose the catalyst performance, and is inversely related to load resistance.

4.2.3 Effect of Carbon Monoxide on PEMFC Performance

A platinum element is commonly used in the catalysts (for both electrodes) of hydrogen PEMFCs. Since the outcome of cells is directly linked to the effectiveness of the used catalysts therefore, when a saturated gas such as methane is used with hydrogen, the presence of carbon monoxide CO will be noted. Hence, this negatively affects the operation of the cells because the platinum causes the attraction of CO on the surface of the catalyst. In addition, when the voltage is between 0.5 to 0.6 volts on the surface of the electrodes, the fuel (hydrogen) will react with oxygen and turn into CO_2, causing the surface to reduce on the affected catalyst (Sato *et al*., 2006). Thus, the CO molecules cause the closing of the separating membrane pores and prevent the ions crossing, which is called poisoning the cells, and this leads to lower output. This can be illustrated in the equations below:

$$CO + Pt \rightarrow Pt - CO \tag{4.1}$$

$$2CO + 2(Pt - H) \rightarrow 2(Pt - CO) + H_2 \tag{4.2}$$

Some approaches can be used to reduce the effect of CO on FCs' performance:

1. Platinum-ruthenium alloy (Pt-Ru) is added to the catalyst as well as platinum element, and this reduces the voltage of the oxidation reaction by 2 to 3 volts on the surface of the catalysts.

$$Pt + H_2O \rightarrow (Pt - OH) + H^+ + e^- \quad (4.3)$$

$$Ru + H_2O \rightarrow (Ru - OH) + H^+ + e^- \quad (4.4)$$

$$(Pt = CO) + (Ru - OH) \rightarrow Pt + Ru + CO_2 + H^+ + e^- \quad (4.5)$$

2. Power electronic converters that are connected to the FC are used to generate current pulses at low frequency, which injects to the anode in order to raise its voltage so creating adequate voltage to force the CO to be electro-oxidised into CO_2, hence freeing enough of the catalyst layers in the PEMFC.
3. A high operating temperature could help to improve the prevention of the cells' tolerance towards CO poisoning. However, high temperature reduces the dynamics of cells.
4. Blowing a little air into the anode with fuel that may cause oxygen availability to oxidise CO, which is absorbed in the layer of catalyst forming CO_2. This would help in cleaning Pt sites (Sato *et al*., 2006; de Beer *et al*., 2015).

Unfortunately, none of these proposed solutions eliminated the effect of CO poisoning on the FC, they only tend to mitigate the problem.

4.3 Transient Faults (Reversible Faults)

As the name implies, transient faults are reversible, so the PEMFC will work normally as soon as the fault is rectified. Usually, this kind of fault is related to the PEMFC state and control technique.

4.3.1 Hydration and Dehydration

Water behaviour and management are amongst the most important parameters influencing the performance and efficiency of PEMFCs. Accordingly, the optimisation of water management throughout cell operation is recognised as

critical, which is the subject of on-going and varied research. Notably, water management needs to be considered in line with processes occurring in gas channels, across the GDLs, electrolyte, catalyst, and within the membrane to minimise the voltage losses. This may be highlighted when considering that, although the membrane needs to be hydrated well in order to ensure good performance, the gas channel and GDL must be safeguarded from flooding (Legros *et a*l., 2007).

The key phenomena and parameters that need to be considered and managed are relative humidity (RH) and the formation of water droplets in the gas channel, in addition to the water level in both the membrane and GDL (Park *et al*., 2012). Importantly, water is produced through the electrochemical reactions, with the reactant gas that needs to be humidified to assist in membrane humidification to enhance ionic conductivity. In contrast, however, in-membrane water transport is led through back-diffusion and electro-osmotic drag. Accordingly, the ideal water level is not easy to establish on an experimental basis, and it is problematic to maintain, particularly without *in situ* water-level measurement.

4.3.1.1 Fuel Cell Flooding

Due to electrochemical reactions, water is produced at the cathode side of the PEMFC. Usually, when the FC is working under normal operating conditions, the water produced is used to humidify the membrane to enhance its ionic conductivity and the rest of water is removed by the airstream. If the water production rate exceeds the removal rate in this case, water will block the membrane pores and GDLs. When this fault happens, degradation of the cell performance is noted because of starvation of gas at both the cathode and anode sides.

The mass transport losses are tightly related to the flooding, especially at the cathode side, owing to the transport rates of the reactants to the electro-catalyst layers being significantly reduced. Output voltage could be recovered relatively quickly as soon as purging both sides of cathode and anode is completed. Table 4.1 shows the location and consequences of flood faults.

Table 4.1: Location and consequences of flood faults.

Fault location	Consequences of faults
Gas diffusion layer (GDL)	• Loss of porosity reduce gas permeability.
Gas Channels	• Low pressure in gas flow channels • Low flow rate of gas channels • Decay and a change in gas channel geometry
Electrodes	• Inhomogeneous pressures in Bps • Decay and a change in flow-field geometry
Membrane	• Reduction of mass transportation

4.3.1.1.1 Cathode Flooding

Water flooding usually occurs at the cathode side, based on the following three mechanisms:

1. Water is generated because of oxygen reduction reactions (ORRs) and the amount of water continues to increase with the increase of current density and load.
2. Water particles, along with protons from the anode to cathode, are pulled by ions which known as the electro-osmotic drag phenomenon, under the effect of an electric field. The amount of water transferred is dependent on the membrane humidification level and may be increased by increasing the current density (Li & Chan, 2013).
3. Flooding may also occur due to over-humidified reactant liquid water injection and gases.

The accumulated water on the cathode may be cleaned out from the porous electrode by using methods like water vapour diffusion or evaporation. Moreover, capillary transfer via the GDL in the flow channels and back-diffusion of water through the membrane to the anode may be used. However, the latter method is not so appropriate in the removal of water because back-diffusion is only possible at lower current densities such as those less than 0.3 A/cm^2 and, at this current, back diffusion can lead to net transport of water towards the anode (Li & Chan, 2013).

Whereas the possibility of cathode flooding is more at higher current densities along with the possibility of excess of back-diffusion due to electro-osmotic drag phenomenon (Chen *et al*., 2012). It may result in an increased water content at the cathode ultimately increasing cathode flooding. Evaporation and water-vapour diffusion methods are usually used to remove water at a higher airflow rate with a higher temperature of cell operation. The process of flushing out the water from the cell is made possible when surface tension and viscosity increase (Speder *et al*., 2014). However, the rise in temperature limits PEMFC applications, especially in transportation, in addition to causing low durability of parts of the cell life, especially of the membrane.

A high airflow rate may cause damage to delicate components such as the membrane. When it becomes impossible to efficiently remove the water which has collected in the cathode, the water flooding affects FC performance badly. At higher current densities, such as above 0.55 A/cm^2, a considerable amount of cell voltage drop occurs due to the reduction of the partial-gas-pressure level at the cathode side because of flooding.

Moreover, by the drop in cathode pressure from 3 KPa to 1.5 KPa, the initial potential (0.9 V) of the cell also drops to one third of the initial 0.9 V. Furthermore, water accumulation and cathode flooding cause oxygen to enter the surface of the catalyst causing hindrance. (Therdthianwong *et al*., 2012).

It is possible for the cathode voltage to drop significantly from 1.23 V to 0.00V at current off and further from 0.8 to 0.1 V at current on with replacement of PRR with ORR. Current flows through the electrode along with the electrode polarisation, which causes a voltage shift in the negative direction, however, anode polarisation occurs towards the positive path. Anode potential tends to shift towards the positive direction with flowing current. Thereby, FC voltage may change from the initial 0.7 V to 0.2 V as shown in figure 4.1.

Cell voltage may be reversed from a positive to a negative value (i.e. from 0.7 V to -0.2V) along with the replacement of PRR with ORR under the oxygen starvation phase. In PEMFCs, this process is known as the voltage reversal effect (VRE) (Therdthianwong *et al*., 2012). However, when VRE occurs within a cell, it not only

contributes to the stack output, but may also balance the partial effective output voltage with a single FC.

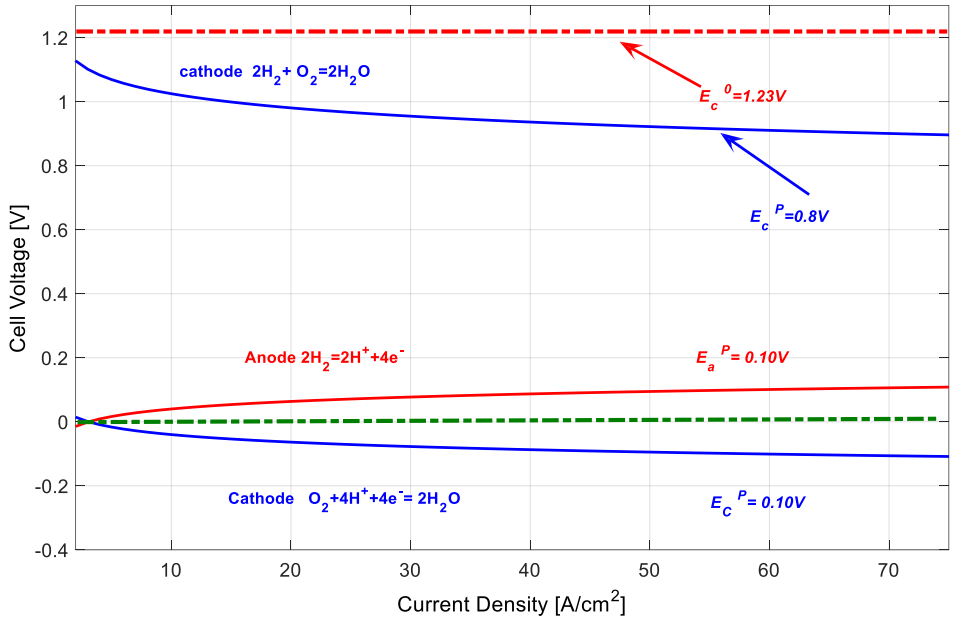

Figure 4.1: The impact of voltage reversal in a PEMFC.

4.3.1.1.2 Anode Flooding

Water requires more time to gather at the anode side due to the production of water at the cathode side of the FC. Less flooding occurrence at the anode may cause serious concerns about the performance of the FC. Fault occurrences due to anode flooding may cause fuel starvation with carbon corrosion in layers of the catalyst. Furthermore, at low flow rates of hydrogen, water may not be removed from the anode. Kim, *et al*. (2014) found that water at the anode may be detected when the cell is operated at low current densities such as 0.2 A/cm^2, however, electro-osmotic drag force may reduce the water content at the anode, especially at higher current densities. Moreover, anode flooding may also occur due to the lower temperature of the cell with higher condensation of water in channels (Yu *et al*., 2005)

Proton flux is high at the inlet of the anode where heavy electro-osmotic phenomenon drags water molecules out of the anode to the cathode, which results in low water content. However, in contrast, at the outflow of the anode, current density is lower with higher water content.

Anode flooding may occur due to back-diffusion of water from the cathode along with a stream of fuel gas with a low hydration state. It is also possible that back-diffusion of water, to the anode through the GDL, may surpass the electro-osmotic effects in which case the hydration state is not as high as that of the cathode. It was also observed by Kim *et al*. (2014) that water vapour which came from the GDL of the anode condensed at the surface. However, water content due to condensation is not much in quantity. Injection of liquid water to cool and humidify is another reason for the occurrence of anode flooding (Tian *et al*., 2008).

4.3.1.1.3 Flow Channel Flooding

It has been observed that the process of flooding may not only be related to porous electrodes (anode or cathode), but it also occurs in the flow-field gas channels. It usually depends on the interaction of the components' properties and the conditions of operation. Reactant gases may be hindered by the flow channel flooding and may weaken the power output of the FC. When serpentine channels are used in flow channel flooding, one of the channels among them may cause starvation in some regions. Water flooding, along with loss of output voltages, may also cause changes such as:

1. Current density will be reduced, due to accumulation of water preventing the reactants from reaching active areas.
2. Released enthalpy of the condensed water may cause unbalanced local distribution of temperature and current density.
3. Gas flow resistance may rise due to accumulation of water in the GDL; this may also result in an increased pressure between outlet and inlet of a FC (Tian *et al*., 2008; Chen *et al*., 2012; Lee and Bae, 2012).

4.3.1.1.4 Membrane Dehydration and Flooding

Water management is a key factor in the occurrence of membrane dehydration or flooding due to a lack or/flooding of water. Although the membrane needs to be hydrated for good conductivity, flooding of the membrane will block the GDL (Lee & Bae, 2012).

Membrane dehydration usually occurs at the anode side. Poor water management is a key factor in the occurrence of membrane dehydration due to lack of water. When the cell works under dry run conditions of the membrane, it will lead to the deterioration of instantaneous and decline in the performance of the cell.

The low conductivity, due to the high resistance cell, is linked to a radical correlation of relative humidity of the membrane. This will lead to a significant reduction in effort and electrical power in the cell. Although the temporary decline of the effort can be recovered by re-hydrating the cell, operating the cell under dry conditions for a long time causes significant damage to cell which is irreversible, especially to the membrane. Recovery time is determined by membrane thickness and water diffusion. Due to higher water, back-diffusion that takes place at the anode in the bottom of the cell, the dehydration of the anode is more important at the inlet of the cell. Moreover, the membrane pores shrink because of the dehydration leading to lower back-diffusion rates. If the membrane worked for long periods under dehydrated conditions, the membrane becomes brittle and it may develop cracks. In this case, the gas crossover causes an uncontrolled reaction for both H_2 and O_2 and hot spots will appear in the membrane leading to pinholes and more gas crossover. There are four reasons for cell dehydration:

1. Inability to maintain adequate humidification of the cell when the cell is fed streams of dry gases or little humidification.
2. High temperature of the cell during operation will increase the water evaporation process.
3. Electro-osmosis can play a role in anode dehydration.
4. The membrane thickness.

Figure 4.2 shows water content as a function in membrane thickness.

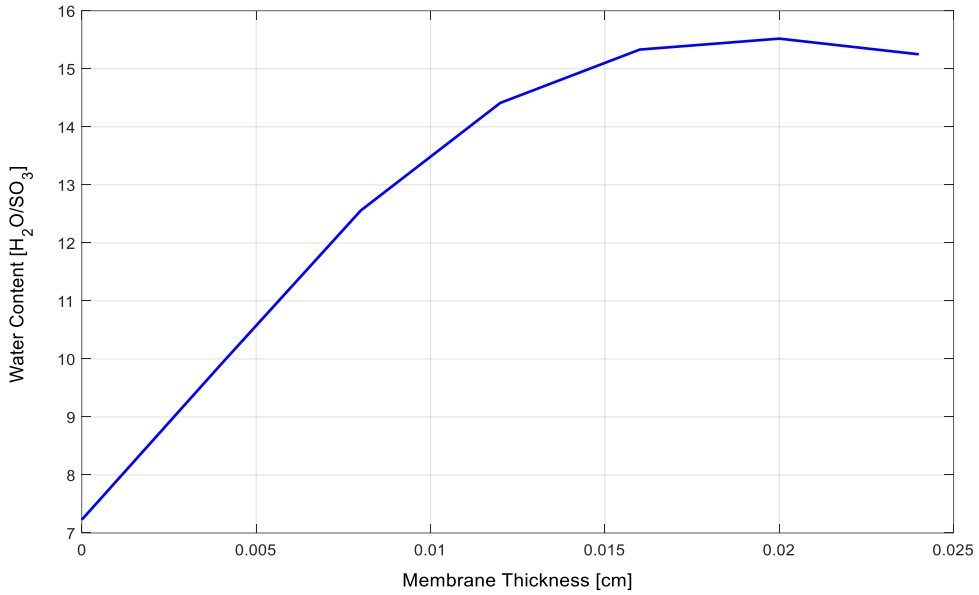

Figure 4.2: Membrane thickness and water content.

4.4 Thermal Management and its Impact on Performance

When a PEMFC is being exposed to freezing temperatures, thermal management becomes important. However, operation of PEMFCs is still not completely understood in cases when it cycles below and above zero temperatures and cold starts. Though research has been carried out in recent years, yet more study is required to completely understand the challenges of operating below zero and at elevated temperatures Srouji *et al*., 2013).

Fuel cell operation at temperatures higher than 100^{o}C has some advantages (Berger, 1968): increased tolerance for pollutants with improved efficiency, water management along with enhancement of the cooling mechanism because of higher temperature differences between coolant and cell. Unsaturated hydrogen may be utilised owing to reduction in CO poisoning and recovery of waste heat (Karthikeyan *et al*., 2015). Degradation of electrode catalysts may also occur at moderate temperatures along with loss of their (Pt^{-}) particles (de Beer et al., 2014). Chemical stability is more important at higher temperatures. Redistribution and accumulation of particles are also accelerated at higher temperatures (Zhang *et al*., 2006).

Another issue may arise at elevated temperatures when the potential is kept higher at the cathode. This may cause oxygen molecules to be split into atoms which may

easily react with carbon or water, at high temperature, to form CO_2 and CO which may also result in carbon corrosion (Srouji *et al*., 2013). As a result, degradation of a catalyst may occur which ultimately affects the performance and lifetime. Moreover, at low relative humidity and elevated temperatures, water acceptance of the membrane worsens with the decrease in proton conductivity. This process may result in resistive loss, which may lower the cell efficiency and performance

Song *et al*. (2001) analysed the impact of Nafion contents on the performance of electrodes under three diverse temperatures namely; 80, 100 and 120ºC. At 120ºC the effect of Nafion was greater than that at lower temperatures. Therefore, lower performance is observed and mass transport problems of non-optimised Nafion content.

4.4.1 Effect of Sub-zero Temperatures on Performance and Efficiency

The performance and efficiency of PEMFCs may be affected by exposing the non-operating PEMFCs to lower temperatures. The residual water may get frozen when the FC is exposed to sub-zero temperatures for long periods of time. This may result in mechanical damage or physical break down of the FC components due to mechanical and thermal stress. It is to be noted that the cause of degradation of the MEA is freezing water on Nafion membrane instead of inside the membrane. The volume of frozen water is expanded about 9% due to different densities of ice and water (Jiao and Lee, 2011). The process of ice formation and melting again in water can separate the catalyst layers from the membrane layer of gas diffusion as well (Hou *et al*., 2009). As the components are no longer in contact within the cell, mechanical damage may also cause a thermal and electrical contact as well. Ge and Wang (2007) have linked the formation of ice at the surface of a membrane with its initial water content and initial thickness. Enclosed liquid water may flow out of the membrane and easily become frozen on the surface because the Nafion membrane has a higher freezing temperature.

The thickness of the developed ice layer depends on the thickness of the membrane and higher content of initial water. For example, ice thickness for Nafion 112 is 5 mm whereas, for Nafion 117 it is 18mm. Moreover, after several freezing cycles, fully hydrated membranes are cracked by carrying out tests by Plug Power

(Theodorakakos *et al*., 2006). However, cracks may be less serious if, after shutdown, the hydration state of the membrane is lower.

Gas crossover due to cracks may lead to an uncontrolled reaction between oxygen and hydrogen along with the formation of pinholes which ultimately damage the membrane and may cause a reduction in the lifetime of the cell (Ge and Wang, 2007). Results from Gebel et al., (2008) show that cells which are being dried during the shut-down period may not experience physical damage and electrochemical losses.

4.5 Starvation

Starvation in PEMFCs occurs due to lack of fuel and/or air. This lack happens as a result of many issues such as faults in pump and compressor as well as clogging in pore layers due to bad water management.

4.5.1 Fuel Starvation

Usually, hydrogen is used as fuel in PEMFCs. The starvation in hydrogen or oxygen will lead to a reduction in output voltage, and thus affect FC reliability and performance.

In the study performed by Gerard, et al. (2010), there was an analysis of performance degradation during fuel starvation of PEMFCs. Fuel starvation occurs for several reasons, such as insufficient oxygen to the cell during peak power demand, compressor delay or water management issues. In the same way, Liu *et al*. (2006), investigated the effect of fuel starvation on PEMFC performance, explored the changes in PEMFC voltage and electrode voltage against the reversible hydrogen electrode (RHE) with time during air starvation and found inhomogeneous degradation of the catalysts.

4.5.2 Air Starvation

Oxygen or air starvation occurs at the cathode due to lack of oxygen or air at the catalyst layers (Scott *et al*., 2014). The net flow-rate of oxygen becomes equal to the oxygen consumed in the electrochemical reaction when steady-state conditions are achieved. However, in transient operating conditions, a sudden increase may occur for the power requirement of the FC. The system’s air supply may lag behind

the requirement causing a lack of air and ultimately creating air starvation in the reaction, thereby increasing the concentration of oxygen at the cathode. However, if a shortage of oxygen occurs at the cathode, a proton (H^+) reduction reaction (PRR) may occur in place of an oxygen reduction reaction (ORR).

Dou, *et al*. (2011) analysed the current distribution during air starvation and observed the decreased current densities in the starvation region. In a similar way, Grigoriev *et al*. (2011) introduced a comprehensive understanding of the reversal process during air starvation. The current distribution measurement system and the local interfacial potential method were utilised in such a way as to find the correlation between the oxidant starvation and performance deterioration.

4.5.3 Reactant Leakage

A certain level of leakage rate must be maintained for hydrogen-fed PEMFCs because hydrogen gas has a higher combustibility level in small non-ventilated spaces. Critical hydrogen accumulation may occur due to an increase in leakage rate. This increment is because of cracks in the graphite plate along with seal ruptures and cross-leaks, which may ultimately lead to explosions. It is argued by Miao *et al*. (2010) that to detect hydrogen leakage accurately, water vapour at the anode must be considered. However, a relative humidity sensor is also required, along with an already employed anode pressure sensor and mass-flow sensor in the PEMFC. Though it is expensive, yet was deployed along with an adaptive alarm threshold in order to remove false alarms.

Miao *et al*. (2010), intended to detect reactant leakage by observing the open circuit cell voltages in aged cells in the region of the crossover and cathode/anode compartment. They analysed them at several different operating conditions, which ultimately helped to locate FCs with defects.

Signal-based fault-detection is usually used for detecting anode/cathode leakage. After stopping the reactant flow, the amount of time needed to reach a certain voltage threshold (0.5V) is studied. It took a while for some cells to reach the set threshold, however, some cells reached their threshold very fast. To differentiate real faults, a normal probability curve is used. By studying the effect of the correlation between the water level in expanded vessels and the reactant gas flow dynamics, anode/cathode compartment leakage can be detected.

The PEMFC simulator model was modified by Escobet, *et al*. (2009) which was designed by Pukrushpan *et al*. [(2004). This was designed to include different faults such as an increment in compressor motor friction, compressor motor overheating because of water channel blockage, flooding in the diffusion layer and cell temperature increase due to malfunctioning of the cooling system.

A knowledge-based fault monitoring system is proposed which is an interface engine with a user interface system conducted on LabView. This is used for monitoring three faults modes:

1. Membrane drying
2. Air and hydrogen starvation of the electro-chemical reaction
3. Leakage of the membrane

The research is based on the reality that membrane leakage is caused by the creation of holes in the membrane. Holes are formed due to hot spots while another reason is fracture caused by mechanical stress. This stress is the result of the cell's operation under dynamic conditions. This may result in a difference in pressure causing the membrane to be broken. To avoid leakage, a hydrogen pressure controller may be deployed.

4.6 Aging and Degradation

In fuel cell (FC) technology, durability is considered as one of the major limiting factors. The lifetime of a PEMFC is considered to be very short and after that the cell performance degrades considerably over time. The operational time of the cell was estimated by Escobet et al. (2009) by utilising a pattern recognition-based approach and the rest of the lifetime was calculated by using dynamic stack information, which is based on the EIS technique.

The process involved a two-step extraction method, which utilised an empirical model for extraction. This featured extraction is used on polarisation curves for the extraction of relevant descriptors while using a regression model. The imaginary part of the spectrum is automatically split, in this model, into several parts which are estimated by polynomials. Real data sets are used for the evaluation of both approaches which estimate the lifetime of a FC. Lifetime has a mean error of twenty-four hours globally, however, the first method has 1,000 hrs mean error, the second

method has 142 hrs of mean error and 95 hrs is the mean error by using featured extraction methods. Furthermore, Pukrushpan et al (2004) developed another method of pattern recognition, which is based on both dynamic and static stack information. This is based on electrochemical impedance spectroscopy (EIS) with a polarisation curve to enhance the estimation of operating time. This enhanced method is used to calculate the lifetime of a FC with a mean error of two hrs with 1,000 hrs of global operating duration. Lechartier et al. (2015) studied the effect of intense operating conditions for PEMFCs' durability. It was done by feeding the cells with low humid air and dry hydrogen. This is done at temperatures greater than the nominal temperature for 1,000 hours. Moreover, EIS and polarisation results were observed during tests conducted for several flow rates of gas. At 450 hrs, only a single cell had stopped operation whereas, other two cells had relatively better performances and a low degradation rate.

Yu and Ye (2007) conducted an experiment to study the impact of ripple current with a high frequency of PEMFC aging. Their modelled analysis proved that the current ripple does not impose many local conditions. However, the analysis and results of the study are still questionable because a specific membrane model should be designed to see the real effect of ripple currents. Two protocols have been designed by Zhang *et al*., (2006) that may be utilised to speed up the estimation of lifetime. One of the protocols was designed to operate at high temperature (300^0C).

Experiments showed that degradation in a stack's performance was found after 24 hrs of the experiment. The second protocol was designed to subject the stack to high current density (2 A/cm^2). Kim *et al*. (2012) conducted two aging tests and proved that the protocol could speed up the performance of the stack. The stack was operated under normal conditions in the first test. A constant current of 50 A was used or 1,000 hrs which was being utilised with dry hydrogen. However, in the second test, a dynamical load current was used for a stack operation for 1,000 hrs, also being fed with dry hydrogen. Polarisation and internal resistance were utilised to evaluate the degradation in performance. Table 4.2 demonstrates important faults along with their causes and the effect of such faults on the performance and efficiency of PEMFCs.

Table 4.2: Common failure modes in PEMFCs.

Modes of faults	Component of fuel cell	Types of faults	Fault consequences
Activation losses	Pt catalysts	Pt accumulation resulting in electrochemically active surface areas (EASA)	1. On/off load cycling repetition 2. Because of residual hydrogen, high voltage is induced at cathode equivalent 3.Carbon support loss
		Migration of Pt resulting in loss of catalyst materials	4. Platinum solubility during cell operation through air-hydrogen open circuit to air–air open circuit
		Loss of EASA due to absorption of atmospheric pollutants on Pt	5. Air impurities such as NO_2, H_2S, and SO_2
		Loss of EASA due to absorption of fuel impurities on Pt	6. Hydrogen impurities such as CO and reduction of CO_2 to CO
		Catalyst losses because of chemical attacks and silicon/oxygen/Pt particle formation	7. Chemical degradation of silicone sealant
	Geometric structure of the catalyst layers	Increase in pore size and reduction in EASA due to deformation of catalyst structure by melting and freezing of water	8. Residual water in catalyst layers
	Carbon support in catalyst layer	FC is supplied with insufficient fuel and corrosion of carbon occurs to support current above provided hydrogen	9. Starvation of fuel 10. Partial coverage of hydrogen on catalyst layers 11. Localised flooding
Increase of mass transportation losses	Porous and void regions of the FC; catalyst layer, GDL, BPP flow-fields	Two-phase flow is induced by flooding caused by condensation of water	12. Low flow rate of channel gases 13. Low pressure in gas-flow channels 14. Flow-field geometry or configuration 15. Degradation of polymer electrolyte in catalyst layers due to impurity ions

		Hydrophobic material is used to treat loss of hydrophobicity in porous regions	16. Loss of material/material properties due to repeated thermal cycling/high operating temperature. 17. Delamination caused by repeated thermal cycling 18. Exposure to sub-zero conditions damage material 19. PEMFC over-compression, impacting the GDL
	Geometric structure of catalyst layer	Presence of isomer for impedance to transport attributable	20. Pores collapse due to ionomer expansion on water 21. Excessive ionomer loading. 22. Formation of ionomer skins on catalyst layers 23. Lack of control during MEA processing
	Gas diffusion layer (GDL)	Ice formation with impedance to transport attributes	24. Presence of residual water from previous shutdown 25. Operation at sub-zero temperatures
		Loss of porosity, increased flooding and reduced gas permeability	26. BPPs transmitted inhomogeneous compression induced during operation
Increase of Ohmic losses	Stainless-steel BPP	Loss of surface electrical conductivity	27. Passivating layer on SS surface causes impedance to electron transfer
	Coated stainless-steel BPP	Loss of electrical conductivity	28. Coating defects such as pinholes and micro-cracks when coated with TiN 29. Degradation of conductive coating 30. Conductive polymer coating degradation
	Injection-moulded BPP	Low electrical conductivity	31. During injection-moulding process polymer-rich boundaries are formed
	Polymer electrolyte membrane	Proton conductivity losses	32. Membrane hydration loss 33. Increase in water transfer coefficients and decrease in water diffusion due to replacement of protons 34. Decrease of water diffusion coefficient due to anisotropic swelling

Increase of efficiency loss, potentially leading to catastrophic cell failure	Polymer electrolyte membrane	Pinholes and cracks formation	35. At sub-zero operating conditions, roughness of electrolyte membrane surface increases 36. Mechanical stresses induced by thermal hotspots in regions of strong electrical contact i.e. BPP and high compression and reaction rates 37. Manufacturing process defects 38. Peroxide radical attacks of polymer end-groups 39. Repetition of swelling and contraction because of hydro-thermal stresses 40. Difference of excessive pressure between anode and cathode gas supply
Catastrophic cell failure	GDL/catalyst layer/membrane	Delamination of layers	41. Exposure and thermal cycling to sub-zero conditions
	Catalyst layer	Excessive adsorption of atmospheric and fuel impurities	42. Loss of tolerance to contaminants
	BPP	Cracking	43. Inhomogeneous compression 44. Mechanical shock/vibration 45. Irregularities in cell/stack construction
	Polymer electrolyte membrane	Gas leakage	47. Oxidation of seals Polymer electrolyte membrane
		Short circuit	48. Formation of electrical network due to platinum distribution within self-humidifying membrane

4.7 Summary

The efficiency and performance of a PEMFC is affected by many internal and external factors, such as degradation of materials, operational conditions, and impurities or poisons.

The faults that occur within fuel cell systems can be classified into three categories that are permanent faults (irreversible faults), transient faults (reversible faults) and external faults.

Undoubtedly, whilst more conventional experimental approaches dedicated to cell-state assessment (electrochemical impedance spectroscopy, current interruption, pressure drop and X-ray methods) are undoubtedly powerful, they remain

unsuitable in terms of handling the heterogeneous, transient and even stochastic elements of the phenomena witnessed in the membrane of the FC. Essentially, due to the cell geometry, chemical, electrical and physical value uniformity is not flawlessly achieved. In some regard, an approach facilitating membrane hydrogen-state measurement, which needs to be sensitive to localised phenomena, would significantly contribute to developments made in water management.

CHAPTER 5

MODELLING OF PROTON EXCHANGE MEMBRANE FUEL CELLS

This chapter presents the types of modelling currently used for the modelling of fuel cells. The advantages and disadvantages of each type have been discussed. This chapter also covers the modelling of some of the phenomena that occur within PEMFCs such as acoustic emission, water concentration, heat management, mass charge and mass transfer. Finally, semi-empirical modelling for the polarisation curve has been fully presented.

5.1 Overview

The fuel cell (FC) is a complicated device, which contains many scientific phenomena, e.g. mechanical, physical, and electrochemical, all occurring simultaneously. By understanding these complex but interesting phenomena, one can effectively improve the performance as well as the efficiency of the FC, and hence the manufacturing costs can be brought down.

The most efficient methods of studying and understanding these phenomena are modelling and empirical observation methods. The experimental method is better and more reliable, but due to the associated cost and the time and effort required to conduct it, the former methods are preferred. Despite its reliability, there are some limitations in the experimental methods. For example, it is not possible to measure the influence of the current density of FC efficiency when the change in current density is small. The current density affects the FC efficiency considerably, as explained in Chapter 2, thus it is important to measure its influence (Mazumder & Cole, 2003; Pasaogullari & Wang, 2005).

Again, although it is possible to obtain data and draw the V-I polarisation curve in the case of experimental techniques, it is extremely hard to discover the variables which influence the shape of the curve, especially when the FCs are working under various operating conditions. Along with this, the modelling techniques for FCs have a great advantage in that they can replicate the effects of a wide range of parameter values. This is highly beneficial since practical experiments can be conducted with a limited set of values in a single cell:

1. Electronic and protonic charge transfer
2. Transfer of mass
3. Electrochemistry of cell reactions
4. Mechanical stress, i.e. compression of internal pressure
5. Although it is a simple principle – the hydrogen and oxygen react with each other to produce electricity, heat and water – the modelling of cell phenomena is quite complex. In short, the phenomena of FCs are:

a. It occurs in the nanometre range and is modelled by the density-functional theory and the principle of molecular dynamics,
b. It occurs in the micrometre range, i.e. the material structure level, and
c. It also occurs in the millimetre to metre scale for the mass, flow dynamics, charge transfer and heat by the process of continuum mechanics.

The prime difference in time is due to the difference in speed between electrochemical reactions and the speed of transmission of heat and mass. Because of the over-complicated nature of PEMFCs, a single model cannot deal with all the possible phenomena that can occur within a PEMFC. This is a general rule which is true for all modelling except for a few systems. The basic underlying physical principles of quantum mechanics are unable to formulate exactly the composition of the model at a macroscopic level. Even in the case of classical physics, the several phenomena which occur in a FC are translated to form a very complicated non-linear differential equation-based system. In addition to this, the thermal expansion and the contact pressure distribution of the FC, along with the other mechanical stresses, are also responsible for the FC performance.

A PEMFC model may have a time dimension to account for current drawn from the PEMFC and changes in operating conditions, but the degradation of the cell must be accounted for. Even with modern computers, it is impossible to solve this system in three dimensions and under dynamic conditions along with handling different length scales ranging from Nano-sized catalyst particles to a macroscopic stack-sized structure. Due to this, any FC model always focuses on studying only a few effects under specific, simple conditions. Typical examples of FC models used are electrochemical modelling of the FC and studying mass transport with the help of different flow-field configurations.

Initial models were one-dimensional and often studied only some of the parts of the PEMFC (examples are the cathode electrode and the GDL), but due to the development of computers, three-dimensional models are now common practice and it is possible to model the whole geometry of the FC (Spiegel, 2011)]. Even after this, many assumptions are still needed to remove complexity to reduce it to a solvable model. For example, sometimes the anode mass transfer is excluded in

modelling due to limitations of performance. Another complexity is due to arbitrary parameter values being chosen due to the absence of experimental data or to the values being theoretically derived. For example, current density exchange is an important parameter for the electrochemical equations that comprise the basis of a FC model. Various factors affect this parameter, such as the amount of catalyst on the electrodes and the temperature of the cell. Hence, the values are different for each FC and it becomes extremely difficult to measure their effects. It is common to simply use the parameter that fits with the model outcome in order to give a reasonable look and a physical feel.

Modelling faults, whether numerical errors or more profound problems, could have been hidden by the parameters chosen so that proper-looking results could be obtained. Hence, there is no guarantee that the given predictions for other parameters will be correct or not, i.e. the results cannot be predicted.

The exchange of current density is only one of the many examples; several other problematic parameters exist as in cases of modelling with two phases, like condensation and evaporation rates, and equations of capillary pressure (Mamzunder and Cole, 2003). It is usually also required to calculate averages for many material properties which are not isotropic such as the porosity of the GDL or the contact resistances between several layers in the cell, due to the absence of more detailed data. The results from these models can be accurate when considering the whole cell, but can also be extremely inaccurate at explaining local phenomena.

5.2 Existing Modelling Techniques

A compact review of how FC modelling has evolved from the initial 1-dimensional analytic models to the complicated 3-D models that have been utilised so far will be provided in this section. The modelling studies discussed in this section have been classified for method, dimension and modelling aim. It is hard to categorise FC models, and there are many models which do not fit into any of these categories, like spherical agglomeration modelling (Spiegel, 2011).

5.2.1 Analytical Models

One of the computational tools used by FC models is the Finite Element Method (FEM). There are many models, which are based on analytically solvable equations. It is seen that the analytical type of FC model is always very simplified and idealised. The range of dimensions in which the model is solved is reduced to zero or one. The inherent physics is also simplified, usually by linearising the equations used, which cannot otherwise be solved analytically. The results are not very accurate, especially when the current density is so large. Analytical models can be used to gain approximate voltage-current dependencies and to perform short calculations on simple systems (Spiegel, 2011). In ideal conditions, the basic view can be provided by analytical models. Following many early analytical models, 3-D modelling is more common nowadays because of powerful computers, but analytical, as well as semi-analytical, studies are performed even today.

5.2.1.1 One-Dimensional Models

1-D models can be analytical, but if the equations are not linearised then they can be solved by using discrete and numerical algorithms. The benefit of this is that it makes the results more reliable. The current, voltage and other FC characteristics are the major limitations of 1-D models.

Many local phenomena are beyond the range of 1-D models because they assume un-directional similarity in every direction; hence, the difference between the flow-field plate-ribs and the channels is not considered. The FC model represented by Milewski, (2011) is a 1-D model with simple assumptions. The focus is mass transport, as well as management of water and cathode flooding.

5.2.2.2 Two-Dimensional Models

The types of 2-D models found are channel models or cross-sectional models. The channel model may be used for studying reactant concentration, which varies along the channel due to consumption of the reactants. The cross-section models provide information regarding the process of electrical conduction and current in the flow-plates. The 2-D models assume an infinite planar plate. The flow-field and 3-D phenomenon cannot be studied using 2-D models. The major components of 2-D

models are MEA and GDLs, and symmetry boundaries are used. The aims of a study make it possible to exclude some components; for example, if cathode mass transport is to be studied, then the anode side, as well as the membrane, can be excluded. The 2-D versions of models are extremely useful in cases where the computational power is not large enough.

This sometimes happens if small geometrical details, like the thin layers of the electrode, are included as a domain of the modelling. The mesh of the computational grid will be very fine in similar cases, thus making the model harder to solve. The 2-D models can provide new local phenomena information (Milewski., 2011). These models are used very widely, as the 3-D models can be either unnecessary or impractical for the study of FC phenomena. A few examples can be seen in the work of Al-Baghdadi (2010). The general form of 2-D models is to focus on membrane transport phenomena, GDLs, and local current distribution.

5.2.2.3 Three-Dimensional Models

Three-dimension models can be considered as the most realistic as the FC geometry and can be modelled exactly as it is, although several simplifications must be made. However, this means that, to solve these models, more computer capacity and time will be required. 3-D models are best used while studying phenomena that cannot be modelled in 2-D, like reactant flow and distribution phenomena. A 3-D model can be used to obtain information about whether the reactants are evenly distributed or whether the distribution of current in the FC is uniform or not. Many early examples of 3-D models, such as that presented by Andersson *et al*. (2010) and Bavarian *et al*. (2010), exclude MEA or the electrodes used, as they are very thinly layered and they greatly increase the computational grid size in a 3-D model. It is typical, rather than conducting studies of the whole FC, that only a section of the flow- field is studied, such as one serpentine channel turn. There are many models which can cover the proper active area of a small-sized FC, such as the one given by Anderson *et al*. (2010). In the literature , a 16-cm^2 FC was properly modelled to study the effects of many channel cross-sections on the FC performance. It is very problematic that large scale models are models of comparatively small-sized FCs, e.g. 49 cm^2 (Vasile *et al*., 2016).

Despite this application to small FCs, most real FCs are part of much larger sections to produce the required amount of power. The main problem is that, although the behaviour of the flow-field is not harder to scale, the geometry of the channels works properly in small FCs but they might not perform properly in the larger-sized FC due to changes in their Reynold's numbers. Hence, more effort is required to model the FCs when they are used in stacks, not just those which can be used in the laboratory. PEMFC modelling has proved that the work carried out until now is important for good FC performance.

5.3 Semi-Empirical Models

There are many conditions in which the FC phenomenon physics are not well understood or the correlations are inaccurate outside a certain parameter range, and failure to detect this may result in wrong conclusions. Due to this, the use of empirical correlations never helps in the purpose of understanding the physics of a FC. Hence, the use of empirical correlations may prevent us from finding fresh mechanisms, which could be manipulated to improve FC performance. Semi-empirical models can be accurate enough in design modelling and for materials that are in use already, but can also predict new alternative materials or, innovative designs which could affect cell operation.

It is hard to model the phenomenon for practical modelling. Hence, researchers sometimes opt for formulas obtained from empirical calculations rather than those obtained from algebraic or differential calculations, which are more accurate mathematically in comparison to the former type. There are many cases in which the FC models have employed empirical correlations; an example of such a case is the partially humidified membrane conductivity calculations. In single FCs, semi-empirical modelling is more accepted. Semi-empirical models are used in stack-modelling in which the models require more details and computing capacity.

The use of semi-empirical relations is necessary sometimes because of a lack of better alternatives, but whenever possible it must be avoided.

5.3.1 Dynamic Models

Models which include the time dimension are called dynamic models. In dynamic models, FC operation is not constant but is dependent on time. Dynamic models are used for predictions of FC response or predictions for stacks, such as system level changes or disturbances in the operating conditions. The start-up, shut-down and voltage cycling can also be studied with the help of this tool.

Dynamic models are extremely dependent upon empirical correlations, since including the time dimension requires significantly more computing capacity and time than those required for solving a steady-state model, for example, in which the FC may be modelled using an equivalent circuit model consisting of electrical components like resistors and capacitors which are connected to simulate a FC (Al-Masri *et al*., 2014). This makes the models much simpler. Hence, in several cases, the FC is not the object of study because the constructed model focuses mainly on the system, for example (Abdollahzadeh *et al*. 2014). Dynamic models using physical as well as electrochemical correlations can provide the required estimations of the reaction times of FCs reaching steady-state operation after changes in the operating conditions.

5.3.2 Two-Phase Models

One of the most important aspects of PEMFCs in terms of modelling, as well as FC operation, is water management. Water is required to enhance the conductivity of ions in the membrane, but if too much water accumulates in the electrodes then it will obstruct mass transport to and from the sites of the reaction. Therefore, water management is very crucial for FC performance.

The two methods which are employed for the modelling of two-phase mass transport are the multiphase mixture type model and the multiplied type model. In the multiphase mixture type model, the phases are considered as a mixture for which equations can be solved (Siegel, 2008; Liu *et al*., 2016). The information for each phase can be calculated from the solution in the mixture. In the multiplied model approach both phases have a set of equations and both sets are solved simultaneously (Hutzenlaub *et al*., 2013). The latter method needs more computational capacity and a more efficient operator, as convergence is

comparatively hard to achieve. It also gives more accurate results and predictions for phenomena which cannot be achieved using the other method mentioned. Both models can only work with porous media flow, meaning cases in which Darcy's law is applicable, and thus it cannot not be used for modelling the behaviour of two-phase gas channels. This is considered problematic because the water accumulation process must be studied in three dimensions and across the field of flow, and not just as a GDL and MEA cross-section.

Some experimental techniques, like neutron imaging technology, electrochemical impedance spectroscopy (EIS) and X-rays can be used to study the transport of water and its accumulation in the FC, but more accurate two-phase models are more useful for studying and improving PEMFC water management. Several parameters for two-phase models are chosen in an arbitrary fashion or are derived from the results of experiments conducted on the coil (Carton *et al*., 2012).

It must be mentioned that several two-phase models sometimes use inaccurate boundary conditions for the channel boundary and the GDL where there is no liquid, but the water is in gaseous form (Abdollahzadeh *et al*., 2014). This is clearly not correct, as many experiments have shown the formation of water droplets in the channels (Liu *et al*., 2016). Several studies have suggested that novel boundary conditions are the solution to this problem; for example, a basic model for droplet formation on the boundary can be used (Carton *et al*., 2012; Hutzenlaub *et al*., 2013). However, the liquid water transported in the channels, which affects evaporation from the channels, has never been modelled correctly because Darcy's law does not apply in the channels. Hence the two-phase models are not modelled properly according to FC theory. After considering these issues, it is quite clear that two-phase modelling needs improvements before it can achieve trustworthy results.

5.4 Modelling Approach Proposed in This Thesis

The numerical modelling of the acoustic emission phenomenon, which takes place inside a FC, is a complicated process involving the coupling of non-linear systems of equations. The acoustic emission phenomenon is dependent on other phenomena that require modelling first. These include species transport, heat transfer and water content.

The 3-D and 2-D finite element dependent commercial type Multiphysics numerical equation solver (COMSOL 4.4) was used here to solve all the non-linear transport-coupled equations which describe the operations of AE.

By using the governing transport equation, the transportation of species is solved. The next step is to solve it using a loop-type algorithm. The PEMFC computational domain is sectioned into a definite number of elements by using a second-order Lagrangian algorithm. The electrochemical engineering COMSOL module is used for this type of analysis, and the COMSOL physics application modes are used for solving the equations formed due to electrochemical phenomena. Many such equations are used, like the prime transport equations, the governing transport equations, and the corresponding dependent variables:

1. The Navier-Stokes equation, which is incompressible, is coupled with Darcy's law, i.e. the Brinkman equation, for the simulating of the behaviour of the reactant fluid flow in porous media;
2. The Maxwell-Stefan multi-component type diffusion and convection module for the transport of reactant species and products along the acoustic emission (AE) domain;
3. General heat transfer in the PEMFC is assumed to be by conduction and convection.

A stationary and non-linear type numerical solver, combined with a direct-type linear solver (UMFPACK), is used because the source charge, in terms of conservation, makes it a non-linear problem. For more accuracy of the model, the comparative tolerance for the error was set at $1x10^{-4}$. In the case of parametric analysis, the parametric type solver of COMSOL is used here and the parametric variables are defined with a specific analytical range. The performance polarisation curves were obtained by varying the FC potential using the parametric solver of COMSOL. The parametric solver uses an iteration loop to change the variable values in the specified range.

The convergent behaviour of this non-linear type problem is very sensitive to the first estimation of the given solution. Hence, to accelerate the process of the numerical convergence of the given non-linear type problem, the incompressible type of Navier-Stokes equations, along with the Brinkman equation, are first solved

together to obtain a better estimation of the convective type viscous properties of the flow of the reactant. After this, the fully coupled type, which involves all the types of physics modes, is solved by using these values for an initial guess. This technique is used to avoid possible numerical instability in the convective type terms in small-sized channels of the gas-flow distributor. This is because the numerical modelling of flow behaviour in such small-sized channels can ultimately lead to fluctuations at the walls, which can further lead to numerical instabilities and may result in the simulation crashing. Hence, to minimise the numerical instabilities in such small flow channels, the useful concept of an artificial kind of diffusion is used in this case. Streamline diffusion is used here with a value tuning parameter of 0.25 and introduces stabilising terms to the Navier-Stokes equations of incompressible type to reduce the numerical instabilities in the given streamline direction for the fluid-flow.

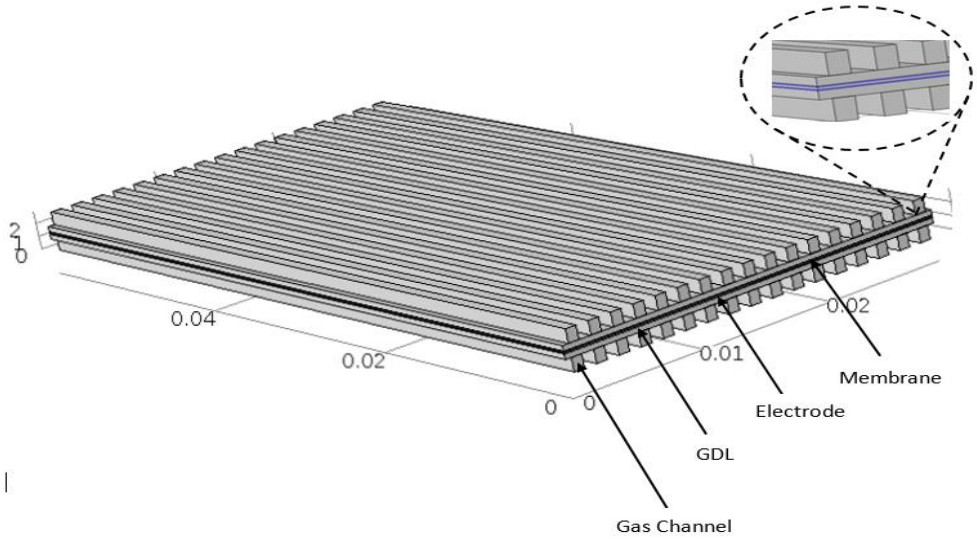

Figure 5.1: Three-dimensional diagram of the proton exchange membrane fuel cell.

5.4.1 Modelling Procedure

This section gives a general view of the underlying physics used in the models employed. The FC phenomena, which are modelled here, consist of the transfer of mass, along with charge, as well as electrochemical reactions and ultimately the acoustic emission (AE).

These are modelled with proper partial differential equations, as well as with boundary conditions which depend on the given model.

5.4.1.1 Assumptions

The assumptions which are made are as follows:

1. Heat transfer is negligible and is achieved by conduction in the gas phase
2. The type of electrode layer used is 'ultrathin'; hence, the diffusion of the gas in the electrode player can be easily neglected
3. The gas mixture used here behaves ideally
4. Liquid water is available in the form of small droplets
5. The electro-osmotic type of coefficient, along with the coefficient of diffusion in the membrane for water are mainly determined by the water activity in the channel of the anode flow. This is especially valid at places with high current densities because at this stage it is most likely that the membrane's anode side is drier in comparison with the cathode side.

Tables 5.1 and 5.2 illustrate the operating conditions and geometric properties of the PEMFC computational domain that is used in this thesis.

Table 5.1: Geometric properties of the PEMFC computational domain.

Parameter's name	Parameter Value	Description
C_L	0.06[m]	Cell length
C_W	0.02884528	Cell width
CH_he	$1*10^{-3}$[m]	Channel height
CH_Wid	0.07875[m]	Channel width
RIB_Wid	$0.90932*10^{-3}$[m]	Rib width
Ele_th	$50*10^{-6}$[m]	Porous electrode thickness
Mem_th	$50*10^{-6}$[m]	Membrane thickness

Table 5.2: Operating conditions values.

Parameter's name	Parameter Value	Description
eps_gdl	0.5	GDL porosity
kappa_gdl	$1.79*10^{-11}[m^2]$	GDL permeability
sigma_gdl	120[S/m]	GDL electric conductivity
wH_2_in Inlet H_2	0.844	mass fraction (anode)
wH_2O_in Inlet H_2O	00.0934	mass fraction (cathode)
wO_2_in Inlet	0.226	oxygen mass fraction (cathode)
U_in_anode	0.3[m/s]	Anode inlet flow velocity
U_in_cathode	0.3[m/s]	Cathode inlet flow velocity
U_anode	$1.19*10^{-5}$[Pa*s]	Anode viscosity
U_cathode	$2.46*10^{-5}$[Pa*s]	Cathode viscosity
MH_2	0.002[kg/mol]	Hydrogen molar mass
MN_2	0.028[kg/mol]	Nitrogen molar mass
MH_2O	0.018[kg/mol]	Water molar mass
MO_2	0.032[kg/mol]	Oxygen molar mass
Def(H_2_H_2O)	$6.8815*10^{-10}$ *(T)^1.75[m^2/s]	Binary gas diffusion coefficient (H_2_H_2O)
Def(N_2_H_2O)	$4.0141*10^{-11}$*(T])^1.75[m^2/s]	Binary gas diffusion coefficient
Deff(O_2_N_2)	$8.5640*10^{-7}$*(T)^1.75[m^2/s]	Binary gas diffusion coefficient
Deff(O_2_H_2O)	$2.4748*10^{-7}$*(T)*$10^{1.75}$[m^2/s]	Binary gas diffusion coefficient
T	298.15 [K]	Cell temperature
p_ref	$1*10^5$[P]	Reference pressure
V_cell	1.1[v]	Cell voltage
cO_2_ref	40.88[mol/m^3]	Oxygen reference concentration
cH_2_ref	40.88[mol/m^3]	Hydrogen reference concentration
eps_l	0.3	
eps_cl	1-eps_l-eps_gdl	Open volume fraction for gas diffusion in porous electrodes
kappa_cl	kappa_gdl/5	Permeability (porous electrode)
sigma	17.69[S/m]	Membrane conductivity
RH_air	95%	Relative humidity (air)
RH_fuel	95%	Relative humidity (Hydrogen)

5.4.1.2 Mass Transfer

Models of the reactant's transport are the building blocks of mass transfer modelling, which consists of the inert substances along with the reaction products in the FC. In a PEMFC, the reactants are H_2 on the anode and O_2 on the cathode and the reaction product is water. The inert phase is N_2, or a mixture of N_2 and air. Both of these gases are very much present in air and hence in the cathode part of a FC which operates in air. They never participate in the reactions but they do affect the transport of mass inside the body of the FC. Mass transport in the anode is excluded from the models used, as the phenomenon of performance limiting usually occurs on the cathode side because of the slower type of reaction kinetics mechanism, which increases the risk of flooding. In this thesis, the distribution of electrode reactants is the focus of mass transport modelling; on the one hand is the flow-field study on the scale of the entire FC, and on the other hand is the study of the scale of individual ribs and channels.

Species are transported on to the cathode through convection as well as by diffusion. A pressure difference of an external nature is applied across the FC creating the FC flow. In the case of free convection, density variations are produced in the air, caused by differences in concentration and temperature. The reactants are consumed on the electrode and reaction products are generated on the electrode as well, which creates a density gradient and concentration gradients. The fluid flow passes into the channels, the electrode and the diffusion layer of porous gas. The membrane can transport water, but it is impermeable to gases.

The fluid flow is modelled in the channels, with the continuity equations and the Navier-Stokes (5.1) and (5.2). These equations model standard laminar equations for flows of an incompressible nature. There is no exact change limit for laminar to turbulent flow, but the flow of the fluid can usually be laminar if the flow's Reynolds number is below 2,300. In the FC type environment, this condition is actually met, and the flows are relatively slower. In the gas diffusion layer as well as the electrode, Darcy's Law is used.

$$\rho\left(\frac{\partial u}{\partial t} + u.\nabla u\right) = -\nabla P + \nabla.\left(\varepsilon(\nabla u + (\nabla u)^T) - \frac{2}{3}\varepsilon(u.\nabla u)I = S\_(SN\ )\right. \quad (5.1)$$

$$\nabla.(\rho u) = S_{con} \quad (5.2)$$

$$\nabla.\left(\rho.\frac{\varepsilon}{k}\nabla p\right) = S_D \tag{5.3}$$

Where:

ρ : the average fluid density;

u : the velocity vector;

P : the fluid pressure;

k : the permeability of the porous medium;

S : the source of the term of every equation;

ε : the viscosity of the fluid.

Equations (5.2) and (5.3) model the velocity pressure, in terms of fluid behaviour in the frame centre mass. For driven flow concentration calculations, diffusion should also be modelled. Using the simple diffusion equation (i.e. Fick's Law) in a FC cathode is considered incorrect; however, the fluid has three constituents (oxygen, water and nitrogen) that have different sources, diffusion and sinks constants. Hence, diffusion equations of the multicomponent type, or of the Maxwell-Stefan type, (5.4) and (5.5), have to be employed *(Hashimoto et al*., 2012).

Although the Maxwell-Stefan equations for each component can be written, they need to be solved only for the first two, as the third component can be calculated from the first two, as the mass fractions will add up to one. Hence, the mass fraction of nitrogen (N_2) is calculated from those of water (H_2O) and oxygen (O_2).

$$\nabla.\left(-\rho\omega_i \sum_{j=O_2,H_2O,N_2} \widetilde{D_{ij}}\left(\nabla x_j\right) + \rho\omega_i u\right) = S_i^{mass} \tag{5.4}$$

Here: $i = O_2, H_2O, and\ N_2$

$$\nabla x_j = \frac{M^2}{M_j}\sum_{\substack{K=O_2,H_2O,N_2 \\ K\neq j}}\left(\frac{1}{M} + \omega_k\left(\frac{1}{M_K} - \frac{1}{M_j}\right)\right)\nabla\omega_k \tag{5.5}$$

Here, ω_i is the species mass fraction of i, $\widetilde{D_{ij}}$ represents the Maxwell-Stefan diffusion coefficient, M_j represents the molar mass and x_j the species molar fraction of j. Maxwell-Stefan equations can be expressed for molar fractions as follows:

$$\nabla.(Cx_i u) - \nabla.\left(C\widetilde{D_{eff}}\nabla x_i\right) = S_i^{molar} \tag{5.6}$$

The formulations in equations (5.4) and (5.6) are similar and both forms are used in this thesis.

The source term, S, used in equations (5.1), (5.2) and (5.3) arise from the reactions in the PEMFC. They consume oxygen (O_2) and produce water (H_2O). Hence, they exist only in the electrodes and not anywhere else. The exceptions are the source terms in the Naiver-Stokes continuity equations in that they are used in the model of the flow-field in which the only PEMFC component modelled is the flow-field and hence the reaction's effects are modelled as if they have occurred inside the channels.

$$S_{NS} = -\frac{i_o A}{2FV_{Ch}} M_{o2} u \tag{5.7}$$

$$S_p = -\frac{i_o}{4F}(M_{Ho2} - M_{o2}) \tag{5.8}$$

$$S_{Con} = -\frac{i_o A}{zFV_{Ch}}(\xi M_{Ho2} - M_{o2}) \tag{5.9}$$

$$S_i^{Mass} = \begin{cases} -\frac{i_o}{4F} M_{o2} \ , i = o_2 \\ \frac{i_o}{2F} M_{Ho2} \ , i = H_{2O} \end{cases} \tag{5.10}$$

$$S_i^{Molar} = \begin{cases} -\frac{i}{4F} \ , i = o_2 \\ \frac{i}{2F} \ , i = H_{2O} \end{cases} \tag{5.11}$$

where i_o represents the electrode current density reactant, A is the active area, z is the number of electrons in the reaction, F is Faraday's number, ξ is the portion of water in the reaction products leaving the FC from the anode, while V_{Ch} is the channel's volume. A part of the reaction's water product can be from the anode to the cathode, driven by diffusion.

The local current density changes along the channel length as the overvoltage of the electrodes, as well as the conductivity of the membrane, varies. The parameter signifies the net water molecules per unit of proton flux ratio (Wang & Nguyen, 2010). The method of calculation is as follows:

$$Net\ water\ flux = N_{w,y,a}(x) = \alpha \frac{I_0}{F} = n_d \frac{I_o}{F} - D_w \frac{dc_w}{dy} \tag{5.12}$$

Where the effect of migration is the first term on the right side, and the second represents diffusion. Manipulation of this yields the following equation:

$$\alpha = n_d - \frac{F}{I_0} D_w \frac{d_{cw}}{d_y} \tag{5.13}$$

This can be simplified by assuming the difference in water accumulation of the cathode with respect to the anode can be approximated by a linear difference of a single step.

$$\alpha = n_d - \frac{F}{I_a} D_w \frac{c_{w,c} - c_{w,a}}{\delta_{thick}} \tag{5.14}$$

Where: δ_{thick} is the thickness of the membrane.

The parameter, '*nd*', is the electro-osmotic drag coefficient, which usually is equal to the number of water molecules that are carried by protons. This quantity is highly dependent on the content of the water in the given membrane, which is a function of the water activity in the gas phase adjacent to that membrane. The partial dehydration that exists along the anode, as well as the saturation which exists along the cathode, is very likely to occur especially at current densities of higher magnitude. This is due to the higher transport rate of water because of the electro-osmosis (also called drag) from the anode to cathode compared to the back-diffusion rate of the water from the cathode and the anode. Physically, this means that the water content of the anode side is lower. For the same reason, the water activity on the anode side may be used to calculate the electro-osmotic coefficient in the membrane. The electro-osmotic coefficient is a function of the water activity in the lower channel of the anode used [Liu *et al*., 2007) and can be expressed as:

$$n_d = \begin{cases} 0.0049 + 2.02a_a - 4.53a_a^2 + 4.09a_a^3 & a_a \leq 1 \\ 1.5 + 0.159(a_a - 1) & a_a > 1 \end{cases} \tag{5.15}$$

The parameter, D_w, needs to be calculated. This gives the coefficient of water diffusion in the membrane. It is believed that the coefficient of diffusion of water in a given membrane is dependent on the content of the water in the membrane, in the same way as the coefficient of electro-osmosis.

$$D_w = n_d D^o exp\left[2416\left(\frac{1}{303} - \frac{1}{T_s}\right)\right] \quad (5.16)$$

The water accumulation is a function of the water activity in the electrodes and is given by:

$$C_{w,k} = \begin{cases} \frac{\rho_{m,dry}}{M_{,m,dry}}(0.043 + 17.8a_k - 39.8a_a^2 + 36.0a_{ak}^3 & a_k \leq 1 \\ \frac{\rho_{m,dry}}{M_{,m,dry}}(14 + 1.4(a_k - 1)) & a_k > 1 \end{cases} \quad (5.17)$$

Either the anode or the cathode is substituted for the subscript k. $\rho_{m,dry}$, and $M_{,m,dry}$ are the dry proton exchange density and the equivalent weight of a. The anode and cathode water activity are as follows:

$$a_a = \frac{x_{w,a}P}{P_{w,a}^{sat}} = \left(\frac{M_{w,a}^v}{M_{w,a}^v + M_{H_2}}\right) * \frac{P}{P_{w,a}^{sat}} \quad (5.18)$$

$$a_c = \frac{x_{w,c}P}{P_{w,c}^{sat}} = \left(\frac{M_{w,c}^v}{M_{w,c}^v + M_{O_2} + M_{N_2}}\right) * \frac{P}{P_{w,c}^{sat}} \quad (5.19)$$

The water vapour can be determined by the following equation:

$$log_{10}P_{w,k}^{sat} = 2.95 * 10^{-2}(T_k - 273.15) - 9.18 * 10^{-5} * (T_k - 273.15)^2 + 1.44 * 10^{-7} * (T_k - 273.15)^3 \quad (5.20)$$

The change in mole number of every reactant can easily be determined by performing a substitution of equations (5.13) – (5.15) into equation (5.18). Equation (5.19) describes the methods by which the reactants can be consumed:

$$\frac{dM_i}{dx} = -hN_{(H_2,O_2,N_2),y,k}(x) \quad (5.21)$$

The change in the number of moles of liquid water in each flow-type channel is determined by the rates of evaporation and condensation (Das *et al*., 2010):

$$\frac{dM_{w,k}^1}{dx} = \left(\frac{K_c h d}{RT_k}\right) * \left(\frac{M_{w,k}^v}{M_{w,k}^v + M_{\frac{H_2}{O_2}}} * P - P_{w,k}^{sat}\right) \quad (5.22)$$

Where:

K_c is the homogeneous rate constant for condensation as well as for water evaporation, whilst *h* and *d* are the width and height of the given channel.

The amount of liquid water in the flow channels is directly proportional to the difference between the partial pressure and the water vapour pressure. Physically, this simply means that liquid H_2O will condense if the partial pressure of water vapour becomes higher than the vapour pressure, while if liquid water is also present and the partial water vapour pressure is lower than its vapour pressure, then the liquid H_2O will surely vaporise. The change in the number of moles of water vapour along the flow-channels is given by the following equation:

$$\frac{dM_w^{v,k}}{dx} = -\frac{dM_w^{1,k}}{dx} - hN_{w,y,k}^{v}(x) \tag{5.23}$$

The factors mentioned above affect the amount of water vapour in the flow channels:

(1) The reaction of oxygen (O_2) with the proton and electron at the cathode produces the water as result of the union between oxygen and hydrogen molecules;

(2) The water (H_2O) generated at the cathode may be used in the membrane up to the anode because of the difference in concentration;

(3) Here, the protons which migrate from the anode up to the cathode can bring the water vapour with them (i.e. via drag or electro-osmosis); and

(4) Water vapour condensation and liquid water evaporation are dependent on the difference between partial pressure and vapour pressure.

The first term on the right-hand side of equation (5.23) signifies condensation as well as evaporation, while the second term is the total water vapour transport across the membrane. The water transport is the result of the difference in concentration, pressure, and number of water molecules, which are carried by the migrating protons.

5.4.1.3 Charge Transfer

The transfer of charge in a PEMFC consists of the movement of electrons and ions. Hence, it is important to model both ionic and electronic potential individually (Lu *et al*., 2011).

The former exists in the membrane and electrodes only, and the latter in the electrodes and GDLs only. Charge transfer, of ionic or electronic nature, is modelled by:

$$-\nabla.\left(\sigma_{membrane\,,GDL}\,\nabla\psi_m\right) = S_m \tag{5.24}$$

The conductivity, $\sigma_{membrane,GDL}$, is a membrane humidity function. The source terms,S_m representing electronic potential as explained in equation (5.25):

$$S_m \begin{cases} i_a \\ -i_c \end{cases} \quad and \begin{cases} -i_a \\ i_c \end{cases} \tag{5.25}$$

The reaction current densities, i_a and i_c, at the electrodes are calculated mathematically as per equation (2.26) in Chapter 2. An aspect of heat and charge transfer in a FC is that the variables are not continuous in different FC components. This is because of the components' contact resistances, like that between the GDL and the electrodes. There is spatial variation in contact resistances, as compression of the components produces such changes on the scale of the completely active area as well as locally in the ribs and the channels (Grimm et al., 2012). The differences in thermal and electric contact resistances have a large effect on FC performance and lifetime.

5.4.1.4 Heat Transfer

Despite PEMFCs operating at a lower temperature compared to FCs such as solid oxide fuel cells (SOFCs) and molten carbonate fuel cell (MCFC), however, heat transfer is an essential factor for the performance of FCs. Due to local temperature variations, as well as in the current density, hot spots occur. The FC performance is not affected significantly by hot spots, but they can cause premature degradation of the membrane and hence they can shorten FC lifetime. Modelling of heat transfer is

very straightforward. There are only two methods of transfer of heat inside the FC namely:

1. Convection
2. Conduction.

Heat transfer by radiation is not very significant in PEMFCs as the temperature, as well as the contact resistances and the thermal bulk, are comparatively low. Heat transfer is modelled according to equation (5.26):

$$\nabla.(k\nabla T) = \sum_i C_{p,i}\,, i\rho_i u.\nabla T + S_T \tag{5.26}$$

Heat is produced from both reactions, and by Ohmic heating due to the electronic and ionic currents. Hence, the thermal source, S_T , in each region is:

$$S_T \begin{cases} {\sigma^s}_{GDL,}(\nabla\psi_G)^2 \\ {\sigma^m}_{membrane,}(\nabla\psi_m)^2 \\ {\sigma^s}_{CL,}(\nabla\psi_s)^2 + {\sigma^m}_{CL,}(\nabla\psi_m)^2 + i_a\phi_a + \frac{i_a T\Delta S_a}{2*F} \\ {\sigma^s}_{CL,}(\nabla\psi_s)^2 + {\sigma^m}_{CL,}(\nabla\psi_m)^2 - i_c\phi_c - \frac{i_c T\Delta S_c}{4*F} \end{cases} \tag{5.27}$$

Here, σ is the ionic or the electronic conductivity of the GDL for catalyst and membrane (CL), ψ_i and ψ_e are the electronic and ionic voltage, ϕ_a and ϕ_c are the overvoltage of the cathode and anode, i_a and i_c are the densities of the reaction current at the cathode and anode, T is the temperature, and ΔS is the change in reaction entropy (Gao *et al*., 2011). From the given equation (5.26), we can note that, as i_c is of negative magnitude, the cathode source terms have negative signs.

The movement of electrons and ions constitutes the transfer of charge in a PEMFC. Hence, it is required to model both electronic and ionic potential individually. The former exists only in the electrodes and membrane while the latter exists in the GDLs and electrodes. The charge transfer, whether ionic or electronic, is modelled by:

$$-\nabla.\left(\sigma_{membrane\,,GDL}\,\nabla\psi_{i,e}\right) = S_{i,e} \tag{5.28}$$

The conductivity, $\sigma_{membrane\,,GDL}$, is a membrane humidity function. The source term,S_i represents the ionic potential, while S_e represents the electronic potential and both are non-zero in the electrodes:

$$S_m = \begin{cases} i_a\,, & at\ anode \\ -i_c, & at\ cathode \end{cases} \quad and \quad S_s = \begin{cases} -i_a\,, & at\ anode \\ i_c, & at\ cathode \end{cases} \tag{5.29}$$

The reaction current densities, i_a and i_c, are calculated at the electrodes according to equation (3.18) given in Chapter 3. An aspect of charge and heat transfer in FCs is that these variables are non-continuous between different components of the FC (Lobato *et al*., 2010; Wang *et al*., 2011). This is because of the contact resistances between the FC components, e.g. the electrodes and the GDL. Spatial variation is present in contact resistances, as the compression applied to these components varies on the local scale of the ribs and channels and on the scale of the completely active area. The differences in electric and thermal contact resistances have an important effect on FC performance and lifetime.

5.4.2 A Novel Semi-Empirical Model

In addition to 3-D and 2-D models, realistic mathematical models were developed and implemented in a MatLab/Simulink® environment to get an overview of the system's behaviour. Some of parameters, such as temperature, pressure, water content and current density have been studied to evaluate the effect of PEMFC system reliability. The proposed model depends on principle equations, combined with equations having experimentally defined parameters, thus resulting in a semi-empirical system. The mathematical model equations describe the operation of the FC composed of the voltage-current characteristics and a relationship for the temperature and pressure as a function of the current density from the FC.

As mentioned earlier in Chapter 3, there three different types of losses that occur within the FC, namely: activation losses, Ohmic losses and concentration losses.

5.4.2.1 Modelling of Activation Polarisation

The activation losses have been considered in two parts: activation losses 1 (Act 1) and activation losses 2 (Act 2). Act 1 occur due to the temperature and current-dependent voltage drop. However, it has been converted into an equation of univalent resistance first, and then it will be combined with concentration losses and the capacitor due to the double–layer changing effect to give the voltage drop (Act 2). The activation polarisation was modelled based on the equation below:

$$\eta_{act} = -0.9514 + T * 0.00312 + T * 7.4 * 10^{-5} * [ln(C * O_2] - 0.000187 * ln(i_o) \quad (5.30)$$

$$C * O_2 = \frac{P_{O2}}{5.08*10^6\, EXP\left(\frac{-498}{T}\right)} \quad (5.31)$$

Where: i_o is the exchange of current density and C*O_2 is the density of the hydrogen on the catalyst layer.

Figure 5.2 illustrates the activation modelling which is dependents on both temperature and current density. The activation polarisation occurs at low current density because of the slowing of the oxidation reaction at the negative electrode. This leads to a reduction in the number of electrons that are emitted.

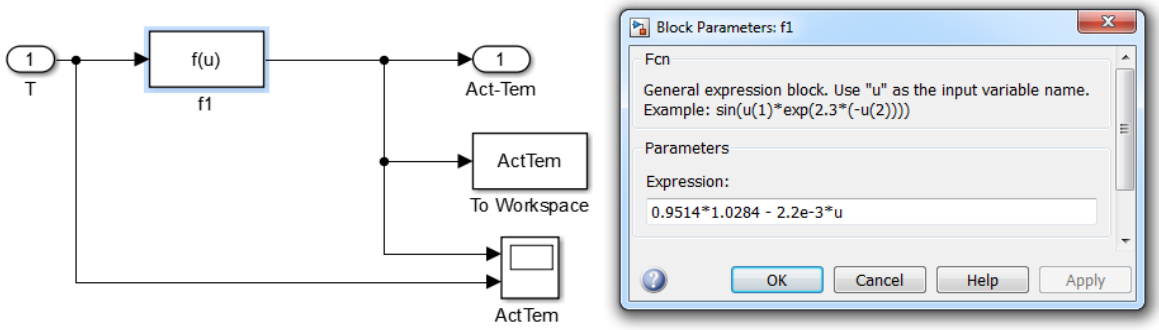

Figure 5.2: Modelling of activation polarisation dependent just on temperature.

Figure 5.3 illustrates the impact of current density on activation losses. The activation voltage has a higher value at low current density because significant numbers of electrons are not emitted, as illustrated in figure 5.3.

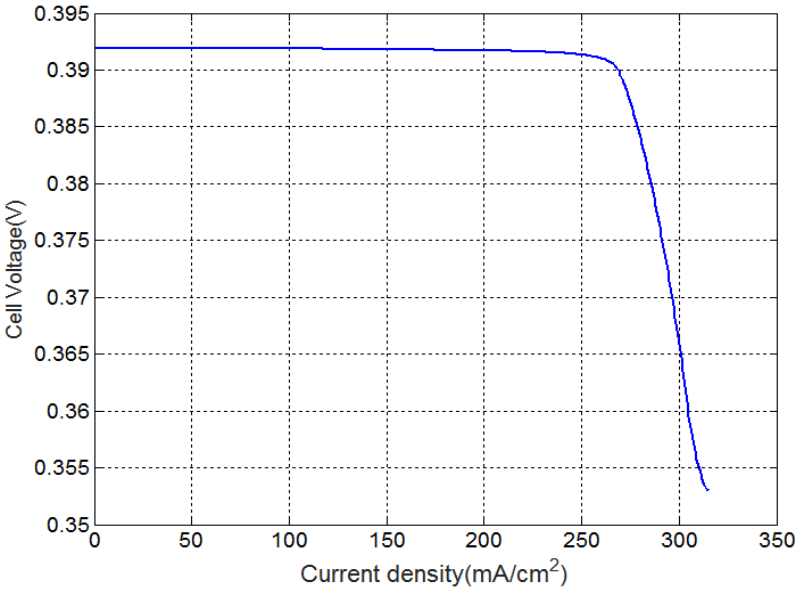

Figure 5.3: Polarisation activation curve dependent only on temperature.

The relationship between the activation polarisation with both current density and temperature is depicted in figure 5.4. The activation losses are decreased when the current density is increased.

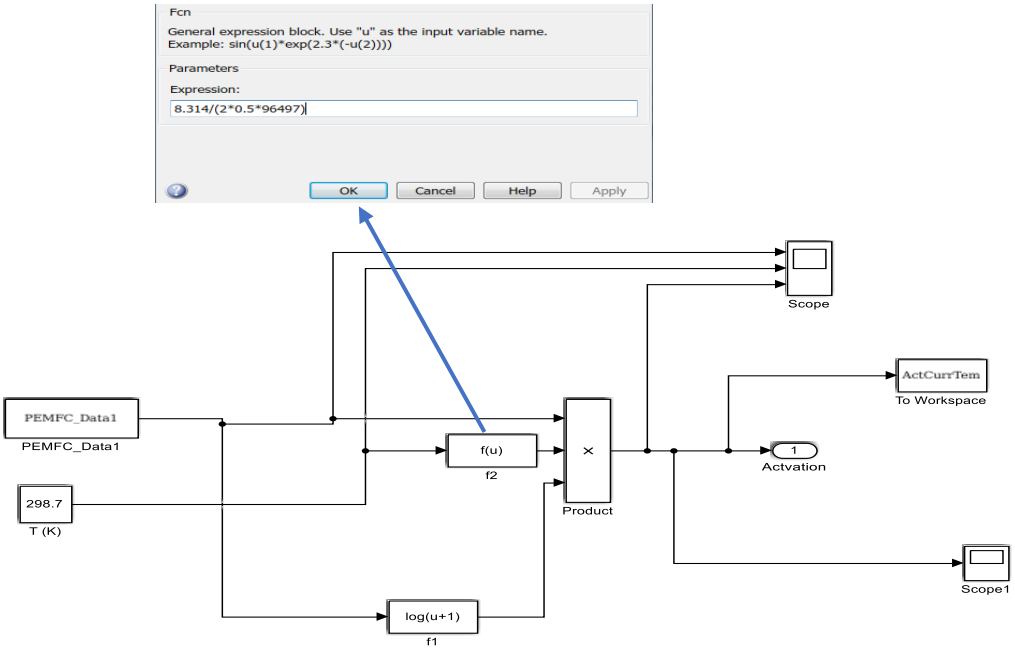

Figure 5.4: Modelling activation losses dependent on temperature and current density.

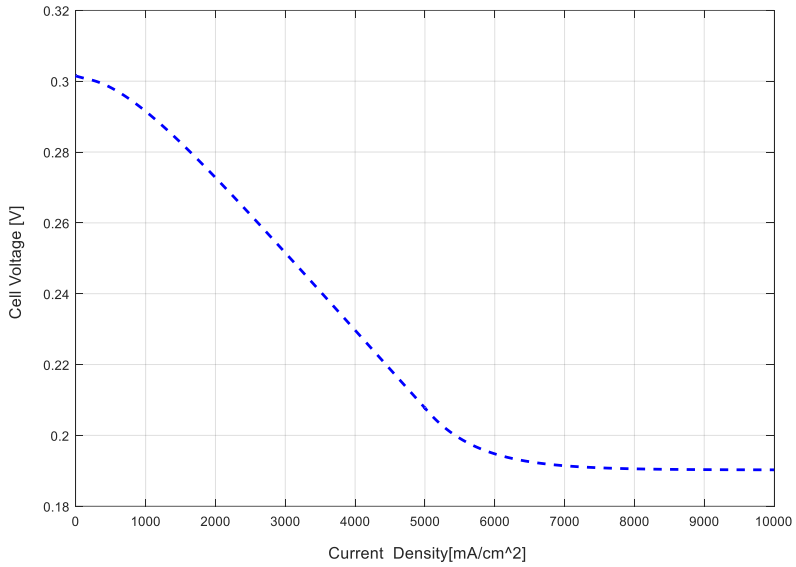

Figure 5.5: Polarisation activation curve dependent on temperature and current density.

5.4.2.2 Modelling of Ohmic Polarisation

The Ohmic polarisation (η_{ohm}) is directly proportional to the current. Since the cell's resistance is almost constant, the Ohmic polarisation changes linearly and this is because of the emergence of resistance during the crossing of ions in the electrolyte and Ohmic resistance in the electrodes. The reduction of these resistances using the appropriate electrolyte and metals in the electrodes can be adopted to overcome this problem, and the equation can be written as follows (Al-Baghdadi *et al*., 2005):

$$\eta_{ohm} = I * R^{internal} \tag{5.32}$$

Where: *I* represents the current of the cell and;

$R^{internal}$ is the internal resistance of the cell, and is modelled using the following relationship (Alrweq & Albarbar, 2016):

$$R^{internal} = 0.01605 - 3.5 * 10^{-5} * T + 8.0 * 10^{-5} * i \tag{5.33}$$

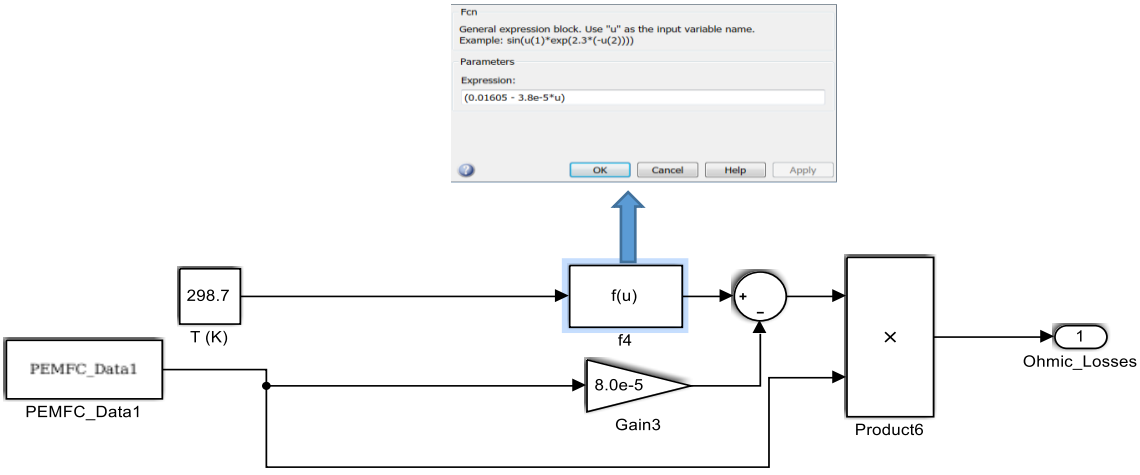

Figure 5.6: Modelling of Ohmic polarisation.

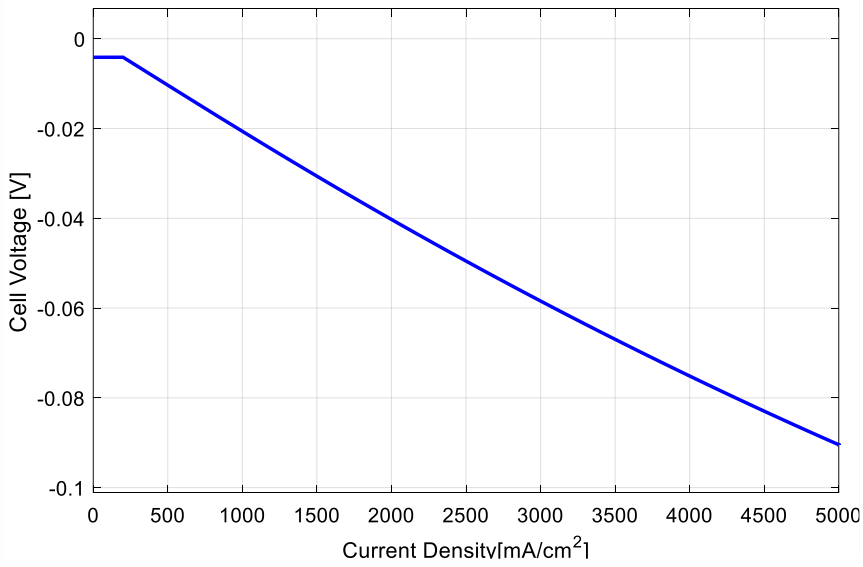

Figure 5.7: Ohmic polarisation as a function in current density.

5.4.2.3 Modelling of Concentration Polarisation

Figure 5.8 illustrates the MatLab Simulink that was used to obtain the concentration polarisation, while figure 5.9 illustrates the concentration polarisation of a PEMFC under typical operating conditions ($80^{o}C$ and 1 atm).

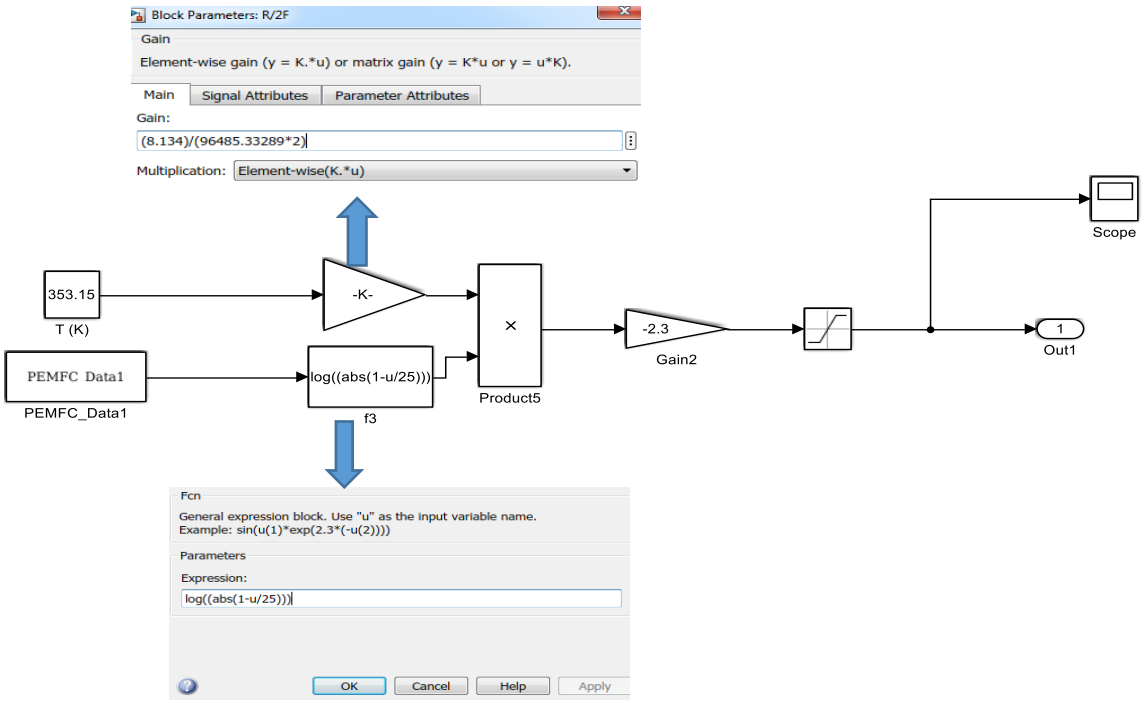

Figure 5.8: Modelling concentration polarisation.

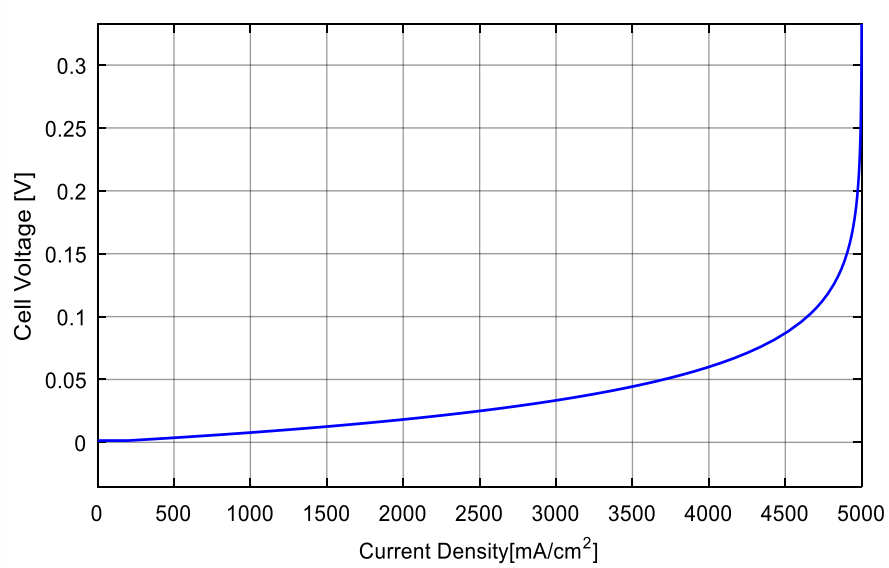

Figure 5.9: Polarisation concentration curve.

To investigate the influence of temperature on the concentration polarisation, equation (2.38) in Chapter 2 is plotted for two values of temperature for the cathode, as depicted in figure 5.9. Figure 5.9 shows clearly that the concentration losses increase slowly with current density. This satisfies the Nernst equation. However, this is counter-balanced by the increase in the kinetics of the chemical reaction as

predicted by the kinetic theory of gases. Nevertheless, the behaviour of concentration losses in a FC is a complex phenomenon and it involves many factors. The main factor is the water that was produced at the cathode due to the chemical reaction, which increases at high current densities. Simultaneously, water evaporation increases at higher temperatures, and this causes the reduction of the species transport limitations and thus the concentration losses, but this could cause membrane dehydration and a reduction in its proton conductivity. Consequently, it is not straightforward to predict the voltage behaviour due to the variation of one parameter without considering the interactions of other parameters, which necessitates the implementation of more advanced analytical tools such as Comsol modelling and simulations. Such simulation tools can be used to virtually describe the effect of some parameters on the concentration losses and the PEMFC V-I curve. There is a need to consider the correlation among these parameters and their effects on the voltage behaviour.

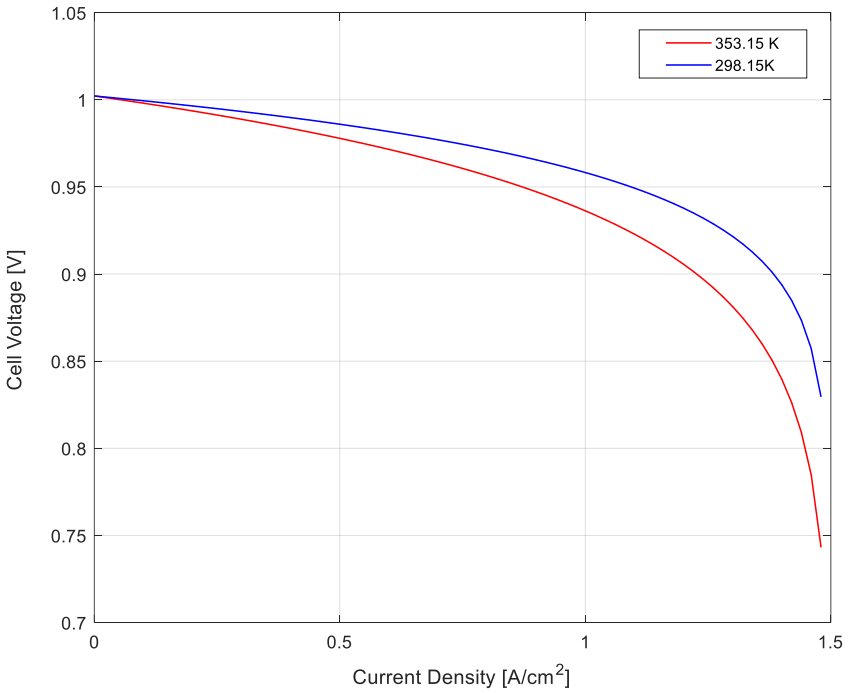

Figure 5.10: Concentration potential at the cathode side vs different temperature values.

5.4.2.4 Modelling of Active Pressure

The circuit in figure 5.11 was used to simulate the active pressure at both the anode and cathode sides. This model helps to find out the effect of the pressure at the anode and cathode on output voltage of the FC. The pressure of hydrogen at the anode side and oxygen pressure at the cathode side are dependent on current density and temperature.

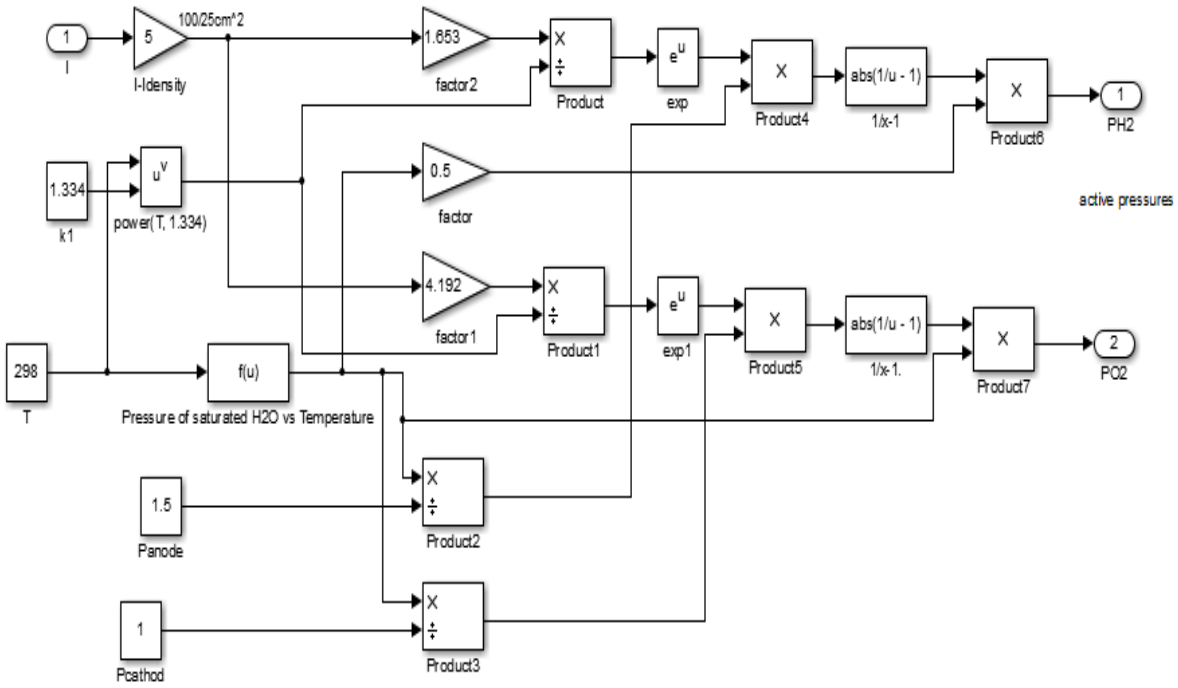

Figure 5.11: Modelling of active pressure.

The result of chemical reactions inside a FC is reversible single electrode voltage, E, given by the Nernst equation as shown in figure 5.12.

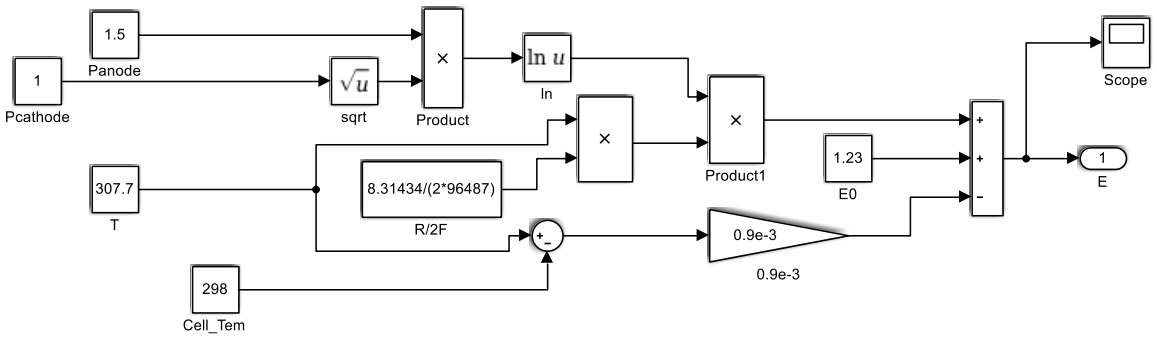

Figure 5.12: Modelling of the Nernst equation.

The output voltage of PEMFC depends on parameters that are contained in three major losses and Nernst Equation. Equations (5.32) and (5.33) are used to calculate the output voltage of the cell. The final system implementation for the output voltage of PEMFC is tackled in figure 5.13.

$$V = E_o - \eta_{act} - \eta_{ohm} - \eta_{con} \tag{5.34}$$

$$V = \left(1.23 - 0.9 * 10^{-3}(T - 298) + \frac{RT}{4F}(ln(P^2H_2 * PO_2)) \right. \left. - \left[-0.9514 + T * 0.00312 + T * 7.4 * 10^{-5}[ln(C * O_2)] + 0.000187 * ln(i) + (-i * (0.01605 * 10^{-5}) * -3.5 * T + 8.0 * 10^{-5} * i)\right) - \left(-\beta * ln\left(1 - \frac{I}{I_{max}}\right)\right)\right] \tag{5.35}$$

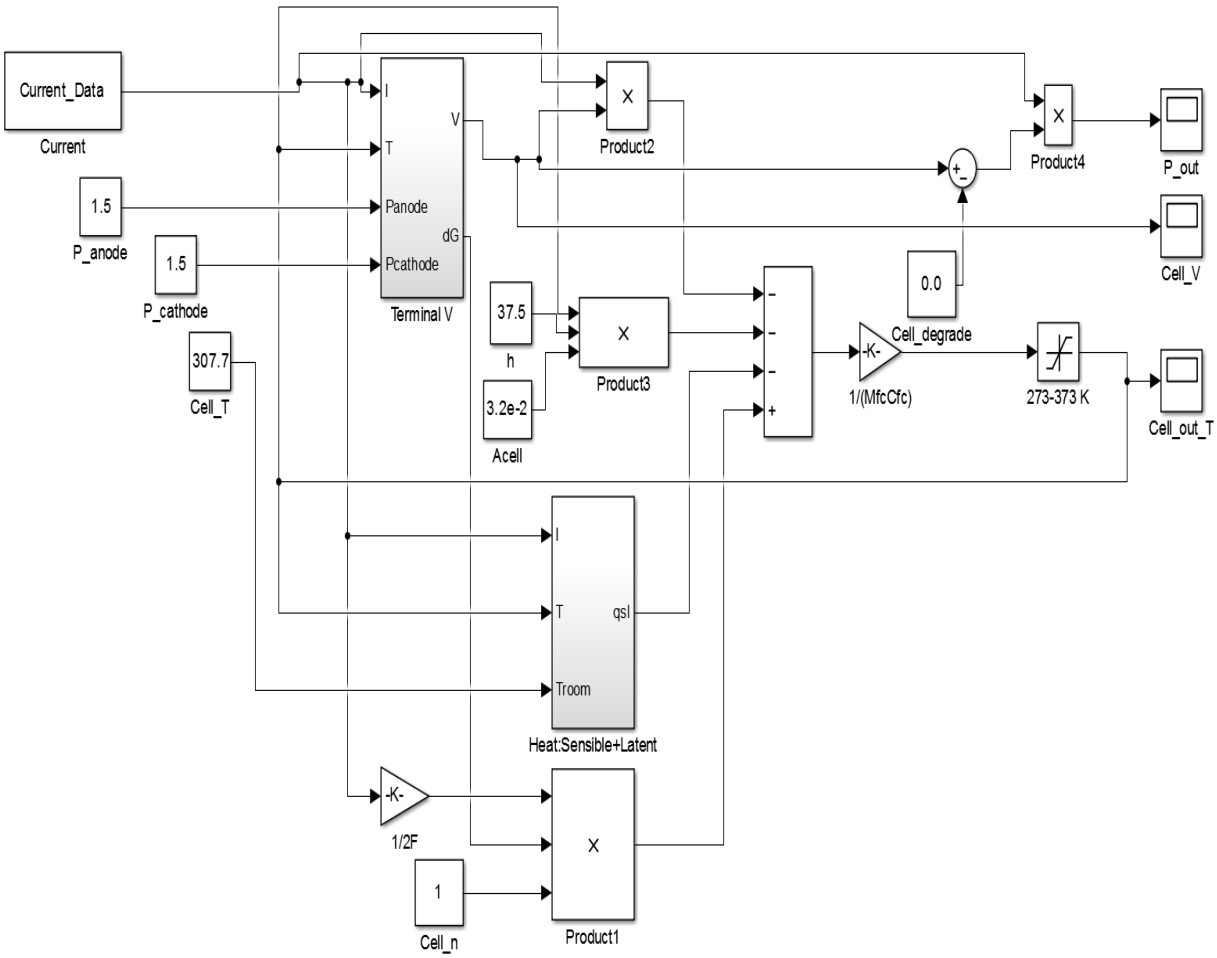

Figure 5.13: Full model to simulate a proton exchange membrane fuel cell.

5.5 Summary

Modelling is performed to capture the aspects of a PEMFC's system that are of interest for study. Knowledge of FC phenomena, such as electrochemical, thermodynamic and transport processes, material properties, and various interactions are useful in formulating a model. 3-D and 2-D models are more accurate in the study of the phenomena that occur in 1-D. However, 3-D and 2-D need additional time and a computer with high specifications to complete the simulation. A mathematical model, which describes certain aspects of a FC system and predicts its behaviour, may be a set of equations, algebraic or differential, or a computer-based procedure or sub-routine.

In this chapter, a dynamic model of a PEMFC system has been presented. This model is based on a combination of experimental data and parametric coefficients in theoretical equations. Such a pattern of modelling is called a semi-empirical dynamic model. The values of the most critical empirical parameters have been determined and an estimation made of their effect on the performance and reliability of the cell. The experimental data have been gathered from a real PEMFC testing unit. The methodology utilised in the underlying experimental study and the model-based validation was implemented. The advantage of this model lies in that it can be used to model different FC types after a proper adjustment of the physical parameters.

CHAPTER 6

RESULTS AND DISCUSSION

This chapter presents the results of the effect of temperature and pressure on proton exchange membrane fuel cell (PEMFC) performance. In addition, the results of acoustic emission and water flooding that have been obtained from experiments and simulations are presented and discussed in depth.

6.1 Overview

Acoustic emissions (AEs) are stress waves produced by the sudden internal stress redistribution of the materials which is caused by changes within the internal structure. AE's are also the spontaneous fluctuations of voltage and/or current generated due to electrochemical processes. Some dynamic chemical systems, especially systems that involve phase transition, are acoustically active. Chemical changes during interactions are usually accompanied by energy transfer and some part of this energy may be converted to AEs.

As explained in chapter 2, in hydrogen fuel cells (HFCs), the fuel (hydrogen) splits into electrons and protons at the anode. Protons travel through the membrane (electrolyte) while electrons migrate into the cathode via an external circuit. At the cathode, oxygen molecules unite with electrons and protons that have migrated from the anode, resulting in generation of water and heat. The movement of water bubbles and collisions with each other will result to emission of acoustic signals. Sufficient understanding of this phenomenon will open the door to non- intrusive monitoring and diagnosis techniques for PEMFC.

To gain clearer understanding on effects of operational parameters on the induced AE signals, a series of experiments were carried out to validate the developed 2-D finite element model, using COMSOL software package.

Furthermore, 3-D finite element model, using COMSOL software package were utilised to investigate the impact of water management on the cell performance and efficiency.

6.2 Effect of Temperature and Pressure on Cell Performance and Efficiency

6.2.1 Effect of Temperature

Figure 6.1a shows the relationship between the temperature and cell performance at constant pressure (1 atm). From the fig it can be noticed that the an increase in the temperature improves the performance of the cell, and reduces voltage losses, which leads to a reduction of voltage dropping factors, especially the decline in the activation losses and improves the overall outcome of the cell. However, under

operational conditions, in order to prevent the loss of humidity, which is significantly important to boost the membrane conductivity, the temperature of the polymeric PEMFC should not exceed 80^{o}C.

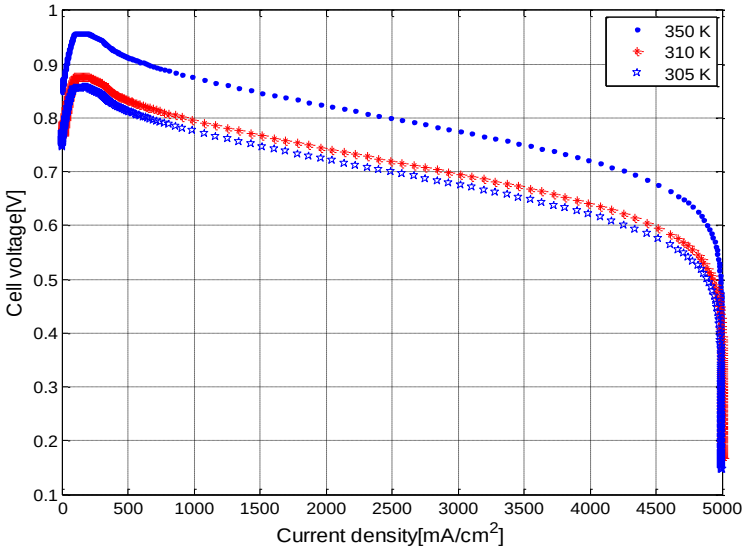

Figure 6.1a: The effect of temperature on PEMFC output voltage.

Figure 6.1b depicts the modelling results of the temperature in the interior layers.

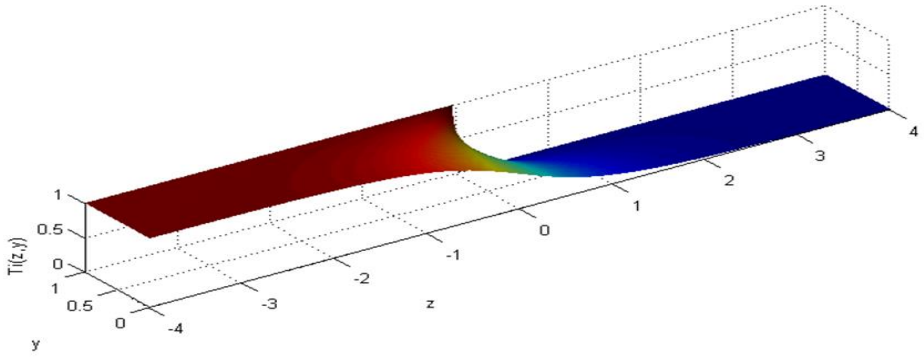

Figure 6.1b: Temperature in interior layers.

6.2.2 Effect of Pressure

Figure 6.2 shows the improvement in the performance of the polymeric PEMFC with three different values of pressure and constant temperature (298.15K). The increase in pressure values must be within the allowable pressure range as instructed by the datasheet (high pressure value may cause damage to the delicate components, such as the membrane). From figure 6.2, it can be seen that increased pressure will

improve the performance only slightly. This increase in the pressure value decreases the temperature.

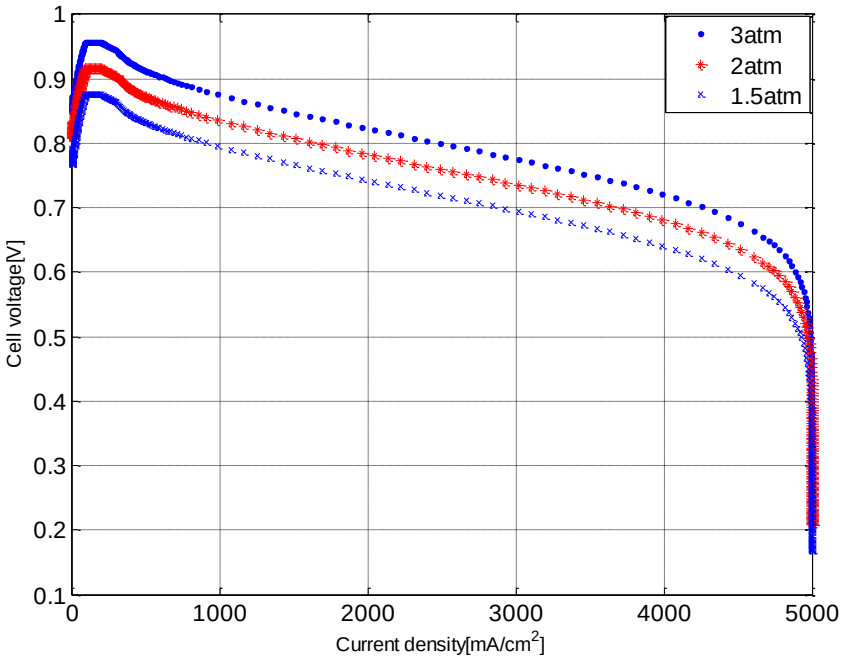

Figure 6.2: Effect of pressure on PEMFC output voltage.

6.2.3 Polarisation Curve and Power Density

Figure 6.3 shows the polarisation curve of the PEMFC for two cases of operation. The first case is of the cell working under the conditions of a set temperature and pressure (353 K and 3 atm). The second case is of operation within the statutory requirements of 323K and 1.5 atm), which shows the decline in output of the cell. Polymeric FCs typically operate at a temperature of 70-90^{O}C and atmospheric pressures of 1.5-3.5 atm since these are when the cell gives its highest output. Therefore, figure 6.3 shows that at low temperature and pressure, the voltage declines 0.1 V, and it causes a decline in the output by 10 % of its nominal value.

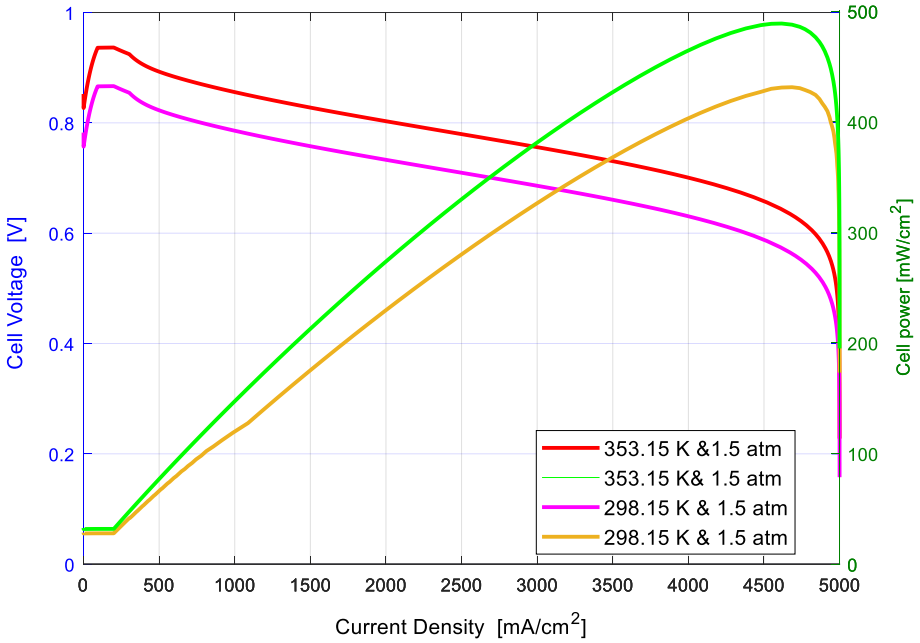

Figure 6.3: The effect of pressure and temperature on both output voltage and power.

6.3 Acoustic Emission Phenomena

Water bubbles are generated as result of the reaction between hydrogen and oxygen at the cathode side. The source of AE signals is the flow and friction between water bubbles.

The Minneart resonance equation can be used to find the bubbles' resonance frequencies f_o at a particular radius as below:

$$f_o = \frac{1}{2\Pi a}\left(\frac{3\Upsilon p_a}{\rho}\right)^{1/2} \tag{6.1}$$

while the volume of the bubbles can be determined by the equation below:

$$V = \frac{1}{(6*\pi^2*f_o)} * \left(\frac{3*\gamma*p_a}{\rho}\right)^{3/2} \tag{6.2}$$

where a is the radius of the bubble, Υ is the polytrophic coefficient, p_a is the ambient pressure, and ρ is the density of water.

Table 6.1 outlines the frequencies of the generated acoustic signals associated with bubble sizes. That confirms two important outcomes; the first is the generation of acoustic signals during this process and the second identifies the frequency bands of such generated signals as being between 100 kHz and 850 kHz.

Figures 6.4 and 6.5 depict the effect of the different load values on AE density.

Table 6.1: Approximation of the size and volume of bubbles based on frequency information of the average power spectrum.

Frequency (kHz)	Bubble radius (m)	Bubble volumes (m^3)
100	$8.6953*10^{-05}$	$2.7539*10^{-12}$
200	$4.3477*10^{-05}$	$3.4424*10^{-13}$
300	$2.8984*10^{-05}$	$1.0200*10^{-13}$
400	$2.1738*10^{-05}$	$4.3030*10^{-14}$
500	$1.739*10^{-05}$	$2.2031*10^{-14}$
600	$1.4492*10^{-05}$	$1.2750*10^{-14}$
650	$1.3377*10^{-05}$	$1.0028*10^{-14}$
700	$1.2422*10^{-05}$	$8.0289*10^{-15}$
750	$1.1594*10^{-05}$	$6.5278*10^{-15}$
800	$1.0869*10^{-05}$	$5.3787*10^{-15}$
850	$1.0230*10^{-05}$	$4.4843*10^{-15}$

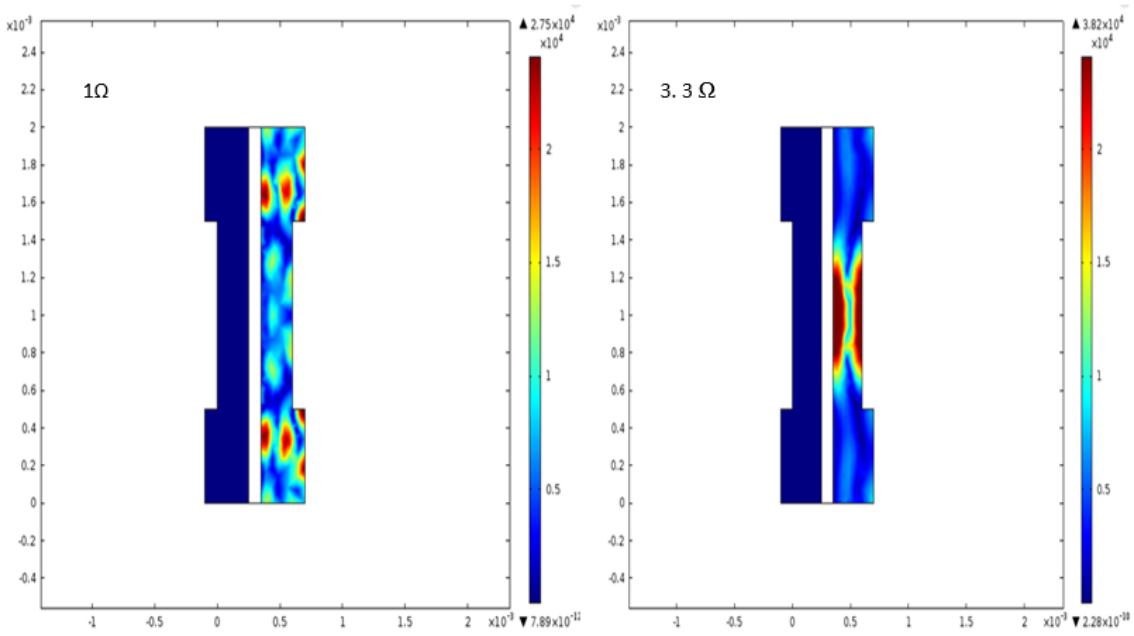

Figure 6.4: Acoustic emission intensity at 1 &3.3 Ω.

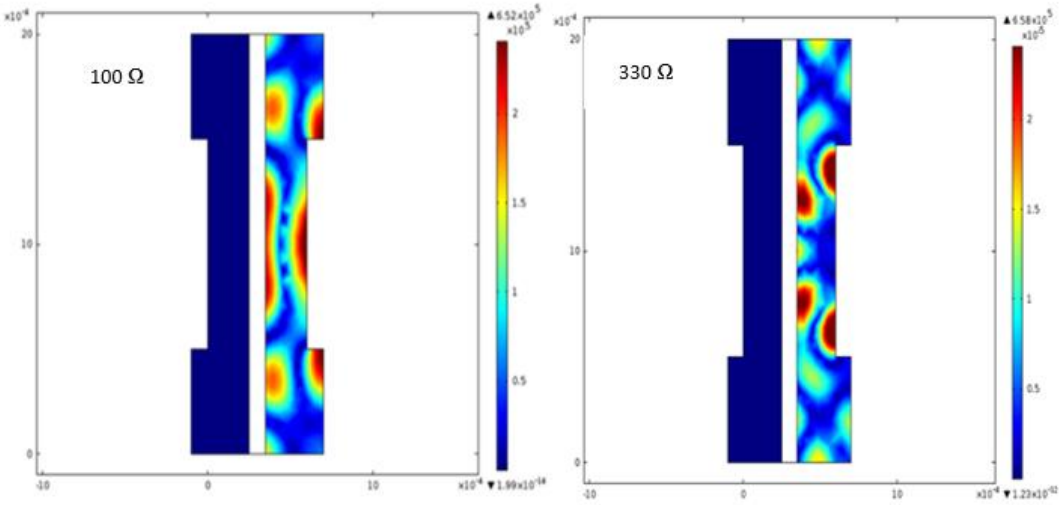

Figure 6.5: Acoustic emission intensity at 100 &330 Ω.

6.3.1 Experimental Setup to Investigate the Impact of Load Variation on Acoustic Emission

The experimental setup is shown in figures 6.6 and 6.7. A single 500mW PEMFC with Nafion 115 membrane of thickness 0.127mm and active area of 9cm^2 was examined. The electrodes were both made of 0.2mg/cm^2 platinum. The catalyst layer was made of carbon-supported platinum, loading 1mg/cm^2.

Six different loads were applied in order to investigate the active levels of AE, namely 20%, 40%, 60%, 80% and 100% of the cell's full load.

The AE monitoring was conducted using a piezoelectric sensor mounted atop the PEMFC. The sensor was attached using special wax, which supported the sensor during the experiment while supplying the necessary acoustic coupling.

The AE signals from the PEMFC were measured using an AE transducer model NS2000, amplified and filtered using a 20 kHz to 5 MHz band pass filter. The gain of the amplifier was set to 30 dB and interfaced to a GDS-1102 - GW Instek digital oscilloscope. For all experiments conducted, a sampling interval of 200 ns was used, necessitating 1024 points per signal. The scope was triggered such that about 100 points were collected before the trigger point. The recorded data was processed using MatLab package.

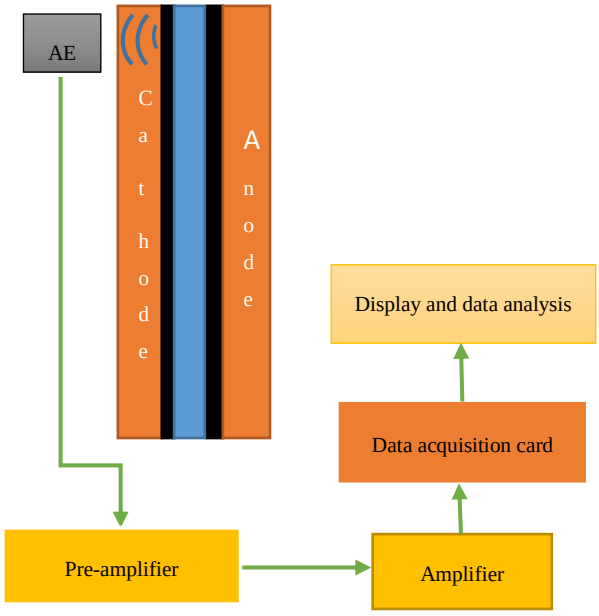

Figure 6.6: Block diagram of the AE signal measuring system.

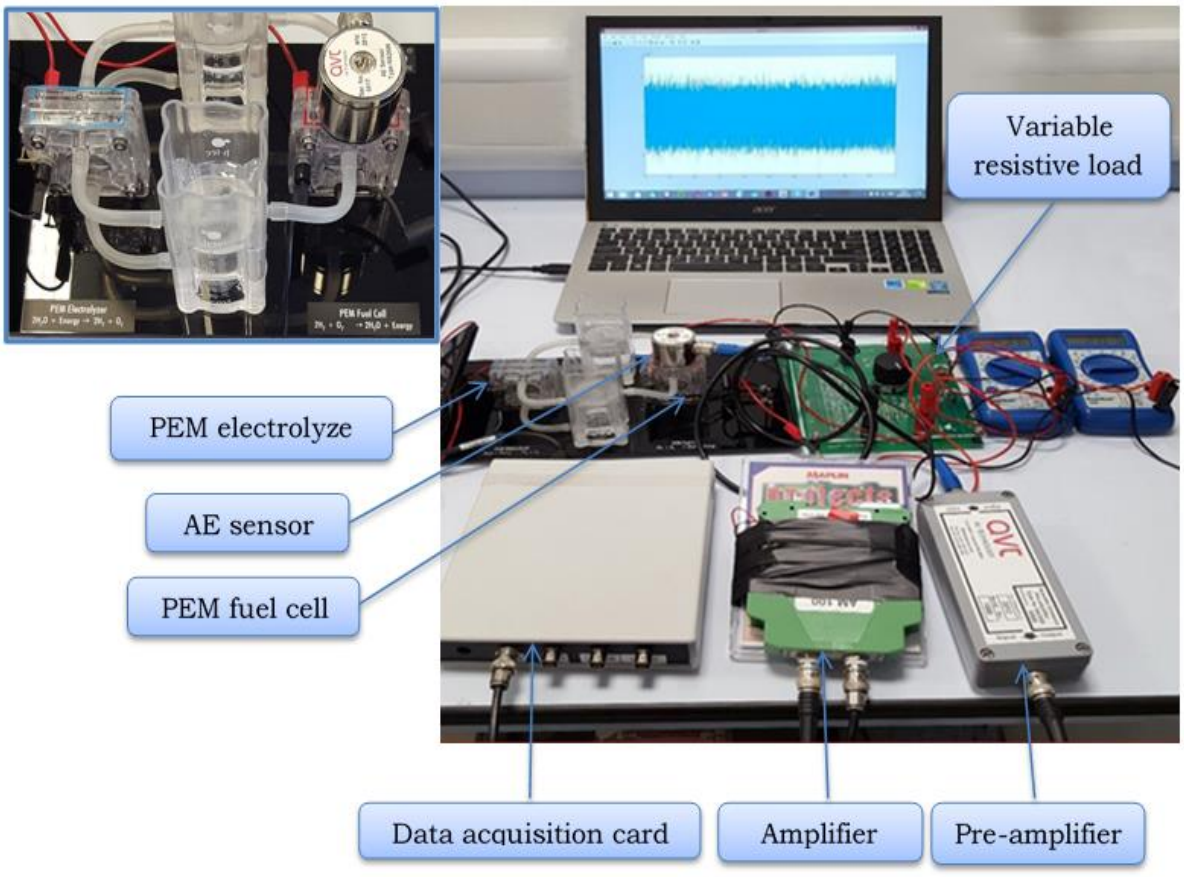

Figure 6.7: The experimental set-up.

6.3.2 Data Acquisition and Analysis of AE

Statistical approaches were utilised to extract information from the AE data. FFT is used to generate a frequency domain to representation the signal.

The system was used to collect data from the PEMFC system that comprises a piezoelectric sensor, preamplifier and amplifier. Due to the frequency spectrum of AE being very large (ranging from 16 kHz to >1 MHz), this means the AE sensor model NS2000m is used to gather the data from the PEMFC system. A pre-amplifier amplified the piezoelectric sensor with 20–1000 kHz bandwidth filters and a 30-dB gain, see figure 6.8.

A fast storage oscilloscope was used as a transient digitiser. This can acquire and digitise input signals and display or store the result. A GDS-1102 - GW Instek Digital Oscilloscope was used for monitoring AE, and can sample data at rates of up to 1MHz. The code in the MatLab environment had been written for data analysis in both time and frequency domains.

Figurer 6.8: AE sensor and pre-amplifier.

6.3.3 Experimental Procedure of Water Flooding

As mentioned in chapter 5, water management plays vital role in enhancing the performance of a PEMFC. In this content, a single PEMFC was utilised to figure out the effect of flooding on cell performance with the following specifications:

- Fuel cell active area: 9cm^2;
- Membrane Electrolyte Assembly (MEA) with Nafion 115, 1 mg. Pt/cm^2 (platinum load at both sides);

- Toray carbon fibre paper with 0.19mm thickness used as the GDL.

In this experiment, operating temperature, pressure, and relative humidity had been taken into consideration due to their significant impact on the water management issue.

Hydrogen and oxygen were used as fuel and oxidiser respectively. Electrolysis was used to ensure both hydrogen and oxygen had a humidity and purity of 100% and 99.9% respectively.

There are two approaches to making the cell operate under flooding conditions. The first method relies on the difference between the temperature of the gases and the cell i.e. if the cell's temperature is higher than the temperature of the gases, the cell will remain under dry conditions. In contrast, if the gases' temperatures are higher than the cell's temperature, the cell will be flooded. The second method depends on control of the water drainage. In the existing work, the authors opted for the second method due to its simplicity.

Fuel cell cleaning of accumulated water can be performed in two ways, one is by raising the level of the cell temperature and the second method uses the air stream. Both these methods have some limitations. For example, raising cell temperatures tends to limit the cell's applications, especially mobile applications. The second method that relies on the air stream may damage the delicate components such as the membrane. Thus, this method should be used carefully and prudently. In this work, the second method was used. To ensure repeatability, several independent flooding experiments were carried out.

In order to characterise the flooding conditions and simplify the experiments' procedure, we assumed that the flow channel of the PEMFC was signal–phase flow, so that the flooding condition can be declared if the measured values of current and voltage drop deviated significantly from its predicted values owing to the presence of liquid water in the system.

The output PEMFC was connected to different electrical loads in order to vary the current drawn from the system.

The data that obtained from output voltage and current was then fed into a personal computer running a developed computer program under the LabVIEW software environment to monitor the water content and cell flooding continually.

6.4 Results and Discussion

6.4.1 Effects of Operating Conditions on the AE Signals

Firstly, the electrical performance of the PEMFC was examined by connecting it to different loads (resistors). The effects of electric loading variations on the generated currents, voltages and power are listed in table 6.2, which was as expected and demonstrates a healthy performance.

Table 6.2: Load effects on power parameters.

Resistance (Ohr	Current (A)	Voltage (V)	Power (W)
∞	0	0.99	0
330	0.01	0.97	0.0097
100	0.02	0.94	0.0188
33	0.03	0.9	0.027
10	0.08	0.83	0.0664
3.3	0.22	0.77	0.1694
1	0.56	0.63	0.3528
0.33	1.05	0.47	0.4935
0.1	1.43	0.32	0.4576
0	1.61	0.24	0.3864

The output of an AE transducer attached on the 500 mW PEMFC with no load is shown figure 6.9. The AE signals shown in figures 6.9 and 6.10 were enhanced by averaging. In practice, it is frequently the case that with a repeated signal, the signal-to-noise ratio can be improved by averaging, particularly where the corruption of the signal is due to unwanted noise occurring because of random events. Time-domain averaging is a way to reduce the content of undesired components in a signal.

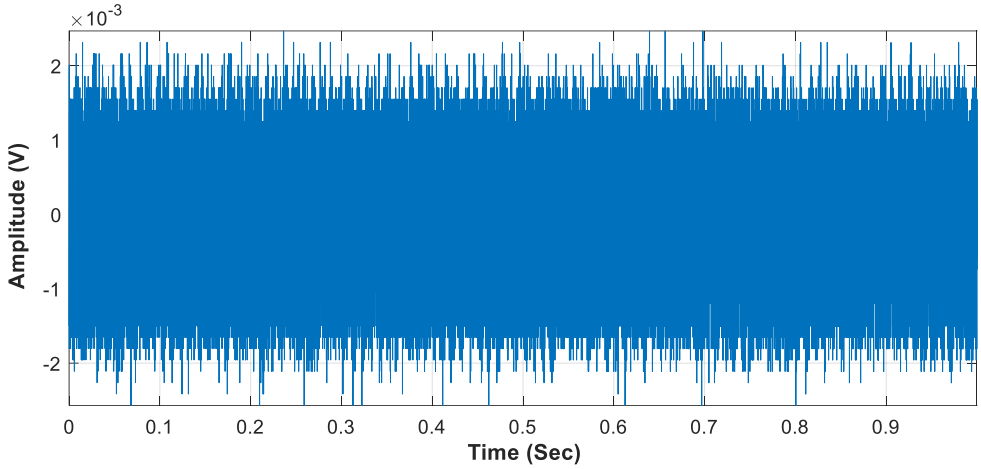

Figure 6.9: AE signals in time domain with no load.

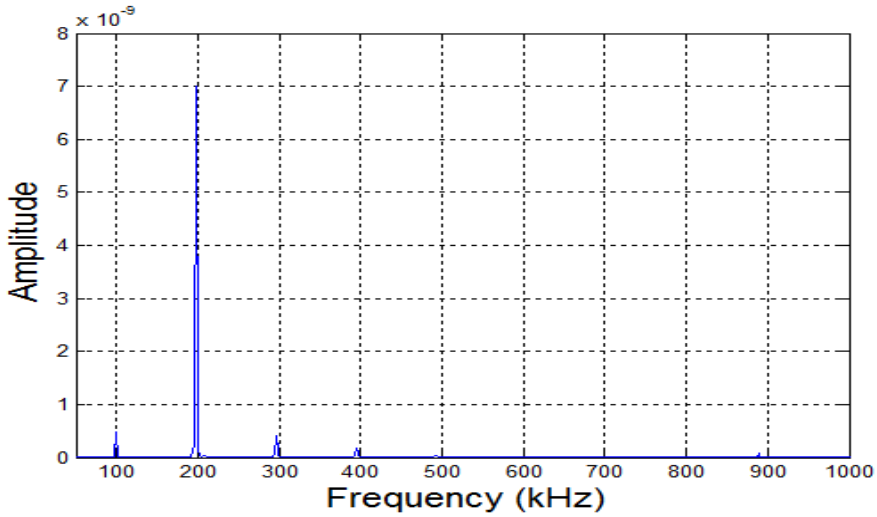

Figure 6.10: AE signals in frequency domain with no load.

The main features, observed from the AE waveform and shown in Figure 6.10, are peaks corresponding to the reaction events between oxygen and hydrogen at the cathode. This waveform is complicated and difficult to extract information from due to the numerous frequency components superimposed on each other. In the associated power spectrum, shown in figure 6.10, no peaks can be seen at 650 kHz; the other peaks that appears are results of random events.

This section reports on how varying the PEMFC electric load affects the characteristics of the AE signals. The PEMFC was operated under six loading conditions. A MatLab code was written to show the measured AE signal in terms of both the time domain and frequency domain. Extensive experiments were made to validate the AE activity with load change. The effect of load changing on AE activity

is described in Figures 6.11 to 6.13. An excellent correlation between load changing and AE has been observed.

Figure 6.11 shows time-domain histories at each of the six loads, with the associated spectrum. It can be observed that the amplitudes of the time domain waveforms increase as the load increases. Figure 6.13 shows the AE signals in the frequency domain.

In the associated power spectrum, shown in figure 6.12, the peaks can be seen; the highest at the resonance frequency of the AE transducer (650 kHz), and the other peaks are multiples of this main frequency component. The amplitudes of any higher harmonics can be ignored because they contain considerably less energy than the first leading terms.

The amplitude of the peaks increases with increasing load, and the frequency at which the peak occurs also increases in direct proportion to the increase in load. Figure 6.13 illustrates the AE signal in the frequency band after the zoom. It is clear that the peak of the signal is at 650 KHz.

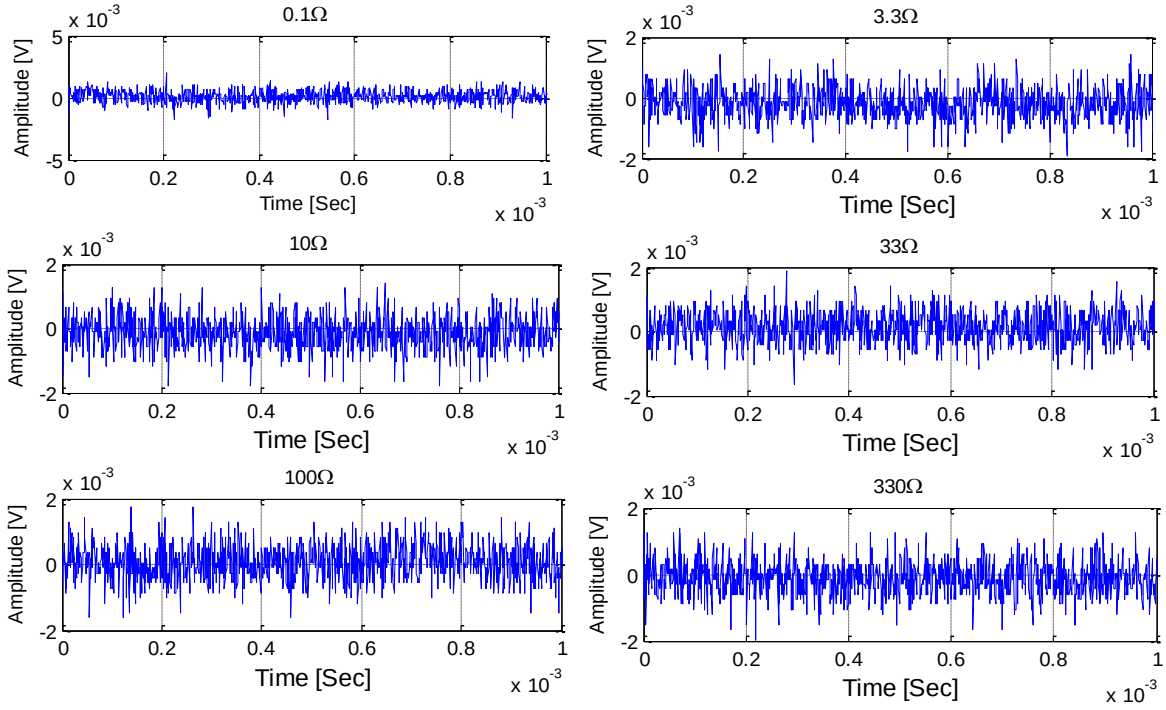

Figure 6.11: Time-domain histories at each of the six loads with the associated spectrum.

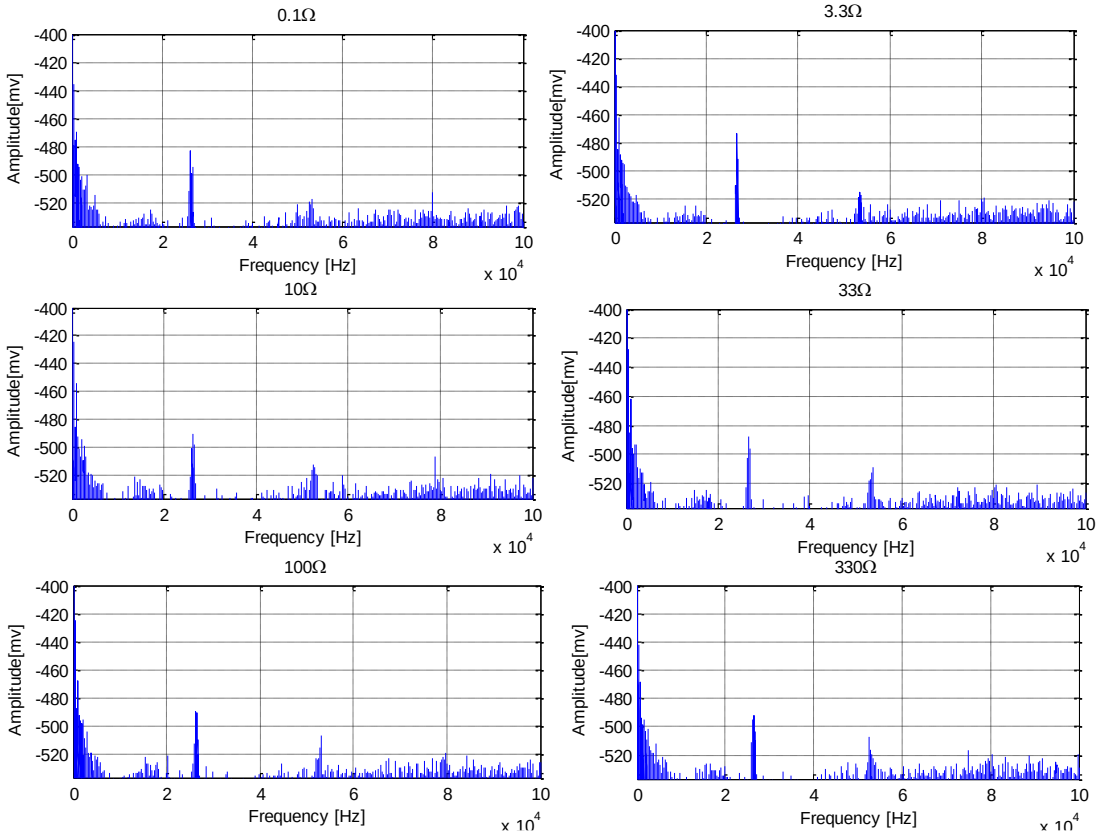

Figure 6.12: Frequency-domain histories at each of the six loads with the associated spectrum.

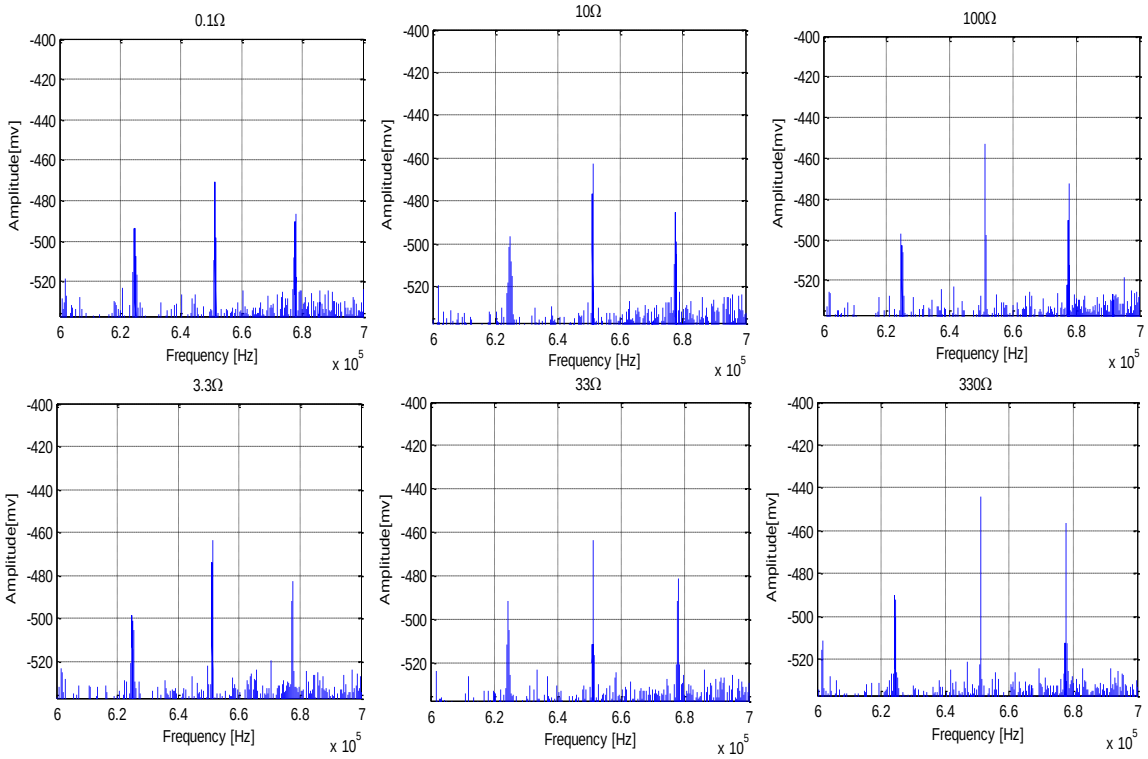

Figure 6.13: AE signals in the frequency domain after the zoom.

6.4.1.1 AE Signals Analysis Using Statistical Parameters

In this section, statistical parameters were used to extract information from the AE signal and used to determine the PEMFC with load variation.

The idea behind testing the PEMFC in this way was to investigate the possibility of utilising AE measurements and simple statistical methods for use as a condition-monitoring tool. Calculating the RMS values, kurtosis and skewness of the AE signals may give a quick indication of the PEMFC in a relatively straightforward way, and information on the PEMFC's condition could be assessed without the need for any special training.

The variance of a population (σ^2) is defined as the sum of squares of the deviations of the observations from the mean divided by the total number of observations, see equation (6.3). The standard deviation (σ) is defined as the positive square root of the variance when the standard deviation is evaluated from a sample, rather than the population as a whole. It is given the symbol, *s,* and (N-1) rather than N is used in equation (6.3).

$$\sigma^2 = \frac{\sum f_i (x_i - \mu)^2}{N} \tag{6.3}$$

Kurtosis and skewness are statistical parameters that could be used to describe the graphical representation of the AE signal population. Kurtosis describes the rate of change of the curve, and skewness reflects the degree to which the curve is skewed to the left or right.

Kurtosis (*k*) characterises the relative peak-ends or flatness of a distribution compared to the Gaussian distribution. Positive kurtosis indicates a relatively peaked distribution. Negative kurtosis indicates a relatively flat distribution.

Skewness characterises the degree of asymmetry of the distribution around its mean. Positive skewness indicates a distribution with an asymmetric tail extending towards values that are more positive. Negative skewness indicates a distribution with an asymmetric tail extending towards values that are more negative. Normal distributions produce a skewness statistic of zero.

The normal distribution is represented by:

$$f(x) = \frac{1}{\sqrt{2\pi\sigma^2}} e^{-(x-\mu)^2/2\sigma^2} \tag{6.4}$$

The formula for evaluating kurtosis (k) is:

$$k = \frac{\Sigma_{i=1}^{N}(x_i - \bar{x})^4 / N}{(s^2)^2} \tag{6.5}$$

Where $\Sigma_{i=1}^{N}$ has its usual meaning of the summation of terms from 1 to *N*, $\bar{x}$ is the sample mean, x_i is the value of the i^{th} score, N is the total number of scores in population, and s^2 is the sample variance.

The formula for measuring skewness (sk) is:

$$sk = \frac{3(\bar{x} - md)}{s} \tag{6.6}$$

Where md the median is score and s is the sample standard deviation.

The Root Mean Square (RMS) of a signal is given by:

$$V_{RMS} = \sqrt{\frac{1}{T}\int_{t_0}^{t_0+T} v(t)^2 dt} \tag{6.7}$$

Where *v (t)* is the instantaneous value of the signal at time t, and V_{RMS} is the RMS-value of *v (t)* for the time *T.*

6.4.1.2 Root Mean Square Value and Variance as Fault Severity Indicators

In this section, RMS values, kurtosis, skewness and variance were used to investigate the PEMFC's loading effects on their emitted acoustic signals. The PEMFC was tested under six loading conditions, one with no load and four where a linear load increase was introduced. The AE data was band pass filtered into three different frequency bands; low frequency band [0 – 100 kHz], medium frequency band [100 – 500 kHz] and high frequency band [500 – 1000 kHz].

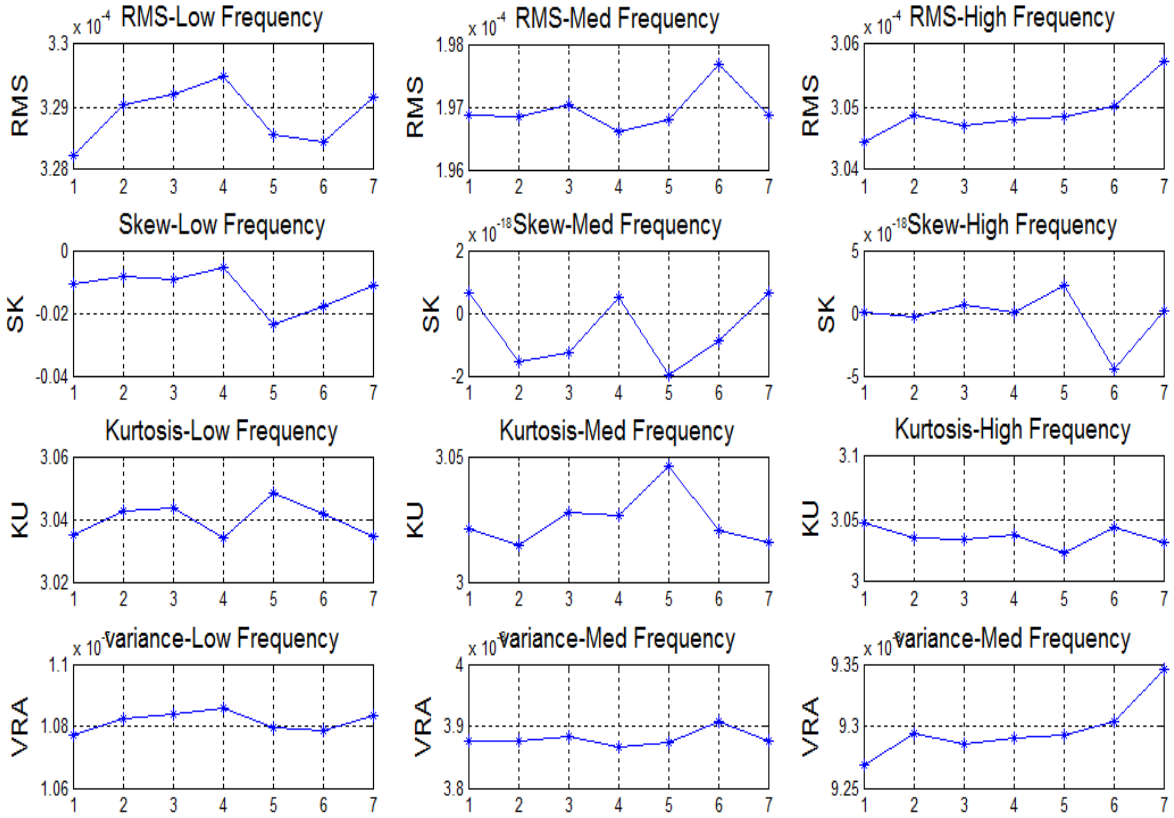

Figure 6.14: Statistical parameters of the AE under different loading conditions.

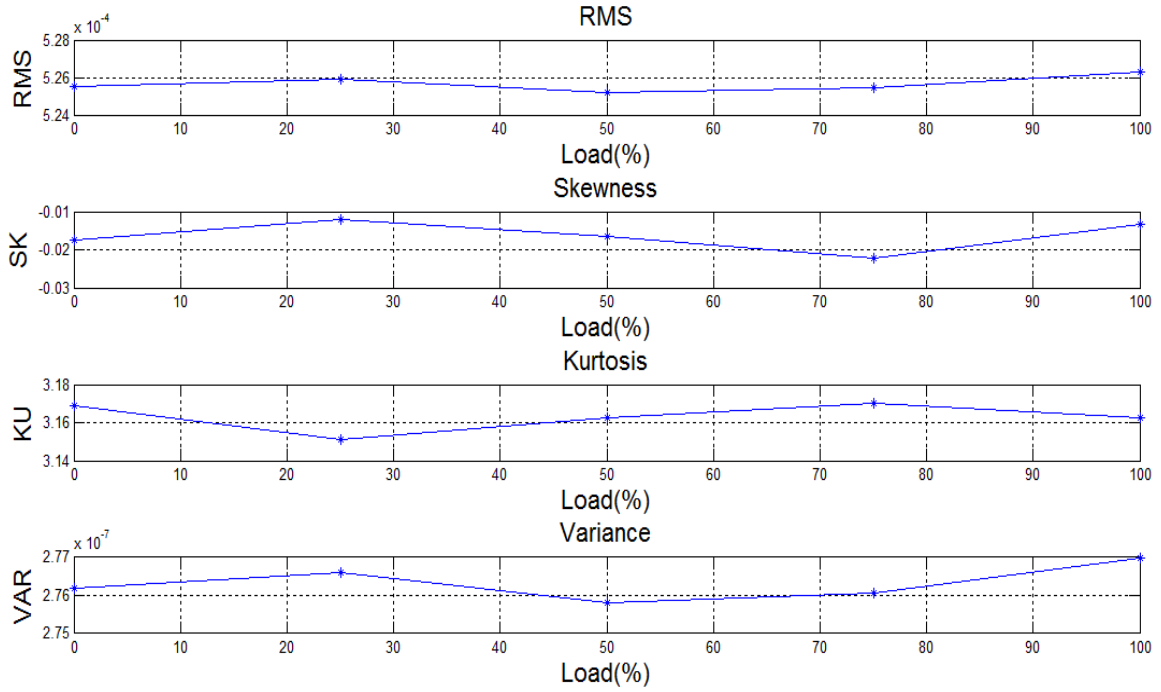

Figure 6.15: Statistical parameters of the AE under different loading conditions at high frequencies.

6.4.2 Results and Comments for Water Flooding

Figure 6.16 shows the flooding of PEMFC at constant pressure, fully humidified gases and a slow increase in the current. At current low density, there was no liquid water in the channels and only a small amount of water was generated at the cathode side due to a reduction in oxygen reduction reaction (ORR). The output voltage and current curves were as same as in normal operating conditions. At 180s, the first water droplet emerged, which was stressed by three forces: gravitation (G), viscous force between the droplet and solid surface (Fs), and the shear drag force induced by the gas flow (FD). The droplet was small at the beginning, FD + G ≤ Fs, and was held on the GDL surface or/and the channel side wall. With continued operation of the PEMFC, more droplets emerged and became larger, which started to block the porous membrane and GDL, thereby hindering the gas flow.

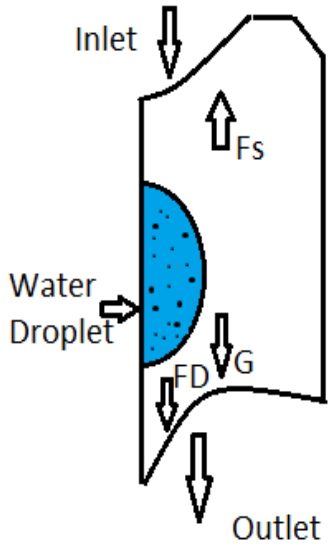

Figure 6.16: Force diagram of a water droplet in the channel.

Figure 6.17 illustrates the water concentration at cathode side. From figure 6.17, it can be noticed that the level of water at the outlet is higher than the inlet, due to pressures at the outlet being lower than at the inlet.

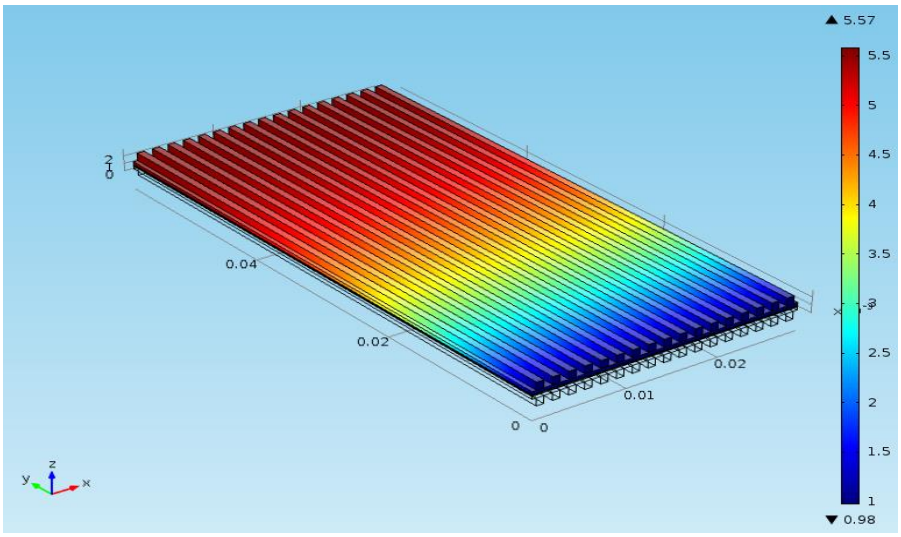

Figure 6.17: Water concentration at the cathode side.

Figure 6.18 shows the presence and accumulation of liquid water at the anode side. Due to the lack of water generation at the anode, the accumulation of water is attributed to the gas humidifying and back diffusion phenomena, hence, the amount of water is less than that at the cathode.

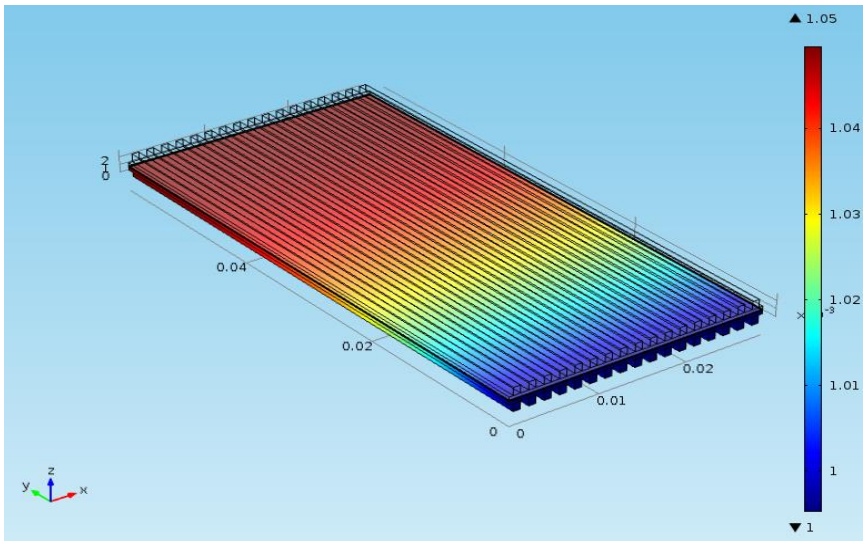

Figure 6.18: Water concentration at the anode side.

The membrane entails more PEMFC components affected by water management issues. The membrane requires adequate water to ensure high ionic conductivity, thus lowering Ohmic losses.

Figure 6.19 shows the water content through the membrane. The water accumulates in the membrane due to electro-osmotic drag as well as the back-diffusion phenomenon.

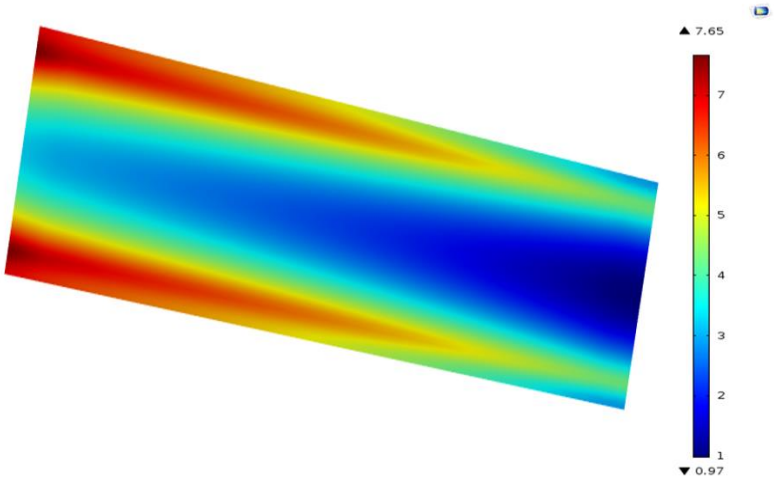

Figure 6.19: Water content through the membrane.

Water vapour concentration in the membrane is depicted in figure 6.20. This figure shows that most of the water in the liquid phase attributed to the PEMFC operates at a relatively low temperature.

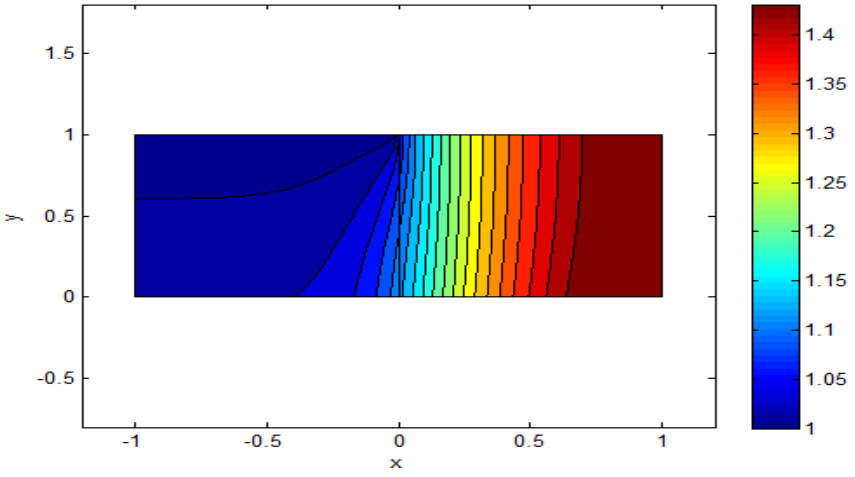

Figure 6.20: Contour plot of water vapour concentration in membrane.

Figures 6.21, 6.22 and 6.23 show water concentration values that were obtained from the MatLab Simulink at the anode, cathode and membrane.

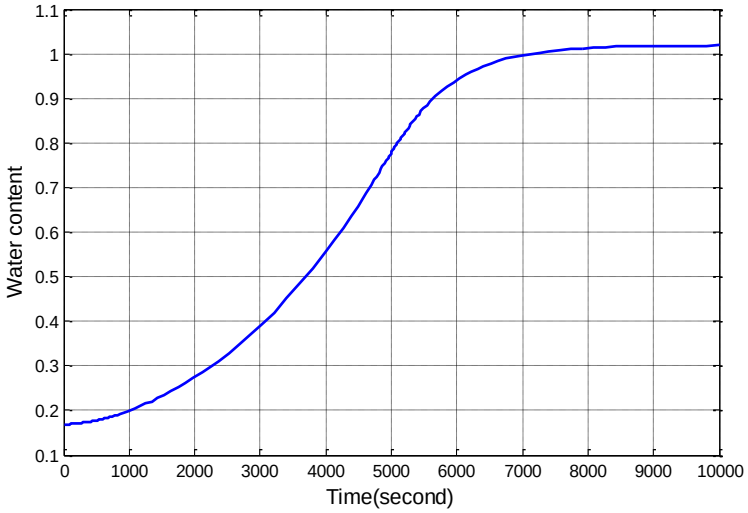

Figure 6.21: Water concentration at the anode.

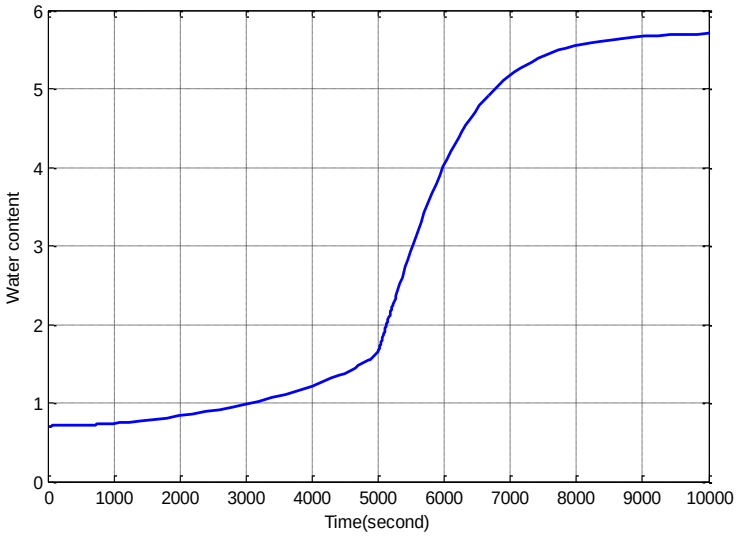

Figure 6.22: Water concentration at the cathode.

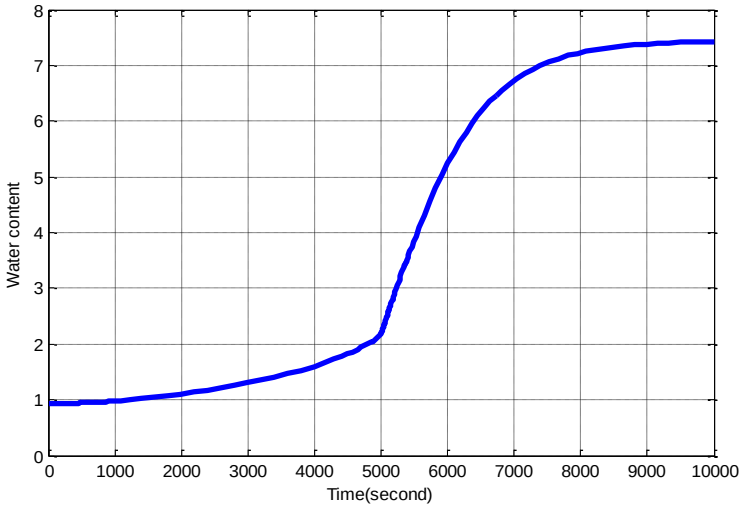

Figure 6.23: Water concentration at the membrane.

Figure 6.24 depicts the pressures of hydrogen, oxygen, and water during the cell under flooding conditions. It is clear that the pressure of water is increased with flooding while reducing the pressure of hydrogen and oxygen. This because the water droplets will clog the GDL and gas channels.

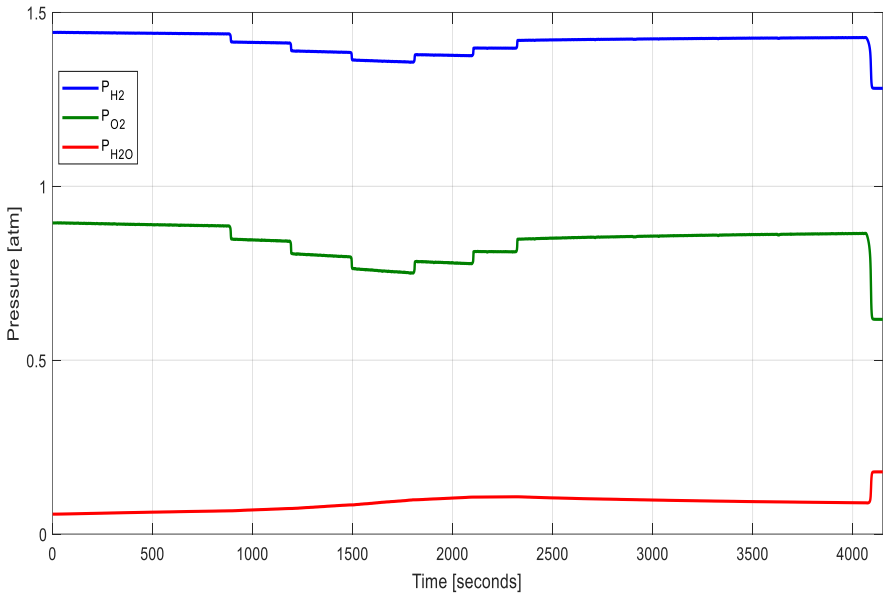

Figure 6.24: Pressures during flooding.

Figure 6.25 shows the output voltage of PEMFC under normal conditions as well as during flooding cases. The voltage curve under flooding conditions can be divided into three parts: the first part describes the water produced and accumulated at the cathode side (the cathode side is the main source of the water because of the electrochemical reaction as described in chapter 1 equation (1.1c). As can be observed from figure 6.25, water takes time to accumulate at the cathode side. This duration depends on many factors, such as current density, pressures and temperatures. The second part represents the water status in the GDL. When water clogs the GDL, the voltage value declines sharply. Meanwhile, the last part in curve illustrates the voltage recovery after water purging.

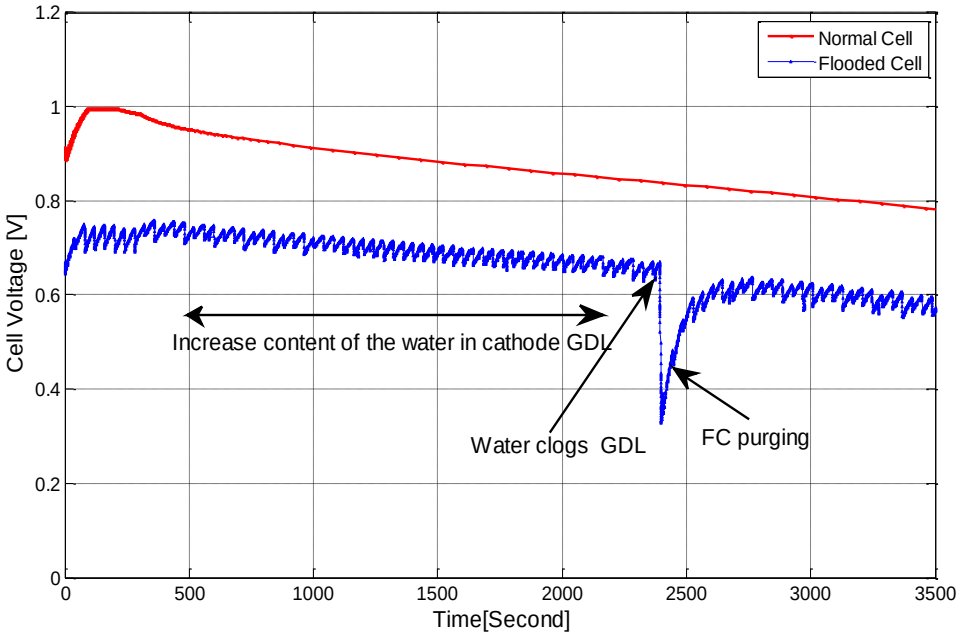

Figure 6.25: Fuel cell output voltage during flooding state.

As mentioned in chapter 2, when the protons are traveling from the anode to the cathode they carry water molecules with them, which is known as the electro-osmotic drag phenomenon. The amount of water molecules transferred depends significantly on the value of the load. Figure 6.26 illustrates the output voltage when different loads are applied to the cell.

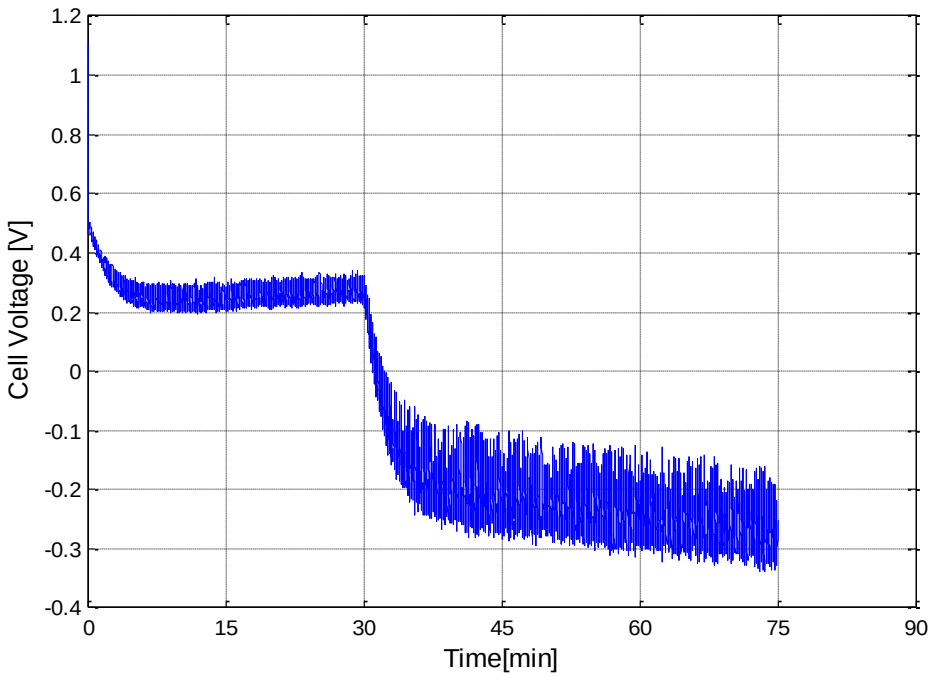

Figure 6.26: Cell flooding due to load.

Figure 6.27 shows the cell output voltage curves that were obtained from both simulation and experimental results. It can be seen that there is a reasonable correlation between the experimental and simulation results.

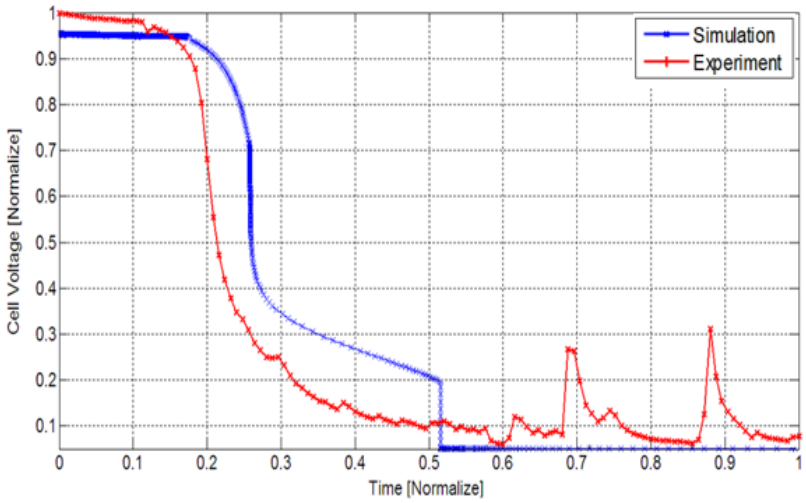

Figure 6.27: Validation of experimental results.

CHAPTER 7

CONCLUSIONS AND FUTURE WORK

This chapter illustrates the conclusions and contribution to knowledge. It also summarises the achievements of the research project and explains how the objectives stated in Section 1.4.2 were achieved. Some suggestions for future directions are also given at the end.

7.1 Conclusions

This thesis has discussed performance and system effectiveness because they are the key attributes to improve and enhance PEMFC as a promising power source. Parameters that affect cell performance has been investigated. This include failure modes that can lead to catastrophic failure and performance degradation below to an acceptable level.

Both COMSOL and MatLab Simulink-based models were implemented to study the reversible degradations and recoverable phenomena involving voltage or/and current density decay.

Acoustic emission was used as tool to diagnose and investigate the load variation and operating conditions and how they can affect the cell performance and its reliability.

- A dynamic model of a proton exchange membrane fuel cell (PEMFC) system has been presented. A semi-empirical dynamic model was built by combining mass-energy conservation and experimentally determined parametric coefficient equations. In order to determine the values of the most critical empirical coefficients, a formal estimation procedure was employed and experimental data was gathered from a real PEMFC testing unit.

  The methodology in the underlying experimental study was utilised and then model-based validation was implemented. The model presented in this thesis could be used with other fuel cell types if physical parameters are adjusted accordingly. In addition, the results showed a good agreement with experimental data under different operating conditions.

- Increases in the temperature will increase the performance of PEMFCs by reducing activation and concentration losses; however, this might affect the conductivity of the membrane, which will lead to an increase in the Ohmic losses. In addition, high temperatures could limit the uses of PEMFCs, particularly in mobile applications.

- Increases in gas pressure particularly at the cathode side will increase the performance of fuel cells; however, this could damage the delicate components such as the membrane.

- At low temperature and pressure, the voltage declines 0.1 V, and it causes a decline in the outcome (voltage and power) by 10 % of its nominal output.
- The AE is emitted from FC as a result of the reaction between the hydrogen and oxygen. The acoustic emission is due to the movement of the bubbles at the cathode side to produce water.
- This study applies only to the changes in both pressure and temperature and their effect on the performance of the FC. However, these changes will also affect the conductivity of the various components and viscosity of the fluids. In addition, some parameters that were assumed to be constant, such as the specific heat at constant pressure, will also vary.
- The polarization curve can be used to present the typical shape of the FC's performance curve. However, under practical conditions, some deviation from this shape is expected, due to the idealistic assumptions made during the derivation of the equation and does not consider all the factors affecting the practical applications.
- Any change in the chemical reaction will lead to a change in AE. The AE activity is increased by an increase in the load value. In addition, the AE amplitude is directly proportional to the increases in pressure and the temperature.
- AE has been analysed to find the correlation between it and PEMFC behaviour during load change. The quantity of bubbles is strictly limited by the small size of the fuel cell. Therefore, it is difficult to observe the signal differences in the time domain. For that, it is better to use statistical approaches to analyse the data based in the frequency domain. The data collected separated into four types of statistical factors, which are root mean square (RMS), skewness, kurtosis, and distribution. The RMS, kurtosis, skewness and variance parameters were calculated from the average of several experiments with different load values. The RMS values have shown a good response in the high frequency band, so it may have a use as a detector for fuel cells. AE has shown good sensitivity to different operating conditions. In particular, changes in the load were closely linked to the evolution of AE activity and its use to detect failure experienced in FCs has been outlined.

- Modelling cell dynamics: a good knowledge of the processes entailed in the operation of the PEMFC, both at the auxiliary subsystems and the membrane level, will help to develop dynamic models for the design of more compact, reliable and efficient devices. This also enlarges the range of PEMFCs' applications, increasing their attractiveness as substitutes in fields usually reserved for other cell types, for example, in high-power stationary installations. Alternatively, precise models of gas circulation and cell fluid dynamics will improve the predictability of electrochemical procedures, with direct consequences for strategies of design.

  From the perspective of failure modes, sufficient effort has been made to develop robust diagnostic strategies that can improve the reliability and efficiency of PEM cells, avoiding irreversible damage to membranes, the GDL and catalysts. There is need for robustness in considering the intrinsic ambiguity in the system model and to avoid cumbersome or expensive determination of variables. Moreover, sim-empirical methods often allow broader operation variables than "local" methods that linearise the system around points of equilibrium. To ensure success in the market, it is important to come up with strategies and models to predict and diagnose situations of failure.

-

- From the perspective of automatic control, sufficient effort is needed to develop robust, nonlinear strategies that can improve the reliability and efficiency of PEM cells, avoiding irreversible damage to membranes.
- There is a need for robustness in considering the intrinsic ambiguity in the system model and to avoid cumbersome or expensive determination of variables. Moreover, nonlinear control methods often allow broad operation varieties than "local" methods that linearize the system around points of equilibrium. To ensure success in the market, it is important to come up with strategies and models to predict and diagnose situations of failure.
- Water management is a critical issue that needs to be addressed to enhance the reliability of PEMFCs.

- Water accumulated in PEMFC is a result of three processes, namely the reaction between oxygen and hydrogen at cathode side, electro-osmotic drag and the back-diffusion phenomenon. All these processes rely on the electrical power produced in the cell.
- In this thesis, PEMFC flooding has been investigated through modelling. The results were then validated experimentally. The proposed technique can give instant information about accumulated water during a fuel cell's operation, and the location of excess water can be indicated. Therefore, the proposed indicator cannot only detect the flooding of the PEMFC, but also shows the amount of accumulated water inside, which can be used to quantify the level of flooding. The results presented here demonstrate the effectiveness of the derived technique especially for deployment in real-time monitoring systems for PEMFCs.

7.2 Contribution to Knowledge

The research work carried out in this thesis has resulted in seven publications and includes a number of important, novel aspects that were not previously implemented by other researchers. These publications and new findings are summarised below:

7.2.1 Contribution through Publications

Alrweq, M. & Albarbar, A. (2016), 'Investigation into the characteristics of proton exchange membrane fuel cell-based power system.' IET Science, Measurement & Technology, DOI: 10.1049/iet-smt.2015.0046, Online ISSN 1751-8830 Inverness conference.

Alrweq, M., & Albarbar, A. (2016), 'An integrated system for enhancing reliability of proton exchange membrane fuel cell.' *SCI Electrochemistry Postgraduate Conference*, University College of London (UCL), May, 2016.

Alrweq, M., & Albarbar, A. (2016), 'Proton exchange membrane fuel cells: recent developments, modelling and challenges. *Proceedings of the 6th International Symposium in Energy Challenges and Mechanics*, Inverness Jul 2016.

Batunlu, C., Alrweq, M., & Albarbar, A. (2016), Effects of Power Tracking Algorithm on Lifetime of Power Electronic Devices Used in Solar Systems. *Energies* 2016, 9(11), 884; DOI: 10.3390/en9110884.

Badawood, C., Alrweq, M., & Albarbar, A. (2017), Acoustic Emission Based Condition Monitoring Technique for Power Electronics in Solar Systems, *Proceedings of 1st BINDT conference on Condition Monitoring*, WCCM 2017. London.

Alrweq, M., & Albarbar, A., (2017), Model-Based System for Water Management in Proton Exchange Membrane Fuel Cells, Under Review, *Catalysts*.

Alrweq, M., Batunlu, C. and Albarbar, A. 'Investigation into the Acoustical Characteristics of Proton Exchange Membrane Fuel Cells', Under Review, Renewable Energy.

Alrweq, M., Viqar Dar, O., Albarbar, A. (2017), 'An investigation to perturb and observe an incremental conductance based maximum power point tracking for photovoltaic system.' The 1st Euro-Mediterranean Conference for Environmental Integration (EMCEI), Sousse, Tunisia, November 2017.

Alrweq, M., & Albarbar, A. (2017) 'Effective technique for improving electrical performance and reliability of fuel cells.' *International Journal of Power Electronics and Drive Systems,*

7.2.2 Novelty of the Work

• Novelty One:

The derivation and validation of realistic user-friendly model, using COMSOL Multiphysics software, that aids design optimisation and the development of an effective condition monitoring system for PEMFCs.

• Novelty Two:

Development of an effective method to determine current density and efficiency of PEMFCs using only the measured current and voltage. This has also been compared with manufacturer's data available from the nameplate and/or datasheet. The developed method was found effective in detecting and diagnosing faults in PEMFCs.

• Novelty Three:

The fundamental acoustical characteristics of PEMFCs were investigated and cells' load sensitive frequency bands, within a wide spectrum, were clearly identified. This opens the doors for the full adoption of AE measurements for control and condition monitoring purposes. This, if fully utilised, would lead to effective and non-intrusive tools for the abovementioned purposes.

7.3 Review of Objectives and Achievements

The main achievements of this work are described below and correlated with the original objectives set out in Section 1.4.2.

Objective 1:

Explore the design and working principles of proton exchange membrane fuel cells (PEMFCs) and their associated parameters.

Achievement 1:

The main features and functionality of PEMFCs have been presented starting with the contents and basic components and the fundamentals of PEMFCs. A thermodynamic investigation followed to establish the relationship between current and voltage and their relationship with other operation conditions, such as pressure, temperature, exchange current density, charge transfer coefficient and gas concentrations in PEMFCs.

A comprehensive study and analysis of PEMFCs has been considered under actual operating conditions, internal currents, fuel utilisation efficiency and thermal and electrical efficiencies. Then these involved expressions for the efficiency and performance of the PEMFC and the formula for PEMFC efficiency were derived and employed to plot the complete curve of efficiency against current density (see chapters 1 and 2).

Objective 2:

Gain a clear understanding of PEMFCs' failure modes and understand condition monitoring techniques e.g. temperature, voltage, power and current analysis.

Achievement 2:

A state-of-the-art review provides readers with a fundamental understanding of insufficient PEMFC performance; identification of failure modes and failure mechanisms of PEMFCs; PEMFCs component degradation testing, and mitigation strategies against degradation has been discussed in depth in chapter 3. In chapter 4, the degradation and failure modes of various PEMFC components have been examined. This includes reversible and irreversible of failure modes, and the effects of operating conditions on performance and efficiency of PEMFCs.

Objective 3:

Develop a mathematical model for Proton Exchange Membrane Fuel Cells (PEMFCs) operations and effect of faults on their efficiency and performance.

Achievement 3:

To meet objective three, realistic mathematical models were developed and implemented in a MatLab/Simulink® environment to get an overview of the system's behaviour. Some parameters have been studied to evaluate their effects on a PEMFC system performance and efficiency.

The proposed model depends on principle equations of PEMFC, which combined with equations that were obtained experimentally, and the results of these equations lead to the production of a semi-empirical system. The mathematical model equations describing the operation of the PEMFC are composed of the voltage-current characteristics and a relationship for the temperatures and pressures as a function of the current density. In addition, both thermodynamic characteristics and double-layer charging, which affect the inside of the PEMFC, are included in the models.

To gain a clearer understanding of the effects of operational parameters on the induced AE signals, a 2-D finite element model, using the COMSOL software package, was developed and examined when operated under different load values. In addition, the impact of water management on the cell performance and efficiency of a 3-D finite element model, was investigated using the COMSOL software package.

Objective 4:

Design and construct a test rig with associated instrumentation for various operating conditions and fault simulation, namely load variations, hydration and dehydration, data collection and subsequent data analysis.

Achievement 4:

The experimental set-up used in this work consisted of a single 500mW PEMFC with a Nafion 115 membrane of 0.127mm thickness and an active area of 9cm^2. The electrodes were made of 0.1mg/cm^2 platinum for both sides of anode and cathode. The catalyst layers were made of carbon-supported platinum, loading 1mg/cm^2.

Membrane electrode assembly (MEA) was first sandwiched between two gaskets and then between two graphite current collector plates.
Six different loads were applied to investigate the active levels of AE, namely 20%, 40%, 60%, 80% and 100% of cell's full load.
The AE monitoring was conducted using a piezoelectric sensor mounted on top of the PEMFC. The sensor was attached using a special wax, which supported the sensor during the experiment while supplying the necessary acoustic coupling.

The system used to collect data from the PEMFC system comprised a pre-amplifier, amplifier and piezoelectric sensor with 20 to 1000 KHz bandwidth filters. As the frequency spectrum of AE was very large (16 KHz to 1 MHz), the AE sensor model NS2000m was used to gather the data from the PEMFC system.

A fast storage oscilloscope was used as a transient digitiser. This could acquire and digitise input signals and display or store the result. A GDS-1102 - GW Instek Digital Oscilloscope was used for monitoring AE, and it could take sample data at rates of up to 1MHz. Code was written in the MatLab environment for data analysis in both time and frequency domains. (See section 6.3.2).

For flooding experiments, in addition to the above instrumentation, the output voltage and current from the PEMFC fed into a personal computer which in turn ran a computer program developed using LabVIEW software in order to monitor the water content and cell flooding continually.

Objective 5:

Carry out experimental investigation on the use of power parameter-based techniques such as current, voltage and power and diagnosis of the seeded condition. This also includes determining their operating efficiency using only the measured current and the manufacturer's data available from the datasheet to detect, diagnose and assess the relative fault severity of the seeded faults.

Achievement 5:

This objective was delivered in chapter 6. The power parameters and efficiency of PEMFCs were studied in detail including the effects of load, pressure, temperature and flow variation.

Objective 6:

Upgrade the developed test rig to include measuring and recording acoustic emissions (AE) data, under varying operating conditions and at different electrical loads.

Achievement 6:

A fully integrated data acquisition system was constructed to collect data from a 500mW PEMFC, which was available at the AID laboratory at Manchester Metropolitan University. Importantly, this data includes conventional electrical power parameters and AE measurements.

The data collected from PEMFC has been analysed in both time and frequency domains. Statistical approaches were utilised to analyse the AE with different loads. FFT was used to transform the time domain signal into the frequency domain signal. The frequency spectrum information is a valuable means of characterising all signals captured over the entire experiment; these were averaged to produce an average power spectrum.

Objective 7: Develop and apply signal-processing methods to assess AE ability to detect load variations. Those processing techniques include multiband filtration, root mean square values, variance, and kurtosis for detecting and diagnosing load variation and quantified faults.

Achievement 7:

Statistical approaches have been used to analyse the data namely, RMS (Root mean square), kurtosis, skewness and variance. A test rig has been developed for the collection and analysis of data; this was achieved by collecting data under different loading conditions and quantified seeded faults. The goal here was centred on obtaining an effective diagnostic signal processing technique. The focus was directed towards making the AE signals as a novel diagnostic tool for supporting the limited capabilities of conventional monitoring approaches. There is also room for optimising the developed model and applying other signal processing methods, such as time frequency domains using wavelet transforms.

7.4 Future Work

Results presented in this work have provided clear performance evaluation and fundamental acoustical characteristics of PEMFCs. However, further investigation should be performed for full utilisation of those findings to develop effective control and condition monitoring systems for PEMFCs. The proposed future work could be as follows:

1- More investigation into experimental aspects

A. Use a different size of PEMFCs.
B. Simulate and seed other types of failure modes.

2- Diagnostic techniques related

Although AE signals show clear capabilities for detecting load variation, more work is required to fully assess their abilities in detecting failures in PEMFCs. This would include the development of more powerful signal processing techniques such as frequency and time-frequency domain analysis.

7.5 Concluding Remarks

Reliability has become an increasingly important requirement for FC systems. In the early stages of market adoption and large-scale demonstration projects, performance and reliability have been recognised as key attributes in ensuring the successful adoption of these new technologies. In this context, the main aim of future work is to investigate the reliability of the PEMFC and how can it be enhanced. The faults that occur in PEMFCs are the main effect on reliability. More work and experiments are needed to investigate e.g., how the AE technique can be used to establish an online state of health and failures under operating conditions for single or a stack of PEMFC units. Output voltage might be used as a performance primary indicator and AE will be used as the main diagnostic tool. Single and stack units can be used in the experiments. The main challenge for AE to act as an effective diagnosis tool for a PEMFC stack system is to find a reliable way to identify faulty PEMFCs. There are many faults that are difficult to deal with such as flooding, drying and fuel starvation, which are highly related with water management - especially in the FC stack. Therefore, future work would involve performing an

experimental study of technique performance, which would be directly applied to the PEMFC stack. Laboratory measurement equipment must be used in order to eliminate possible influences caused by the measurement system (noise). By using the above-mentioned techniques, the following questions can be answered:

- How accurate the method is when used with a stack of cells
- Where the biggest computation problems are to be expected
- How accurate the measurement equipment should be.

REFERENCES

Abdo, N. and Easton, E.B. (2016). 'Nafion/Polyaniline composite membranes for hydrogen production in the Cu–Cl thermochemical cycle'. International Journal of Hydrogen Energy, 41(19), pp.7892-7903.

Abdollahzadeh, M., Pascoa, J.C., Ranjbar, A.A. and Esmaili, Q. (2014). Analysis of PEM (Polymer Electrolyte Membrane) fuel cell cathode two-dimensional modeling. Energy, 68, pp. 478-494.

Adzic, R.R., Zhang, J., Sasaki, K., Vukmirovic, M.B., Shao, M., Wang, J.X., Nilekar, A.U., Mavrikakis, M., Valerio, J.A. and Uribe, F., 2007. Platinum monolayer fuel cell electrocatalysts. Topics in Catalysis, 46(3-4), pp.249-262.

Adjemian, K.T., Srinivasan, S., Benziger, J. and Bocarsly, A.B. (2002). 'Investigation of PEMFC operation above 100 C employing perfluorosulfonic acid silicon oxide composite membranes'. Journal of Power Sources, 109(2), pp. 356-364.

Al-Baghdadi, M.A. (2010). CFD modeling and analysis of different novel designs of air-breathing PEM fuel cells. Nova Science Publishers.

Al-Baghdadi, M.A.S. (2005). 'Modelling of proton exchange membrane fuel cell performance based on semi-empirical equations'. Renewable Energy, 30(10), pp. 1587-1599.

Alink, R., Gerteisen, D. and Oszcipok, M. (2008). 'Degradation effects in polymer electrolyte membrane fuel cell stacks by sub-zero operation — An in situ and ex situ analysis'. Journal of Power Sources, 182(1), pp. 175-187.

Al-Masri, A., Peksen, M., Blum, L. and Stolten, D. (2014). A 3D CFD model for predicting the temperature distribution in a full scale APU SOFC short stack under transient operating conditions. Applied Energy, 135, pp. 539-547.

Alrewq, M. and Albarbar, A. (2016). 'Investigation into the characteristics of proton exchange membrane fuel cell-based power system'. IET Science, Measurement and Technology, 10(3), pp. 200-206.

Al-Zahrani, A., Dincer, I. and Li, X. (2015). 'A performance assessment study on solid oxide fuel cells for reduced operating temperatures'. International Journal of Hydrogen Energy, 40(24), pp.7791-7797.

Andersson, M., Yuan, J. and Sundén, B. (2010). Review on modelling development for multiscale chemical reactions coupled transport phenomena in solid oxide fuel cells. Applied Energy, 87(5), pp. 1461-1476.

Antunes, R.A., Oliveira, M.C.L., Ett, G. and Ett, V. (2010). 'Corrosion of metal bipolar plates for PEM fuel cells: a review'. International Journal of Hydrogen Energy, 35(8), pp. 3632-3647.

Arvay, A., Yli-Rantala, E., Liu, C.H., Peng, X.H., Koski, P., Cindrella, L., Kauranen, P., Wilde, P.M. and Kannan, A.M., 2012. Characterization techniques for gas diffusion layers for proton exchange membrane fuel cells–A review. Journal of Power Sources, 213, pp. 317-337.

Assarabowski, R.J., Unkert, W.T., Bach, L.A., Grasso, A.P. and Olsommer, B.C., Utc Fuel Cells, Llc. (2004). 'Method and apparatus for preventing water in fuel cell power plants from freezing during storage'. U.S. Patent 6,797,421.

Bavarian, M., Soroush, M., Kevrekidis, I.G. and Benziger, J.B. (2010). Mathematical modelling, steady-state and dynamic behaviour, and control of fuel cells: A review. Industrial & Engineering Chemistry Research, 49(17), pp. 7922-7950.

Belvedere, B., Bianchi, M., Borghetti, A., De Pascale, A., Paolone, M. and Vecci, R. (2013). 'Experimental analysis of a PEM fuel cell performance at variable load with anodic exhaust management optimization.' International Journal of Hydrogen Energy, 38(1), pp. 385-393.

Berger, C. ed. (1968) 'Handbook of FC Technology., Prentice-Hall, Inc., Englewood Cliffs, New Jersey, USA, p. 607 .

Bianchi, F.D., Ocampo-Martinez, C., Kunusch, C. and Sánchez-Pena, R.S., 2015. Fault-tolerant unfalsified control for PEM fuel cell systems. IEEE Transactions on Energy Conversion, 30(1), pp. 307-315.

Borup, R., Meyers, J., Pivovar, B., Kim, Y.S., Mukundan, R., Garland, N., Myers, D., Wilson, M., Garzon, F., Wood, D. and Zelenay, P. (2007). 'Scientific aspects of polymer electrolyte fuel cell durability and degradation'. Chemical Reviews, 107(10), pp. 3904-3951.

Bose, S., Kuila, T., Nguyen, T.X.H., Kim, N.H., Lau, K.T. and Lee, J.H. (2011). Polymer membranes for high temperature proton exchange membrane fuel cell: recent advances and challenges. Progress in Polymer Science, 36(6), pp. 813-843.

Brady, M.P., Elhamid, M.A., Dadheech, G., Bradley, J., Toops, T.J., Meyer, H.M. and Tortorelli, P.F. (2013). 'Manufacturing and performance assessment of stamped, laser welded, and nitrided FeCrV stainless steel bipolar plates for proton exchange membrane fuel cells'. International Journal of Hydrogen Energy, 38(11), pp. 4734-4739.

Carmo, M., Fritz, D.L., Mergel, J. and Stolten, D. (2013). 'A comprehensive review on PEM water electrolysis'. International Journal of Hydrogen Energy, 38(12), pp. 4901-4934.

Carton, J.G., Lawlor, V., Olabi, A.G., Hochenauer, C. and Zauner, G. (2012). Water droplet accumulation and motion in PEM (Proton Exchange Membrane) fuel cell mini-channels. Energy, 39(1), pp. 63-73.

Chandan, A., Hattenberger, M., El-Kharouf, A., Du, S., Dhir, A., Self, V., Pollet, B.G., Ingram, A. and Bujalski, W. (2013). 'High temperature (HT) polymer electrolyte membrane fuel cells (PEMFC) – A review'. Journal of Power Sources, 231, pp. 264-278.

Chatenet, M., Dubau, L., Job, N. and Maillard, F. (2010). 'The (electro) catalyst| membrane interface in the proton exchange membrane fuel cell: similarities and differences with non-electrochemical catalytic membrane reactors. Catalysis Today, 156(3), pp. 76-86.

Chen, L., Luan, H.B., He, Y.L. and Tao, W.Q. (2012). 'Pore-scale flow and mass transport in gas diffusion layer of proton exchange membrane fuel cell with interdigitated flow fields'. International Journal of Thermal Sciences, 51, pp. 132-144.

Cheng, S., Liu, H. and Logan, B.E. (2006). 'Power densities using different cathode catalysts (Pt and CoTMPP) and polymer binders (Nafion and PTFE) in single chamber microbial fuel cells.' Environmental Science and Technology, 40(1), pp. 364-369.

Crowther, T.G., Wade, A.P., Wentzell, P.D. and Gopal, R. (1991). 'Characterization of acoustic emission from an electrolysis cell'. Analytica Chimica Acta, 254(1-2), pp. 223-234.

Das, P.K., Li, X. and Liu, Z.S. (2010). Analysis of liquid water transport in cathode catalyst layer of PEM fuel cells. International Journal of Hydrogen Energy, 35(6), pp. 2403-2416.

De Beer, C., Barendse, P.S., Pillay, P., Bullecks, B. and Rengaswamy, R. (2015). 'Electrical circuit analysis of CO poisoning in high-temperature PEM fuel cells for fault diagnostics and mitigation'. IEEE Transactions on Industry Applications, 51(1), pp. 619-630.

De Bruijn, F.A., Dam, V.A.T. and Janssen, G.J.M., 2008. Durability and degradation issues of PEM fuel cell components. Fuel cells, 8(1), pp.3-22.

Devanathan, R. (2013). 'Proton Exchange Membranes for FCs. Energy Production and Storage: Inorganic Chemical Strategies for a Warming World', Journal of Physical Chemistry B, 117(51), pp. 16522-16529.

Dou, M., Hou, M., Liang, D., Shen, Q., Zhang, H., Lu, W., Shao, Z. and Yi, B. (2011). Behaviour of proton exchange membrane fuel cells under oxidant starvation. Journal of Power Sources, 196(5), pp. 2759-2762.

Dubau, L., Castanheira, L., Maillard, F., Chatenet, M., Lottin, O., Maranzana, G., Dillet, J., Lamibrac, A., Perrin, J.C., Moukheiber, E. and El Kaddouri, A. (2014). 'A review of PEM fuel cell durability: materials degradation, local heterogeneities of aging and possible mitigation strategies'. Wiley Interdisciplinary Reviews: Energy and Environment, 3(6), pp. 540-560.

Dutta, S., Shimpalee, S., and Van Zee, W. (2001) 'Numerical prediction of mass-exchange between cathode and anode channels in a PEM fuel cell. International Journal of Heat and Mass Transfer 11(44) pp. 2029-2042.

Ercolino, G., Ashraf, M.A., Specchia, V. and Specchia, S. (2015). 'Performance evaluation and comparison of fuel processors integrated with PEM fuel cell based on steam or autothermal reforming and on CO preferential oxidation or selective methanation'. Applied Energy, 143, pp. 138-153.

Escobet, T., Feroldi, D., De Lira, S., Puig, V., Quevedo, J., Riera, J. and Serra, M. (2009). Model-based fault diagnosis in PEM fuel cell systems. Journal of Power Sources, 192(1), pp. 216-223.

Fecarotti, C., Andrews, J. and Chen, R., 2016. A petri net approach for performance modelling of polymer electrolyte membrane fuel cell systems. International Journal of Hydrogen Energy, 41(28), pp. 12242-12260.

Gabreab, E.M., Hinds, G., Fearn, S., Hodgson, D., Millichamp, J., Shearing, P.R. and Brett, D.J. (2014). 'An electrochemical treatment to improve corrosion and contact resistance of stainless steel bipolar plates used in polymer electrolyte fuel cells'. Journal of Power Sources, 245, pp. 1014-1026.

Gancs, L., Hult, B.N., Hakim, N. and Mukerjee, S. (2007). 'The impact of Ru contamination of a Pt⁄C electrocatalyst on its oxygen-reducing activity. Electrochemical and Solid-state Letters, 10(9), pp. B150-B154.

Gao, F., Blunier, B., Simoes, M.G. and Miraoui, A., 2011. PEM fuel cell stack modelling for real-time emulation in hardware-in-the-loop applications. IEEE Transactions on Energy Conversion, 26(1), pp.184-194.

Ge, S. and Wang, C.Y., 2007. Characteristics of sub-zero start-up and water/ice formation on the catalyst layer in a polymer electrolyte fuel cell. Electrochemical Acta, 52(14), pp. 4825-4835.

Gebel, G., Diat, O., Escribano, S. and Mosdale, R., 2008. Water profile determination in a running PEMFC by small-angle neutron scattering. Journal of Power Sources, 179(1), pp.132-139.

Gerard, M., Poirot-Crouvezier, J.P., Hissel, D. and Pera, M.C., 2010. Oxygen starvation analysis during air feeding faults in PEMFC. International Journal of Hydrogen Energy, 35(22), pp. 12295-12307.

Gittleman, C.S., Coms, F.D. and Lai, Y.H. (2011). 'Membrane durability: physical and chemical degradation'. In Polymer Electrolyte Fuel Cell Degradation, Eds: Mench, M., Kumbur, E.C. and Veziroglu, T.N. Elsevier 1st edition, chapter 2, pp. 15-88.

Grigoriev, S.A., Shtatniy, I.G., Millet, P., Porembsky, V.I. and Fateev, V.N., 2011. Description and characterization of an electrochemical hydrogen compressor/concentrator based on solid polymer electrolyte technology. International Journal of Hydrogen Energy, 36(6), pp. 4148-4155.

Grimm, M., See, E.J. and Kandlikar, S.G., 2012. Modelling gas flow in PEMFC channels: Part I–Flow pattern transitions and pressure drop in a simulated ex situ channel

with uniform water injection through the GDL. International Journal of Hydrogen Energy, 37(17), pp. 12489-12503.

Gubler, L. and Scherer, G.G. (2009). 'Durability of Radiation-Grafted Fuel Cell Membranes'. In Polymer Electrolyte Fuel Cell Durability, pp. 133-155. Springer, New York.

Ha, T., Cho, J., Park, J., Min, K., Kim, H.S., Lee, E. and Young, J.Y. (2011). 'Experimental study on carbon corrosion of the gas diffusion layer in polymer electrolyte membrane fuel cells'. International Journal of Hydrogen Energy, 36(19), pp. 12436-12443.

Hashimoto, S., Watanabe, H., Sakamoto, T., Kawada, T., Yashiro, K., Mizusaki, J., Kumada, K., Changsheng, D., Sato, K. and Hashida, T. (2012). 'The design and development of an evaluation system for redox characteristics of anode supported SOFCs using in-situ acoustic emission and electrochemical technique'. In ASME 2012 10th International Conference on Fuel Cell Science, Engineering and Technology collocated with the American Society of Mechanical Engineers' 2012 6th International Conference on Energy Sustainability, pp. 521-525.

Hou, J., Yu, H., Zhang, S., Sun, S., Wang, H., Yi, B. and Ming, P. (2006). 'Analysis of PEMFC freeze degradation at − 20 C after gas purging'. Journal of Power Sources, 162(1), pp. 513-520.

Hu, Q., Zhang, D., Fu, H. and Huang, K. (2014). 'Investigation of stamping process of metallic bipolar plates in PEM fuel cell — Numerical simulation and experiments'. International Journal of Hydrogen Energy, 39(25), pp. 13770-13776.

Hutzenlaub, T., Becker, J., Zengerle, R. and Thiele, S. (2013). Modelling the water distribution within a hydrophilic and hydrophobic 3D reconstructed cathode catalyst layer of a proton exchange membrane fuel cell. Journal of Power Sources, 227, pp. 260-266.

Inaba, M., Kinumoto, T., Kiriake, M., Umebayashi, R., Tasaka, A. and Ogumi, Z. (2006). 'Gas crossover and membrane degradation in polymer electrolyte fuel cells'. Electrochimica Acta, 51(26), pp. 5746-5753.

International Energy Agency (2015) Key world energy statistics 2015. Available at: http://www.iea.org/publications/freepublications/publication/KeyWorld_Statistics_2015.pdf.

Iranzo, A., Muñoz, M., Rosa, F. and Pino, J. (2010). 'Numerical model for the performance prediction of a PEM fuel cell. Model results and experimental validation'. International Journal of Hydrogen Energy, 35(20), pp. 11533-11550.

James, B.D. and Spisak, A.B. (2012). 'Mass Production Cost Estimation of Direct H2 PEM Fuel Cell Systems for Transportation Applications: 2012 Update'. Report by Strategic Analysis, Inc., under Award Number DEEE0005236 for the US Department of Energy, 18. and Sustainable Energy Reviews, 11(8), pp.1720-1738.

Jaouen, F., Goellner, V., Lefèvre, M., Herranz, J., Proietti, E. and Dodelet, J.P. (2013). 'Oxygen reduction activities compared in rotating-disk electrode and proton exchange membrane fuel cells for highly active Fe N C catalysts'. Electrochimica Acta, 87, pp. 619-628.

Jeon, Y., Na, H., Hwang, H., Park, J., Hwang, H. and Shul, Y.G. (2015). 'Accelerated life-time test protocols for polymer electrolyte membrane fuel cells operated at high temperature'. International Journal of Hydrogen Energy, 40(7), pp. 3057-3067.

Jeon, Y., Park, J.I., Ok, J., Dorjgotov, A., Kim, H.J., Kim, H., Lee, C., Park, S. and Shul, Y.G. (2016). 'Enhancement of catalytic durability through nitrogen-doping treatment on the CNF-derivatized ACF support for high temperature PEMFC'. International Journal of Hydrogen Energy, 41(16), pp. 6864-6876.

Jiao, K. and Li, X. (2011). 'Water transport in polymer electrolyte membrane fuel cells'. Progress in Energy and Combustion Science, 37(3), pp. 221-291.

Jia, Q., Li, J., Caldwell, K., Ramaker, D.E., Ziegelbauer, J.M., Kukreja, R.S., Kongkanand, A. and Mukerjee, S., 2016. Circumventing Metal Dissolution Induced Degradation of Pt-Alloy Catalysts in Proton Exchange Membrane Fuel Cells: Revealing the Asymmetric Volcano Nature of Redox Catalysis. ACS Catalysis, 6(2), pp.928-938.

Jouin, M., Gouriveau, R., Hissel, D., Péra, M.C. and Zerhouni, N. (2014) 'Prognostics of PEM fuel cell in a particle filtering framework'. International Journal of Hydrogen Energy, 39(1) pp. 481-494.

Jouin, M., Gouriveau, R., Hissel, D., Péra, M.C. and Zerhouni, N. (2013). 'Prognostics and Health Management of PEMFC–State of the art and remaining challenges'. International Journal of Hydrogen Energy, 38(35), pp.15307-15317.

Jung, H.M. and Um, S. (2011). 'An experimental feasibility study of vanadium oxide films on metallic bipolar plates for the cold start enhancement of fuel cell vehicles'. International Journal of Hydrogen Energy, 36(24), pp. 15826-15837.

Kakati, B.K., Ghosh, A. and Verma, A. (2013). 'Efficient composite bipolar plate reinforced with carbon fiber and graphene for proton exchange membrane fuel cell'. International Journal of Hydrogen Energy, 38(22), pp. 9362-9369.

Kangasniemi, K.H., Condit, D.A. and Jarvi, T.D. (2004). 'Characterization of vulcan electrochemically oxidized under simulated PEM fuel cell conditions'. Journal of the Electrochemical Society, 151(4), pp. E125-E132.

Karimi, S., Fraser, N., Roberts, B. and Foulkes, F.R. (2012). 'A review of metallic bipolar plates for proton exchange membrane fuel cells: materials and fabrication methods.' Advances in Materials Science and Engineering, Article ID 828070.

Karthikeyan, P., Li, H.C., Lipscomb, G., Neelakrishnan, S., Abby, J.G. and Anand, R. (2012). 'Experimental investigation of the water impact on performance of proton exchange membrane fuel cells (PEMFC) with porous and non-porous flow channels'. In

ASME 2012 International Mechanical Engineering Congress and Exposition pp. 781-788.

Kim, J.H., Jang, M.H., Choe, J.S., Kim, D.Y., Tak, Y.S. and Cho, B.H. (2011). 'An experimental analysis of the ripple current applied variable frequency characteristic in a polymer electrolyte membrane fuel cell'. Journal of Power Electronics, 11(1), pp. 82-89.

Kim, M., Jung, N., Eom, K., Yoo, S.J., Kim, J.Y., Jang, J.H., Kim, H.J., Hong, B.K. and Cho, E. (2014). 'Effects of anode flooding on the performance degradation of polymer electrolyte membrane fuel cells'. Journal of Power Sources, 266, pp. 332-340.

Kim, S.K., Choi, S.W., Jeon, W.S., Park, J.O., Ko, T., Chang, H. and Lee, J.C., 2012. Cross-linked benzoxazine–benzimidazole copolymer electrolyte membranes for fuel cells at elevated temperature. Macromolecules, 45(3), pp.1438-1446.

KIRCHEVA, N., TANT, S., LEGROS, B., GENIES, S., ROSINI, S. and THIVEL, P.X., Acoustic Methods as a Tool for Management of Electrochemical Process of Energy.

Kirsten, S 'Renewable Energy Sources Act and Trading of Emission Certificates: a National and a Supranational Tool Direct Energy Turnover to Renewable Electricity-Supply in Germany., Energy Policy, 64: pp. 302-312.

Koh, S., Leisch, J., Toney, M.F. and Strasser, P. (2007). 'Structure-activity-stability relationships of Pt-Co alloy electrocatalysts in gas-diffusion electrode layers'. Journal of Physical Chemistry C, 111(9), pp.3 744-3752.

Kraytsberg, A. and Ein-Eli, Y. (2014). 'Review of advanced materials for proton exchange membrane fuel cells'. Energy and Fuels, 28(12), pp. 7303-7330.

Kumar, A., Sharma, S., Kumar K., Kaushik, N., and Mishra, S. (2010) 'Renewable Energy in India: Current Status and Future Potentials.' Renewable and Sustainable Energy Reviews 14(7) pp. 2434-2442.

Kusoglu, A., Karlsson, A.M., Santare, M.H., Cleghorn, S. and Johnson, W.B. (2006). 'Mechanical response of fuel cell membranes subjected to a hygro-thermal cycle'. Journal of Power Sources, 161(2), pp. 987-996.

Laberty-Robert, C., Valle, K., Pereira, F. and Sanchez, C. (2011). 'Design and properties of functional hybrid organic–inorganic membranes for fuel cells'. Chemical Society Reviews, 40(2), pp. 961-1005.

Lechartier, E., Laffly, E., Péra, M.C., Gouriveau, R., Hissel, D. and Zerhouni, N. (2015). Proton exchange membrane fuel cell behavioural model suitable for prognostics. International Journal of Hydrogen Energy, 40(26), pp. 8384-8397.

Lee, D. and Bae, J. (2012). 'Visualization of flooding in a single cell and stacks by using a newly-designed transparent PEMFC'. International Journal of Hydrogen Energy, 37(1), pp. 422-435.

Lee, K., Zhang, J., Wang, H. and Wilkinson, D.P. (2006). 'Progress in the synthesis of carbon nanotube-and nanofiber-supported Pt electrocatalysts for PEM fuel cell catalysis'. *Journal of Applied Electrochemistry*, 36(5), pp. 507-522.

Legros, B., Thivel, P.X., Druart, F., Bultel, Y. and Nogueira, R. (2009), July. Diagnosis and modelling of proton-exchange-membrane fuel cell via electrochemical-impedance-spectroscopy and Acoustic-Emission measurements. In *Advanced Electromechanical Motion Systems & Electric Drives Joint Symposium, 2009. ELECTROMOTION 2009. 8th International Symposium on* IEEE, pp. 1-6.

Li, A. and Chan, S.H. (2013). 'Understanding the role of cathode structure and property on water management and electrochemical performance of a PEM fuel cell'. *International Journal of Hydrogen Energy*, 38(27), pp. 11988-11995.

Lim, C., Ghassemzadeh, L., Van Hove, F., Lauritzen, M., Kolodziej, J., Wang, G.G., Holdcroft, S. and Kjeang, E. (2014). 'Membrane degradation during combined chemical and mechanical accelerated stress testing of polymer electrolyte fuel cells'. *Journal of Power Sources*, 257, pp. 102-110.

Liu, F., Lu, G. and Wang, C.Y. (2007). Water transport coefficient distribution through the membrane in a polymer electrolyte fuel cell. *Journal of Membrane Science*, 287(1), pp. 126-131.

Liu, Y., Lehnert, W., Janßen, H., Samsun, R.C. and Stolten, D. (2016). A review of high-temperature polymer electrolyte membrane fuel-cell (HT-PEMFC)-based auxiliary power units for diesel-powered road vehicles. *Journal of Power Sources*, 311, pp. 91-102.

Liu, Z., Yang, L., Mao, Z., Zhuge, W., Zhang, Y. and Wang, L., 2006. Behaviour of PEMFC in starvation. Journal of Power Sources, 157(1), pp. 166-176.

Lobato, J., Cañizares, P., Rodrigo, M.A., Pinar, F.J., Mena, E. and Úbeda, D. (2010). Three-dimensional model of a 50 cm 2 high temperature PEM fuel cell. Study of the flow channel geometry influence. *International Journal of Hydrogen Energy*, 35(11), pp. 5510-5520.

Lohoff, A.S., Günther, D., Hehemann, M., Müller, M. and Stolten, D. (2016). 'Extending the lifetime of direct methanol fuel cell systems to more than 20,000 h by applying ion exchange resins'. *International Journal of Hydrogen Energy*, 41(34), pp. 15325-15334.

Lu, Z., Rath, C., Zhang, G. and Kandlikar, S.G. (2011). Water management studies in PEM fuel cells, part IV: effects of channel surface wettability, geometry and orientation on the two-phase flow in parallel gas channels. *International Journal of Hydrogen Energy*, 36(16), pp. 9864-9875.

Maiyalagan, T. (2008). 'Synthesis and electro-catalytic activity of methanol oxidation on nitrogen containing carbon nanotubes supported Pt electrodes'. *Applied Catalysis B: Environmental*, 80(3), pp. 286-295.

Mazumder, S. and Cole, J.V., 2003. Rigorous 3-D mathematical modelling of PEM fuel cells II. Model predictions with liquid water transport. *Journal of the Electrochemical Society*, 150(11), pp. A1510-A1517.

Meier, J.C., Galeano, C., Katsounaros, I., Topalov, A.A., Kostka, A., Schüth, F. and Mayrhofer, K.J. (2012). 'Degradation mechanisms of Pt/C fuel cell catalysts under simulated start–stop conditions'. *Acs Catalysis*, 2(5), pp. 832-843.

Meng, H. (2008). 'Numerical analyses of non-isothermal self-start behaviour of PEM fuel cells from subfreezing start-up temperatures'. *International Journal of Hydrogen Energy*, 33(20), pp. 5738-5747.

Miao, Z., Yu, H., Song, W., Hao, L., Shao, Z., Shen, Q., Hou, J. and Yi, B. (2010). Characteristics of proton exchange membrane fuel cells cold start with silica in cathode catalyst layers. *International Journal of Hydrogen Energy*, 35(11), pp.5552-5557.

Milewski, J., 2011. Theory. In Advanced Methods of Solid Oxide Fuel Cell Modelling (pp. 17-39). Springer London.

Murray, E. Perry, T. Tsai, and S. A. Barnett. (1999) 'A direct-methane fuel cell with a ceria-based anode'. *Nature* 400 (6745) pp. 649-651.

Najafi, B., Mamaghani, A.H., Rinaldi, F. and Casalegno, A. (2015). 'Long-term performance analysis of an HT-PEM fuel cell based micro-CHP system: operational strategies'. *Applied Energy*, 147, pp. 582-592.

Nakagawa, T., Nakabayashi, K., Higashihara, T. and Ueda, M. (2010). 'A high performance polymer electrolyte membrane based on sulfonated poly (ether sulfone) with binaphthyl units'. *Journal of Materials Chemistry*, 20(32), pp.6662-6667.

Ni, M. (2013). 'Modeling and parametric simulations of solid oxide fuel cells with methane carbon dioxide reforming'. *Energy Conversion and Management*, 70, pp. 116-129.

Niu, X.D., Munekata, T., Hyodo, S.A. and Suga, K. (2007). 'An investigation of water-gas transport processes in the gas-diffusion-layer of a PEM FC by a multiphase multiple-relaxation-time lattice Boltzmann model'. *Journal of Power Sources*, 172(2), pp.542-552.

Oberholzer, P., Boillat, P., Siegrist, R., Perego, R., Kästner, A., Lehmann, E., Scherer, G.G. and Wokaun, A. (2011). 'Cold-start of a PEFC visualized with high resolution dynamic in-plane neutron imaging'. *Journal of the Electrochemical Society*, 159(2), pp. B235-B245.

Offer, G.J., Mermelstein, J., Brightman, E. and Brandon, N.P. (2009). 'Thermodynamics and kinetics of the interaction of carbon and sulfur with solid oxide FC anodes'. *Journal of the American Ceramic Society*, 92(4), pp.763-780.

Okada, T., Møller-Holst, S., Gorseth, O. and Kjelstrup, S. (1998). 'Transport and equilibrium properties of Nafion® membranes with H^+ and Na^+ ions'. *Journal of Electroanalytical Chemistry*, 442(1), pp.137-145.

Panwar, N., Kaushik, S., & Kothari, S. (2011) 'Role of renewable energy sources in environmental protection: a review' *Renewable and Sustainable Energy Reviews* 15(3) pp. 1513-1524.

Park, S., Lee, J.W. and Popov, B.N. (2012). 'A review of gas diffusion layer in PEM fuel cells: materials and designs'. *International Journal of Hydrogen Energy*, 37(7), pp. 5850-5865.

Pasaogullari, U. and Wang, C.Y. (2005). Two-phase modelling and flooding prediction of polymer electrolyte fuel cells. *Journal of the Electrochemical Society*, 152(2), pp. A380-A390.

Pedersen, C.M., Escudero-Escribano, M., Velázquez-Palenzuela, A., Christensen, L.H., Chorkendorff, I. and Stephens, I.E. (2015). 'Benchmarking Pt-based electrocatalysts for low temperature fuel cell reactions with the rotating disk electrode: Oxygen reduction and hydrogen oxidation in the presence of CO (review article)'. *Electrochimica Acta*, 179, pp. 647-657.

Peighambardoust, S.J., Rowshanzamir, S. and Amjadi, M. (2010). 'Review of the proton exchange membranes for fuel cell applications'. *International Journal of Hydrogen Energy*, 35(17), pp.9349-9384.

Pukrushpan, J.T., Stefanopoulou, A.G. and Peng, H. (2004). 'Control of fuel cell breathing.' *IEEE Control Systems*, 24(2), pp.30-46.

Raunija, T.S.K., Gautam, R.K., Bhradwaj, V.M., Nandikesan, N., Shaneeth, M., Sharma, S.C. and Verma, A., 2016. Low Cost and Rapidly Processed Randomly Oriented Carbon/Carbon Composite Bipolar Plate for PEM Fuel Cell. *Fuel Cells*, 16(6), pp.801-809.

Robin, C., Gérard, M., Quinaud, M., d'Arbigny, J. and Bultel, Y. (2016). 'Proton exchange membrane fuel cell model for aging predictions: Simulated equivalent active surface area loss and comparisons with durability tests'. *Journal of Power Sources*, 326, pp.417-427.

Rodrigues, S., Restrepo, C., Kontos, E., Pinto, R.T. and Bauer, P. (2015).' Trends of offshore wind projects.' Renewable and Sustainable Energy Reviews, 49: pp.1114-1135.

Rowshanzamir, S., Peighambardoust, S.J., Parnian, M.J., Amirkhanlou, G.R. and Rahnavard, A. (2015). 'Effect of Pt-Cs 2.5 H 0.5 PW 12 O 40 catalyst addition on durability of self-humidifying nanocomposite membranes based on sulfonated poly (ether ether ketone) for proton exchange membrane fuel cell applications'. *International Journal of Hydrogen Energy*, 40(1), pp.549-560.

Sato, K., Hashida, T., Yugami, H., Yashiro, K., Kawada, T. & Mizusaki, J. (2006). 'Characteristics of damage and fracture process of solid oxide fuel cells under simulated

operating conditions by using AE method'. *Journal of Acoustic Emission*, 24, pp. 215-221.

Schmittinger, W. and Vahidi, A. (2008). 'A review of the main parameters influencing long-term performance and durability of PEM fuel cells'. *Journal of Power Sources*, 180(1), pp. 1-14.

Scott, K., Xu, C. and Wu, X. (2014). 'Intermediate temperature proton-conducting membrane electrolytes for fuel cells'. *Wiley Interdisciplinary Reviews: Energy and Environment*, 3(1), pp.24-41.

Shao, M., Shoemaker, K., Peles, A., Kaneko, K. and Protsailo, L. (2010). 'Pt monolayer on porous Pd−Cu alloys as oxygen reduction electrocatalysts'. *Journal of the American Chemical Society*, 132(27), pp. 9253-9255.

Shao, M.H., Huang, T., Liu, P., Zhang, J., Sasaki, K., Vukmirovic, M.B. and Adzic, R.R. (2006). 'Palladium monolayer and palladium alloy electrocatalysts for oxygen reduction'. *Langmuir*, 22(25), pp. 10409-10415.

Shao, Y., Yin, G. and Gao, Y. (2007). 'Understanding and approaches for the durability issues of Pt-based catalysts for PEM fuel cell'. *Journal of Power Sources*, 171(2), pp.558-566.

Shao, Y., Yin, G., Gao, Y. and Shi, P. (2006). 'Durability study of Pt/C and Pt/CNTs catalysts under simulated PEM fuel cell conditions'. *Journal of the Electrochemical Society*, 153(6), pp. A1093-A1097.

Siegel, C. (2008). Review of computational heat and mass transfer modelling in polymer-electrolyte-membrane (PEM) fuel cells. *Energy*, 33(9), pp.1331-1352.

Song, J.M., Cha, S.Y. and Lee, W.M. (2001). 'Optimal composition of polymer electrolyte fuel cell electrodes determined by the AC impedance method'. *Journal of Power Sources*, 94(1), pp. 78-84.

Speder, J., Zana, A., Spanos, I., Kirkensgaard, J.J., Mortensen, K., Hanzlik, M. and Arenz, M. (2014). 'Comparative degradation study of carbon supported proton exchange membrane fuel cell electrocatalysts – The influence of the platinum to carbon ratio on the degradation rate'. *Journal of Power Sources*, 261, pp. 14-22.

Spiegel, C. (2011). *PEM fuel cell modeling and simulation using MATLAB*. Academic press.

Spurgeon, J.M., Walter, M.G., Zhou, J., Kohl, P.A. and Lewis, N.S. (2011). 'Electrical conductivity, ionic conductivity, optical absorption, and gas separation properties of ionically conductive polymer membranes embedded with Si microwire arrays'. *Energy and Environmental Science*, 4(5), pp.1772-1780.

Srouji, A.K., Zheng, L.J., Dross, R., Turhan, A. and Mench, M.M. (2013). 'Ultra-high current density water management in polymer electrolyte fuel cell with porous metallic flow field'. *Journal of Power Sources*, 239, pp. 433-442.

Subban, C.V., Zhou, Q., Hu, A., Moylan, T.E., Wagner, F.T. and DiSalvo, F.J. (2010). Sol− Gel Synthesis, Electrochemical Characterization, and Stability Testing of Ti0. 7W0. 3O2 Nanoparticles for Catalyst Support Applications in Proton-Exchange Membrane Fuel Cells. *Journal of the American Chemical Society*, *132*(49), pp.17531-17536.

Subianto, S., Pica, M., Casciola, M., Cojocaru, P., Merlo, L., Hards, G. and Jones, D.J. (2013). 'Physical and chemical modification routes leading to improved mechanical properties of perfluorosulfonic acid membranes for PEM fuel cells'. *Journal of Power Sources*, 233, pp .216-230.

Sutharssan, T., Montalvao, D., Chen, Y.K., Wang, W.C., Pisac, C. and Elemara, H. (2017). A review on prognostics and health monitoring of proton exchange membrane fuel cell. *Renewable and Sustainable Energy Reviews*, 75, pp. 440-450.

Taherian, R. (2014). 'A review of composite and metallic bipolar plates in proton exchange membrane fuel cell: Materials, fabrication, and material selection'. *Journal of Power Sources*, 265, pp. 370-390.

Tang, H., Peikang, S., Jiang, S.P., Wang, F. and Pan, M. (2007). 'A degradation study of Nafion proton exchange membrane of PEM fuel cells'. *Journal of Power Sources*, 170(1), pp.85-92.

Tang, H., Qi, Z., Ramani, M. and Elter, J.F. (2006). 'PEM fuel cell cathode carbon corrosion due to the formation of air/fuel boundary at the anode'. *Journal of Power Sources*, 158(2), pp.1306-1312.

Tanrioven, M. and Alam, M.S. (2006). Reliability modelling and analysis of stand-alone PEM fuel cell power plants. Renewable Energy, 31(7), pp.915-933.

Tanuma, T. and Kinoshita, S. (2011). 'Impact of gas diffusion layers (GDLs) on water transport in PEFCs'. *Journal of the Electrochemical Society*, 159(2), pp. B150-B154.

Theodorakakos, A., Ous, T., Gavaises, M., Nouri, J.M., Nikolopoulos, N. and Yanagihara, H. (2006). 'Dynamics of water droplets detached from porous surfaces of relevance to PEM fuel cells.' *Journal of Colloid and Interface Science*, 300(2), pp.673-687.

Therdthianwong, A., Saenwiset, P. and Therdthianwong, S. (2012). 'Cathode catalyst layer design for proton exchange membrane fuel cells'. *Fuel*, 91(1), pp. 192-199.

Tian, G., Wasterlain, S., Endichi, I., Candusso, D., Harel, F., François, X., Péra, M.C., Hissel, D. and Kauffmann, J.M. (2008). 'Diagnosis methods dedicated to the localisation of failed cells within PEMFC stacks'. Journal of Power Sources, 182(2), pp. 449-461.

Ural, Z., Gencoglu, M.T. and Gumus, B. (2007), 'Dynamic simulation of a PEM fuel cell system.' In Proceedings of the 2nd International Hydrogen Energy Congress and Exhibition IHEC 2007, pp. 1-12.

Vasile, N.S., Doherty, R., Videla, A.H.M. and Specchia, S. (2016). 3D multi-physics modeling of a gas diffusion electrode for oxygen reduction reaction for electrochemical energy conversion in PEM fuel cells. *Applied Energy*, 175, pp .435-450.

Vengatesan, S., Panha, K., Fowler, M.W., Yuan, X.Z. and Wang, H. (2012). 'Membrane electrode assembly degradation under idle conditions via unsymmetrical reactant relative humidity cycling'. *Journal of Power Sources*, 207, pp. 101-110.

Vielstich, W., Lamm, A., Yokokawa, H. and Gasteiger, H.A., (2009). *Handbook of fuel cells: fundamentals technology and applications* (Vol. 2). John Wiley & Sons.

Wandschneider, F.T., Finke, D., Grosjean, S., Fischer, P., Pinkwart, K., Tübke, J. and Nirschl, H. (2014). 'Model of a vanadium redox flow battery with an anion exchange membrane and a Larminie-correction.' *Journal of Power Sources*, 272, pp.436-447.

Wang, C.Y. (2004). 'Fundamental models for FC engineering.' *Chemical Reviews*, 104(10), pp.4727-4766.

Wang, L., Husar, A., Zhou, T. and Liu, H. (2003). 'A parametric study of PEM FC performances'. *International Journal of Hydrogen Energy*, 28(11), pp.1263-1272.

Wang, S., Jiang, S.P., White, T.J., Guo, J. and Wang, X. (2009). 'Electrocatalytic activity and interconnectivity of Pt nanoparticles on multi-walled carbon nanotubes for FCs.' *Journal of Physical Chemistry C*, 113(43), pp.18935-18945.

Wang, X. and Van Nguyen, T. (2010). Modelling the effects of the microporous layer on the net water transport rate across the membrane in a PEM fuel cell. *Journal of the Electrochemical Society*, 157(4), pp. B496-B505.

Wang, Y., Chen, K.S., Mishler, J., Cho, S.C. and Adroher, X.C. (2011). A review of polymer electrolyte membrane fuel cells: technology, applications, and needs on fundamental research. *Applied Energy*, 88(4), pp.981-1007.

Wang, Y.J., Qiao, J., Baker, R. and Zhang, J. (2013). 'Alkaline polymer electrolyte membranes for fuel cell applications.' *Chemical Society Reviews*, 42(13), pp. 5768-5787.

Wu, B., Lin, G., Fu, Y., Hou, M. and Yi, B. (2010). 'Chromium-containing carbon film on stainless steel as bipolar plates for proton exchange membrane fuel cells'. *International Journal of Hydrogen Energy*, 35(24), pp. 13255-13261.

Wu, J., Yuan, X.Z., Martin, J.J., Wang, H., Zhang, J., Shen, J., Wu, S. and Merida, W. (2008). 'A review of PEM fuel cell durability: degradation mechanisms and mitigation strategies'. *Journal of Power Sources*, 184(1), pp.104-119.

Wu, J., Yuan, X.Z., Wang, H., Blanco, M., Martin, J.J. and Zhang, J. (2008).' Diagnostic tools in PEM fuel cell research: Part I Electrochemical techniques'. *International Journal of Hydrogen Energy*, 33(6), pp.1735-1746.

Xie, J., Wood, D.L., Wayne, D.M., Zawodzinski, T.A., Atanassov, P. and Borup, R.L. (2005). 'Durability of PEFCs at high humidity conditions'. *Journal of the Electrochemical Society*, 152(1), pp. A104-A113.

Xin, H.L., Mundy, J.A., Liu, Z., Cabezas, R., Hovden, R., Kourkoutis, L.F., Zhang, J., Subramanian, N.P., Makharia, R., Wagner, F.T. and Muller, D.A. (2011). 'Atomic-resolution spectroscopic imaging of ensembles of nano-catalyst particles across the life of a fuel cell.' *Nano Letters,* 12(1), pp.490-497.

Yang, L., Larouche, N., Chenitz, R., Zhang, G., Lefèvre, M. and Dodelet, J.P. (2015). 'Activity, performance, and durability for the reduction of oxygen in PEM fuel cells, of Fe/N/C electrocatalysts obtained from the pyrolysis of metal-organic-framework and iron porphyrin precursors'. *Electrochimica Acta*, 159, pp. 184-197.

Young, A.P. (2010). 'Characterization of structural degradation in a polymer electrolyte membrane fuel cell cathode catalyst layer' (Doctoral dissertation, University of British Columbia).

Yu, J.R., Matsuura, T., Yoshikawa, Y., Islam, M.N., Hori, M. (2005). 'In situ analysis of performance degradation of a PEMFC under non-saturated humidification'. *Electrochemist Solid-State Letters*, 8, pp. 156- 158.

Yu, X. and Ye, S. (2007). Recent advances in activity and durability enhancement of Pt/C catalytic cathode in PEMFC: Part II: Degradation mechanism and durability enhancement of carbon supported platinum catalyst. *Journal of Power Sources*, 172(1), pp.145-154.

Yuan, X.Z., Li, H., Zhang, S., Martin, J. and Wang, H. (2011). 'A review of polymer electrolyte membrane fuel cell durability test protocols'. *Journal of Power Sources*, 196(22), pp. 9107-9116.

Zarrin, H., Higgins, D., Jun, Y., Chen, Z. and Fowler, M. (2011). 'Functionalized graphene oxide nanocomposite membrane for low humidity and high temperature proton exchange membrane fuel cells'. *Journal of Physical Chemistry C*, 115(42), pp .20774-20781.

Zhang, H. and Shen, P.K. (2012). 'Recent development of polymer electrolyte membranes for fuel cells'. *Chemical Reviews*, 112(5), pp.2780-2832.

Zhang, J., Xie, Z., Zhang, J., Tang, Y., Song, C., Navessin, T., Shi, Z., Song, D., Wang, H., Wilkinson, D.P. and Liu, Z.S. (2006). High temperature PEM fuel cells. *Journal of Power Sources*, 160(2), pp.872-891.

Zhang, J.B.; Kramer, D., Shimoi, R., Ono, Y.; Lehmann, E.; Wokaun, A.; Shinohara, K.; Scherer, G.G. (2006) 'In situ diagnostic of two-phase flow phenomena in polymer electrolyte fuel cells by neutron imaging: Part B. Material variations'. *Electrochimica Acta*, 51, pp. 2715-2727.

Zhou, X., Qiao, J., Yang, L. and Zhang, J. (2014). ‘A review of graphene-based nanostructural materials for both catalyst supports and metal-free catalysts in PEM fuel cell oxygen reduction reactions. *Advanced Energy Materials*, 4, p. 8.

Zhou, Y., Neyerlin, K., Olson, T.S., Pylypenko, S., Bult, J., Dinh, H.N., Gennett, T., Shao, Z. and O'Hayre, R. (2010). ‘Enhancement of Pt and Pt-alloy fuel cell catalyst activity and durability via nitrogen-modified carbon supports’. *Energy and Environmental Science*, 3(10), pp.1437-1446

APPENDICES

Appendix A: Parameters used to model PEMFCs

Name	Value	Description
L	0.06[m]	Cell length
H_ch	1e-3[m]	Channel height
W_ch	9.474e-3[m]	Channel width
W_rib	9.0932e-3[m]	Rib width
H_gdl	640e-6[m]	GDL width
H_electrode	50e-6[m]	Porous electrode thickness
H_membrane	100e-6[m]	Membrane thickness
eps_gdl	0.4	GDL porosity
kappa_gdl	1.18e-11[m^2]	GDL permeability
sigma_gdl	222[S/m]	GDL electric conductivity
wH2_in	0.743	Inlet H2 mass fraction (anode)
wH2O_in	0.023	Inlet H2O mass fraction (cathode)
wO2_in	0.228	Inlet oxygen mass fraction (cathode
U_in_anode	0.2[m/s]	Anode inlet flow velocity
U_in_cathode	0.5[m/s]	
mu_anode	1.19e-5[Pa*s]	Anode viscosity
mu_cathode	2.46e-5[Pa*s]	Cathode viscosity
MH2	0.002[kg/mol]	Hydrogen molar mass
MN2	0.028[kg/mol]	Nitrogen molar mass
MH2O	0.018[kg/mol]	Water molar mass
MO2	0.032[kg/mol]	Oxygen molar mass
D_H2_H2O	9.15e-5*(T/307.1[K])^1.75[m^2/s]	H2-H2O
D_N2_H2O	2.56e-5*(T/307.15[K])^1.75[m^2/s]	N2-H2
D_O2_N2	2.2e-5*(T/293.2[K])^1.75[m^2/s]	O2-N2
D_O2_H2O	2.82e-5*(T/308.1[K])^1.75[m^2/s]	O2-H2O
T	20+273.15[K]	Cell temperature
p_ref	101e3[Pa]	Reference pressure
V_cell	0.9	Cell voltage
cO2_ref	40.88[mol/m^3]	Oxygen reference concentration
cH2_ref	40.88[mol/m^3]	Hydrogen reference concentration
eps_l	0.3	
eps_cl	1-eps_l-eps_gdl	Open volume fraction for fusion in porous electrodes
kappa_cl	kappa_gdl/5	Permeability (porous electrodes
sigma_m	9.825[S/m]	Membrane conductivity

Appendix B: Current Distribution and Water Concentration in the GDL

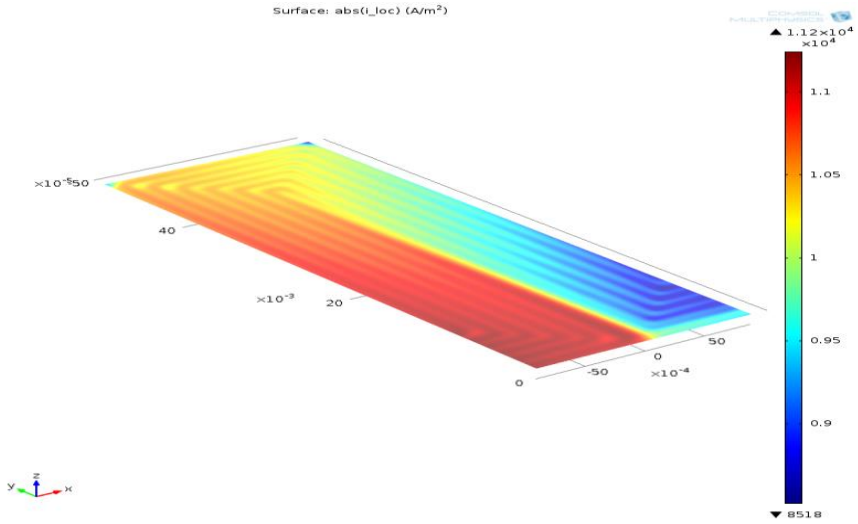

Current density in the GDL under operating conditions 298.15K & 1.5 atm.

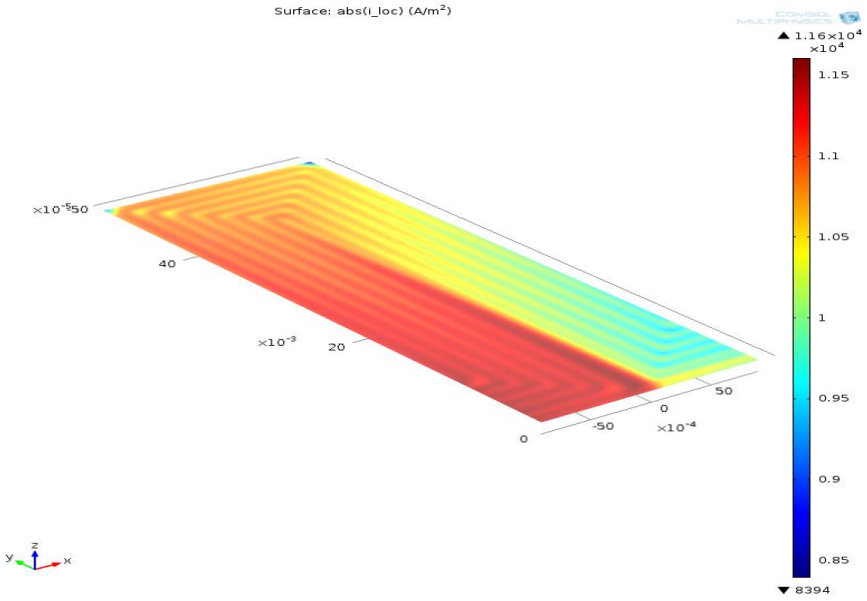

Current density in the GDL under operating conditions 323.15K & 1.5 atm.

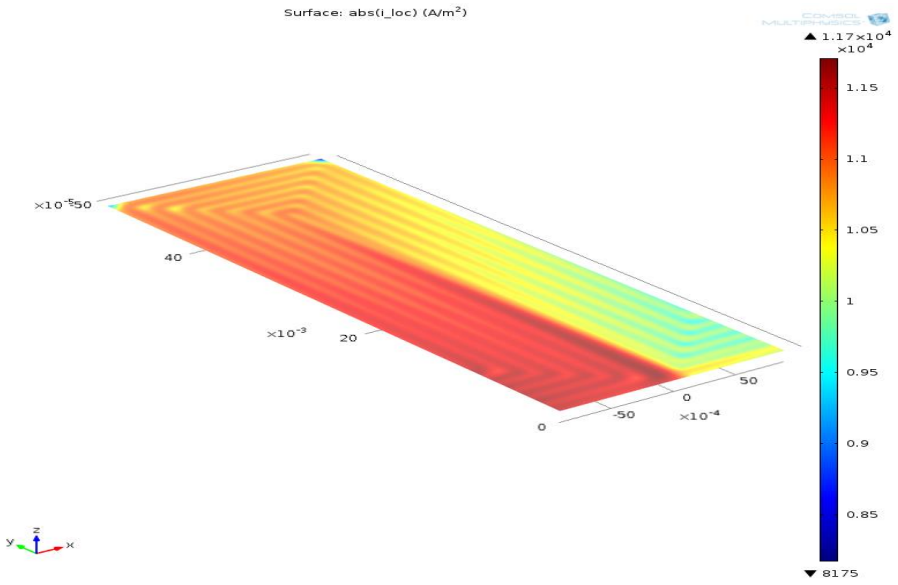

Current density in the GDL under operating conditions 348.15K & 1.5 atm.

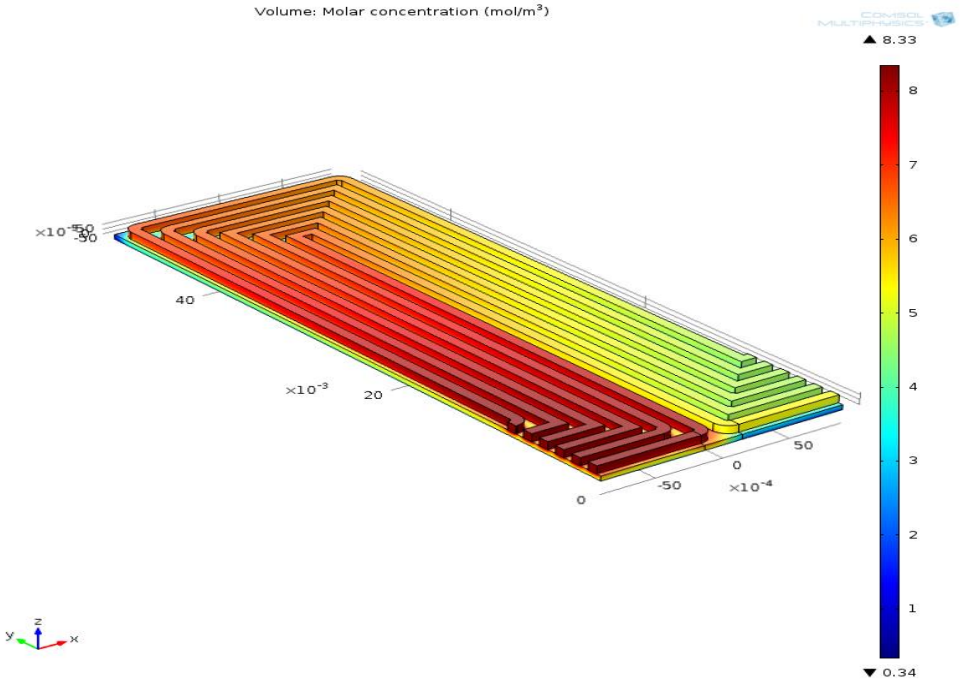

Water concentration in the GDL at 298.15K & 1.5 atm.

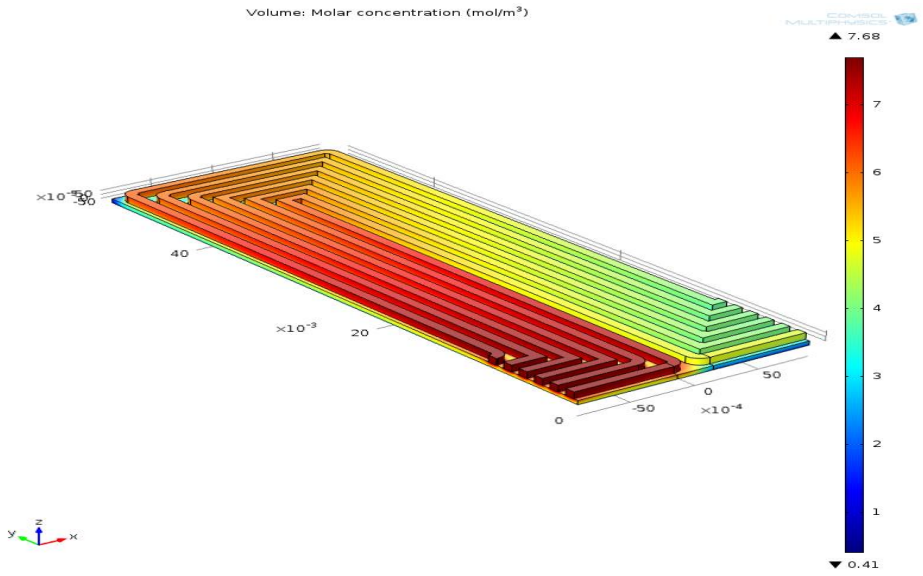

Water concentration in the GDL at 323.15K & 1.5 atm.

Appendix C: Current Density in the Membrane

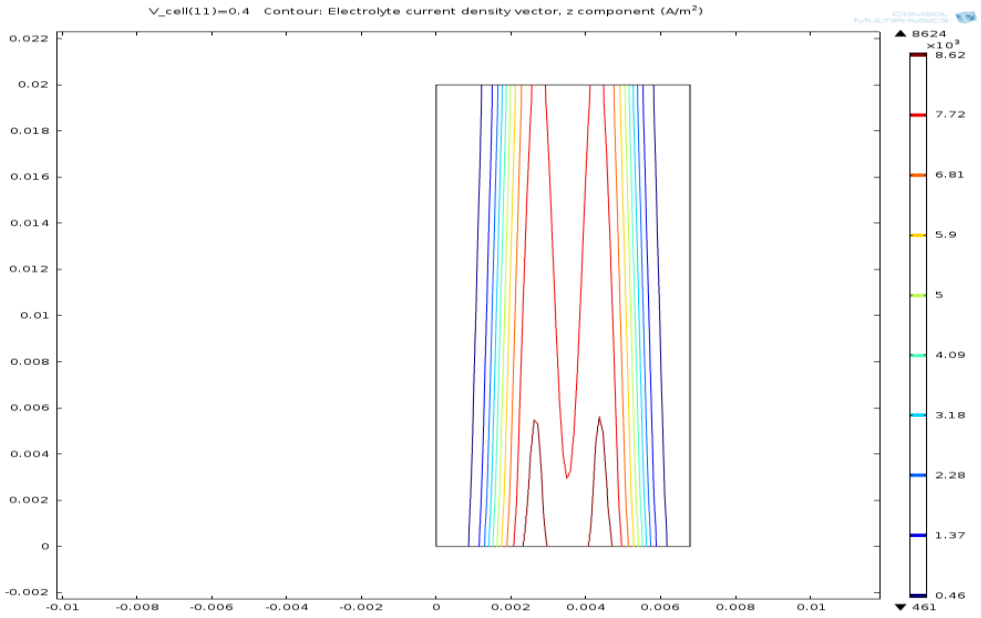

Current density distribution in the membrane at 298.15 K & 1.5 atm.

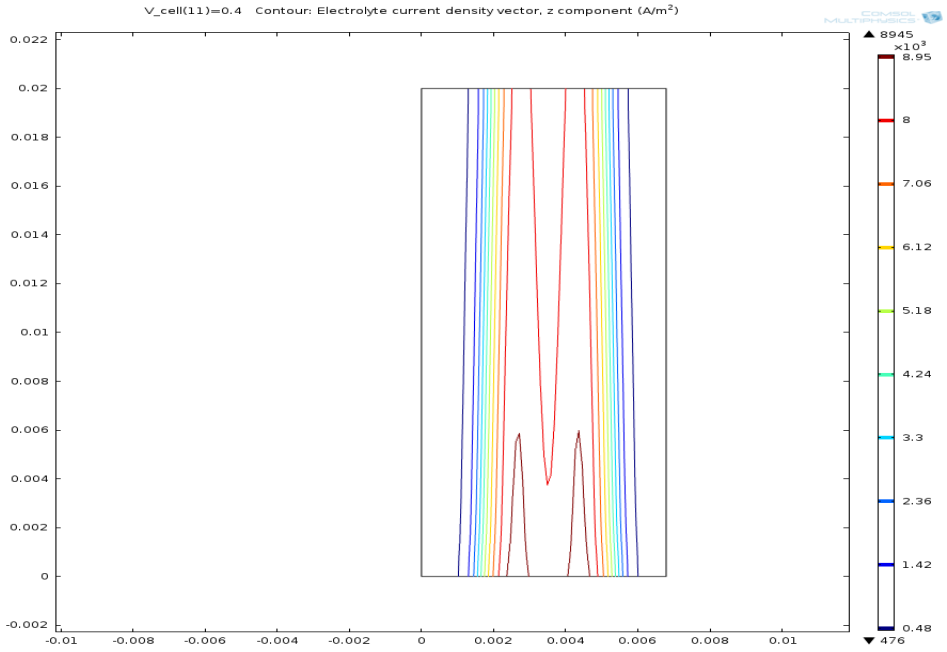

Current density distribution in the membrane at 223.15 K & 1.5 atm.

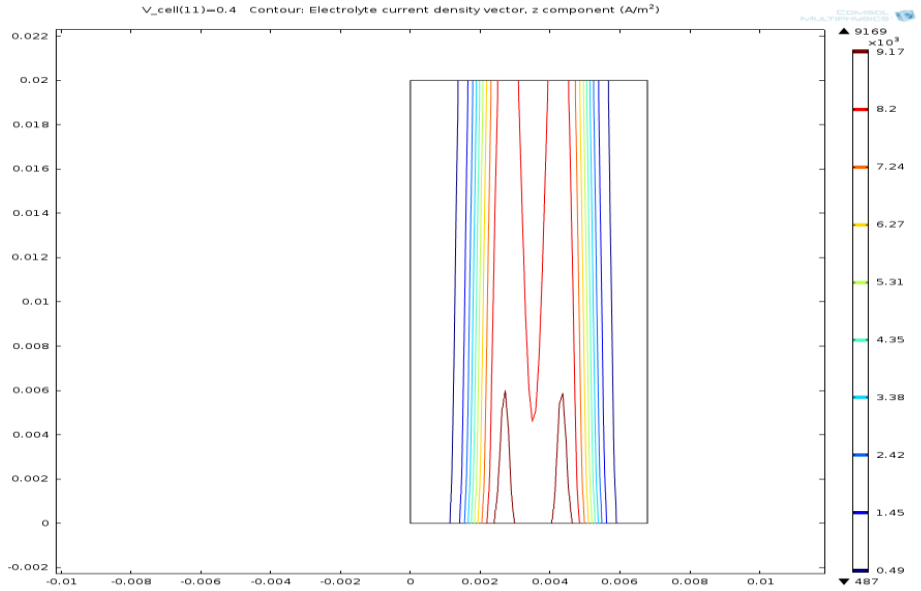

Current density distribution in the membrane at 248.15 K & 1.5 atm.